

AL-TR-90-040

AD:

②

1990 11 10 10 10

Final Report  
for the period  
July 1986 to  
February 1990

## Boundary Layer Study

November 1990

Authors:  
D.E. Coats  
D.R. Berker  
S.S. Dunn

Software & Engineering Associates, Inc.  
1000 E. William Street, Suite 200  
Carson City NV 89701

F04611-86-C-0055

DTIC  
ELECTE  
JAN 30 1991  
S E D

### Approved for Public Release

Distribution is unlimited. The AL Technical Services Office has reviewed this report, and it is releasable to the National Technical Information Service, where it will be available to the general public, including foreign nationals.

Prepared for the: **Astronautics Laboratory (AFSC)**  
Air Force Space Technology Center  
Space Systems Division  
Air Force Systems Command  
Edwards AFB CA 93523-5000

91 1 29 079

AD-A231 343

## NOTICE

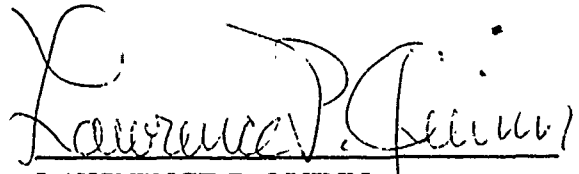
When U.S. Government drawings, specifications, or other data are used for any purpose other than a definitely related Government procurement operation, the fact that the Government may have formulated, furnished, or in any way supplied the said drawings, specifications, or other data, is not to be regarded by implication or otherwise, or in any way licensing the holder or any other person or corporation, or conveying any rights or permission to manufacture, use or sell any patented invention that may be related thereto.

## FOREWORD

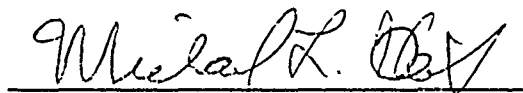
This final report was submitted by Software and Engineering Associates, Inc., Carson City NV on completion of contract F04611-86-C-0055 with the Astronautics Laboratory (AFSC), Edwards AFB CA 93523-5000. AL Project Manager was Jay Levine.

This report has been reviewed and is approved for release and distribution in accordance with the distribution statement on the cover and on the DD Form 1473.

  
JAY N. LEVINE  
Project Manager

  
LAWRENCE P. QUINN  
Chief, Aerothermochemistry Branch

FOR THE DIRECTOR

  
MICHAEL L. HEIL, Lt Col, USAF  
Deputy Director  
Astronautical Sciences Division

## REPORT DOCUMENTATION PAGE

Form Approved  
OMB No. 0704-0188

1a. REPORT SECURITY CLASSIFICATION UNCLASSIFIED			1b. RESTRICTIVE MARKINGS			
2a. SECURITY CLASSIFICATION AUTHORITY			3. DISTRIBUTION/AVAILABILITY OF REPORT Approved for Public Release; Distribution is Unlimited			
2b. DECLASSIFICATION/DOWNGRADING SCHEDULE						
4. PERFORMING ORGANIZATION REPORT NUMBER(S)			5. MONITORING ORGANIZATION REPORT NUMBER(S) AL-TR-90-040			
6a. NAME OF PERFORMING ORGANIZATION Software and Engineering Associates, Inc.		6b. OFFICE SYMBOL (if applicable)	7a. NAME OF MONITORING ORGANIZATION Astronautics Laboratory (AFSC)			
6c. ADDRESS (City, State, and ZIP Code) 300 E. William St., Suite 200 Carson City NV 89701			7b. ADDRESS (City, State, and ZIP Code) AL/LSCF Edwards AFB CA 93523-5000			
8a. NAME OF FUNDING/SPONSORING ORGANIZATION		8b. OFFICE SYMBOL (if applicable)	9. PROCUREMENT INSTRUMENT IDENTIFICATION NUMBER F04611-86-C-0055			
8c. ADDRESS (City, State, and ZIP Code)			10. SOURCE OF FUNDING NUMBERS			
			PROGRAM ELEMENT NO. 62302F	PROJECT NO. 5730	TASK NO. 00VH	WORK UNIT ACCESSION NO. 340830
11. TITLE (Include Security Classification) Boundary Layer Study (U)						
12. PERSONAL AUTHOR(S) Coats, D.E.; Berker, D.R.; Dunn, S.S.						
13a. TYPE OF REPORT Final		13b. TIME COVERED FROM 8607 TO 9002		14. DATE OF REPORT (Year, Month, Day) 9009		
15. PAGE COUNT 128						
16. SUPPLEMENTARY NOTATION						
17. COSATI CODES			18. SUBJECT TERMS (Continue on reverse if necessary and identify by block number)			
FIELD	GROUP	SUB-GROUP				
21	08					
20	04					
19. ABSTRACT (Continue on reverse if necessary and identify by block number)						
<p>The report details the work performed under the Boundary Layer Study contract sponsored by the Astronautics Laboratory. The purpose of this work effort was to produce new and better tools for predicting delivered nozzle performance (I<sub>sp</sub>) for very high area ratio liquid propellant rocket engines. The motivation for this <sup>sp</sup>work is the current interest in space propulsion systems and the high impact that delivered performance has on system design. Design margins can be significantly reduced if the accuracy and reliability of predictive procedures is improved. Two computer programs were developed under this effort. The first of these programs was an extension to the JANNAF standard TDK/BLM code. The second code, called VIPER, was a Parabolized Navier-Stokes solver with finite rate chemistry. An experimental plan to validate the predictive capabilities of the two codes was also formulated. Comparison of both TDK/BLM and VIPER to available data shows excellent agreement.</p>						
20. DISTRIBUTION/AVAILABILITY OF ABSTRACT <input type="checkbox"/> UNCLASSIFIED/UNLIMITED <input type="checkbox"/> SAME AS RPT <input type="checkbox"/> DTIC USERS			21. ABSTRACT SECURITY CLASSIFICATION UNCLASSIFIED			
22a. NAME OF RESPONSIBLE INDIVIDUAL Jay N. Levine			22b. TELEPHONE (Include Area Code) (805) 275-5366		22c. OFFICE SYMBOL AL/LSCF	

# TABLE OF CONTENTS

	<u>Page No.</u>
1.0 Introduction and Executive Summary	1
2.0 Phase I Work Effort - Improvements to Current Technology	5
2.1 Investigation Into Extensions of Current Technology	5
2.2 Implementation	15
2.3 Phase I, Results and Conclusions	16
3.0 Phase 2 Work Effort - Thick Boundary Layer Assessment	21
4.0 Phase 3.0 Effort - New Model Development	23
5.0 Phase 4 Work Effort - Experimental Test Plan	32
Nomenclature	42
References	44
Appendix A: Technical Papers from the Phase 1 Work Effort	A-1
Appendix B Technical Papers from the Phase 2 Work Effort	B-1
Appendix C Technical Papers from the Phase 3 Work Effort	C-1

Accession For	
NTIS GRA&I	<input checked="checked" type="checkbox"/>
DTIC TAB	<input type="checkbox"/>
Unannounced	<input type="checkbox"/>
Justification	
By _____	
Distribution/	
Availability Codes	
Dist	Avail and/or Special
A-1	



## LIST OF FIGURES

<u>Figure No.</u>		<u>Page No.</u>
1	Flow by Longitudinally Curved Walls	10
2	Streamline pattern of Taylor-Gortler Vortices	10
3	Nozzle Wall Schematic	17
4	Damping Study ASE Engine	27
5	Effect of Damping on Wall Shear Stress	28
6	Illustration of Thrust Chamber Losses from Ideal Performance	33
7	Boundary Layer Isp Losses	33

## LIST OF TABLES

<u>Table No.</u>		<u>Page No.</u>
1	Equivalent Sand Roughness for Several Types of Surfaces	14
2	Boundary Layer Thrust Deficit for Variety of Engines in the Absence and Presence of the Longitudinal Curvature. Cold Wall Case	19
3	Boundary Layer Thickness at the Exit Plane for Four Nozzles. Cooled Wall $T_w = 1000^\circ R$	21
4	Nozzle Characteristics for VIPER Verification Test Cases	24
5	Engine Performance	25
6	Conservation Checks	26
7	Effect of 4th Order Damping	29
8	Minimum Test Environment Criteria	35
9	Summary of Velocity Techniques	38

## 1.0 Introduction and Executive Summary

The trend towards very large area ratio nozzles, which result in performance gains for space propulsion applications, has increased the need for detailed knowledge of the momentum losses due to nozzle viscous effects (i.e., boundary layer). These losses degrade overall system performance, such as increasing system weight, decreasing useful payload weight, and/or decreasing effective system range. Another important factor in the designing of propulsive nozzles is the detailed knowledge of heat transfer at the wall for regeneratively cooled walls and/or material performance.

Because of the importance to rocket propulsion, the Astronautics Laboratory (AL/AFSC) has sponsored the Boundary Layer Study Contract to improve the understanding and computational predictive capabilities for boundary layers in rocket nozzles with very high area ratios.

The contractual effort was broken down into 4 work tasks with 2 deliverable computer programs plus documentation and two technical reports. The basic thrust of the effort was to develop an increased analytical capability to predict the performance loss of thick boundary layers in high area ratio propulsive nozzles. This objective has been successfully met.

A description of the four work tasks under this contract, along with the accomplishments made during each task, are:

- 1) Extension of Current Boundary Layer Technology:
  - o Extended the Boundary Layer capability of the JANNAF TDK/BLM code to predict thick boundary layer losses including the effects of longitudinal curvature
  - o Established the deficiency of the current JANNAF method of computing the boundary layer thrust loss for thick boundary layers

## 2) Thick Boundary Layer Assessment

- o Surveyed existing codes (both full and parabolized Navier–Stokes solvers) for solutions to the nozzle flow problem
- o Assessed the effects of various assumptions on computed boundary layer parameters
- o Established the course of action to be taken for the development of the new code developed in the Phase 3 effort

## 3) New Analytical Methods

- o Produced a new code for predicting the performance (including very thick boundary layers) of propulsive nozzles. The new code is called VIPER (Viscous Performance Evaluation Routine)
- o Validated the VIPER against data and the existing JANNAF Standard Code, TDK/BLM.

## 4) Experimental Validation Test Plan

- o Assessed the state of the art of diagnostics techniques for boundary layer measurements in nozzles flows
- o Visited and discussed methods and techniques with sources in industry and government
- o Made recommendations for a test plan to validate the turbulence models used in the codes developed under this contract

A series of 4 technical reports were written which describe in detail all of the technical effort under this contract. These reports are:

#### Phase 1 Effort

AFAL-TR-87-031, "Two-Dimensional Kinetics (TDK) Nozzle Performance Program - Thick Boundary Layer Version", February 1988

#### Phase 2 Effort

AL-TR-90-041, "Boundary Layer Study Thick Boundary Layer Assessment"

#### Phase 3 Effort

AL-TR-90-042, "Viscous Interaction Performance Evaluation Routine for Nozzle Flows with Finite Rate Chemistry"

#### Phase 4 Effort

AL-TR-90-043, "Boundary Layer Study Experimental Validation Test Plan"

#### Conclusions

- o The more general form of the JANNAF Boundary Layer Loss Equation should be adopted as the JANNAF standard
- o That longitudinal curvature is not an important effect for conventional propulsive nozzles
- o That PNS codes, such as the VIPER code, are required to supply the necessary accuracy to resolve the boundary layer and core flow for propulsive nozzles with thick boundary layers
- o The VIPER code represents a significant advancement in nozzle performance prediction capability
- o That direct experimental measurement of the boundary layer loss parameters are required to validate the analytical loss models



### Recommendations

- o That the VIPER code be considered as a JANNAF standard for high area ratio propulsive nozzles
- o That the VIPER code be extended to add:
  - particulate flows,
  - real nozzle effects, such as tangential slot injection,
  - chamber/injector models,
  - better shock capturing capability, and
  - a more robust  $k-\epsilon$  turbulence model
- o That the experimental test plan recommended in the Phase 4 work be executed

## 2.0 Phase I Work Effort - Improvements to Current Technology

The purpose of the Phase I work effort was to investigate ways in which the current performance prediction methodologies could be extended, and to select the most promising approaches and implement them in the current performance code(s). The objectives of the Phase I work were met. Section 2.1 describes the investigation of methods to extend current technology, section 2.2 describes the actual modifications and results, and section 2.3 describes the results and conclusions.

### 2.1 Investigation Into Extensions of Current Technology

At the start of the Boundary Layer Study Contract, the April 1985 Version of the TDK<sup>1</sup> program was the JANNAF standard code for computing the performance of liquid propellant rocket engine nozzles. This code represented the state of the art in nozzle performance prediction. The boundary layer module incorporated into TDK at that time was the BLM model<sup>1,2,3</sup>. This module would compute the boundary layer in a nozzle assuming a non-calorically perfect gas for either laminar or turbulent flow. The turbulence model used was the Cebeci-Smith eddy viscosity model<sup>4</sup>, which also included the effect of transverse curvature.

Since the purpose of the Phase I work was to extend current technology in computing boundary layer losses, it was important to understand the underlying assumptions which are present in the boundary layer equations as used for performance calculations.

The boundary layer equations are "deduced" using an order of magnitude argument<sup>\*</sup>. Reference 4, pp 39-44, contains an excellent presentation of the TSL (thin shear layer) equation derivation. Classical derivations of the TSL equations, e.g., Schlichting<sup>5</sup>, pp 128-131, Laudau and Lifshitz<sup>6</sup>, pp 145-147, tend to ignore the fact that the normal pressure gradient,  $\partial P / \partial y$ , vanishes not because the shear layer is thin ( $\delta / \ell \ll 1$ ), but because they have assumed that the surface is relatively flat, i.e., that the radius of curvature,  $R_c$ , is large, or

---

\* There are more mathematically rigorous derivations of the boundary layer equations than these, for example, Van Dyke<sup>7</sup>. However, the choice of the perturbation parameter and form of the series expansion are based on order of magnitude analysis.

more precisely  $R_c / \ell \gg 1$ . The term that is normally neglected is the "centrifugal force" equation, i.e.,

$$\frac{\partial P}{\partial y} = \frac{\rho u^2}{R_c}$$

The neglect of this term is justified when  $R_c / \ell \gg \delta / \ell$  which is usually the case in propulsive nozzles ( $\delta$  is usually very small when  $\ell$  is small). However, when the shear layer thickens to the point that  $\delta / \ell = O(1)$ , then we can no longer assume a priori that the normal pressure gradient has a negligible effect on the flow in the shear layer.

There are two effects which can have a potentially significant impact on the viscous thrust loss which are not normally accounted for in classical boundary layer theory:

- o transverse curvature
- o longitudinal curvature

The effect of transverse curvature was already treated in the BLM module and is not discussed here. In the following sections, the effect of longitudinal curvature will be examined in light of its impact on the mean flow and the eddy-viscosity models. Also not included in the JANNAF boundary layer codes is the effects of wall roughness. These effects are also discussed.

## Longitudinal Curvature Effects

The effect of longitudinal curvature on the flow results (i.e., nozzle performance) manifests itself in several ways, the most important are

- on the mean flow in the boundary layer (centrifugal force and normal stresses)
- in the turbulent shear stress model (eddy viscosity models)
- in the interaction with the core flow

The variation in mean flow due to the centrifugal force balance has been estimated by Beddini<sup>8</sup> to be about two percent in momentum thickness on the J2 nozzle. This change in thickness translates into a like amount in thrust loss. Note that while none of the commonly used boundary layer codes are accurate to within 5%, (probably not even 10%), it is important to be able to predict the trends accurately in order to know the relative amount of performance increase (or decrease) if the nozzle area ratio is enlarged.

Cebeci & Bradshaw<sup>4</sup> discuss the mean flow terms and their order of magnitude relative to the other boundary-layer terms. They point out that centrifugal force terms are generally intractable and normal stresses are usually negligible in weakly turbulent flows. For this reason the thin boundary-layer approach is usually adopted even in cases where it isn't strictly applicable.

The contribution of turbulence to the normal stresses have received relatively little attention in the literature. Finley<sup>9</sup> analyzed experimental data from cooled-wall and adiabatic hypersonic flow nozzles. He attributed the large variation of static pressure in hypersonic nozzle boundary-layer flows to be the combined effects of longitudinal curvature of the mean streamlines and the increasing importance, as the Mach number rises, of the Reynolds stress contribution to the total normal stress perpendicular to the wall. He concluded that at its peak value the Reynolds stress may provide a normal stress contribution equal to that of the mean static pressure.

The influence of longitudinal curvature on the mean boundary-layer flow can be modeled in several ways. The first way, pointed out by many authors, is to simply include the

centrifugal force term in the y-momentum equation, i.e.

$$\frac{\partial P}{\partial y} \approx \rho u \frac{\partial v}{\partial x} \approx \frac{\rho u^2}{R_c}$$

where  $R_c$  is the longitudinal radius of curvature of the body.

Two rigorous approaches to modeling the effects of longitudinal curvature (on the mean flow) have been taken in the literature. These are the singular perturbation analysis of Van Dyke<sup>7,10</sup> and the metric influence of curvature method of Schultz-Grunow and Breuer<sup>11</sup>.

The singular perturbation theory is too complex to go into here. Suffice it to say that starting with the Navier-Stokes equations the problem is solved by a scheme of successive approximations by the method of inner and outer expansions. Two complementary expansions are constructed simultaneously, and matched in their overlap region of common validity. To lowest order in the inner region the Prandtl boundary-layer theory is recovered while the outer region is an inviscid flow. Higher-order solutions in each region give the perturbations to the boundary-layer and external flows. For example, the boundary-layer displacement effect shows up in both the inner and outer regions. The perturbation method simplifies the problem because viscous effects are confined to the inner region which is parabolic and hence easier to solve than the full (elliptic) Navier-Stokes equations.

The approach of Schultz-Grunow and Breuer<sup>11</sup> is considerably different from the perturbation approach. They adopt a curvilinear system of coordinates and take the arc length along the surface as the x-coordinate. This brings the longitudinal curvature directly into the problem since any differentiation with respect to x carries a factor of the ratio of curvature radii (wall position to actual position). Schultz-Grunow and Breuer derive the boundary-layer equations from an order of magnitude analysis performed on the complete Navier-Stokes equations. They obtain the following set of equations:

Continuity:  $\frac{\partial u}{\partial x} + \frac{\partial}{\partial y} (1+ky)v = 0$

$$\begin{aligned} \text{x-momentum} \quad u \frac{\partial u}{\partial x} + (1+ky)v \frac{\partial u}{\partial y} + kuv = \frac{1}{\rho} \frac{\partial P}{\partial x} + (1+ky)v \frac{\partial^2 u}{\partial y^2} \\ + vk \left[ \frac{\partial u}{\partial y} - \frac{ku}{1+ky} \right] \end{aligned}$$

$$\text{y-momentum} \quad ku^2 = \frac{1+ky}{\rho} \frac{\partial P}{\partial y}$$

where  $k = 1/R_c$ . These equations are valid for concave as well as convex surfaces ( $k > 0$  for convex walls and  $k < 0$  for concave walls).

The authors point out that these equations contain all the second-order terms of the second-order perturbation theory (Van Dyke<sup>10</sup>), namely those of order  $1/\sqrt{\text{Re}}$ , and the exact metric influence of curvature. An additional term was included in the equations as well (the only justification given is that the main flow is then an analytic solution of the boundary-layer equations [sic]). Also note that these equations reduce to the classical boundary-layer equations when  $k = 0$ .

Cebeci, Hirsch, & Whitelaw<sup>12</sup> analyzed the turbulent boundary layer on a (convex) longitudinally curved surface using the mean flow equations of Schultz-Grunow and Breuer<sup>11</sup> discussed above. In their treatment they replaced the laminar viscosity with an effective viscosity,  $\nu + \epsilon_m$ . The eddy viscosity ( $\epsilon_m$ ) was specified to be the standard Cebeci and Smith<sup>13</sup> eddy-viscosity formulation modified by Bradshaw's<sup>14</sup> correction for longitudinal curvature.

Cebeci and Smith<sup>13</sup> point out that streamline curvature may increase or decrease the turbulent mixing, depending on the degree of wall curvature, and it can strongly affect the skin friction and heat transfer coefficients. They also included the streamwise curvature effect into the eddy-viscosity expression. (This will be discussed later). Eghlima et.al.<sup>15</sup> used a similar approach.

Longitudinal curvature has an effect on the structure of turbulence as well. In a boundary layer on a convex wall, see Figure 1, the centrifugal forces exert a small stabilizing effect. In contrast with that, concave walls have a de-stabilizing effect due to instabilities known as Taylor-Gortler vortices, (see Figure 2). Physically, the fluid element in a curved stream whose angular momentum decreases with increasing distance from the center of

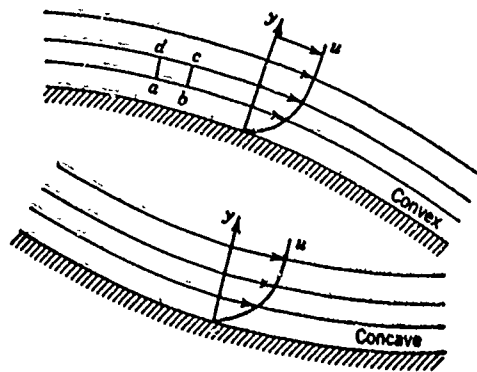


Figure 1: Flow by Longitudinally Curved Walls  
(From Reference 16)

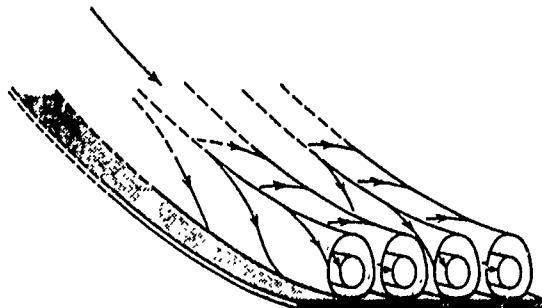


Figure 2: Streamline pattern of Taylor-Görtler Vortices  
(From Reference 16)

curvature is unstable. If the element is slightly displaced outward from the center, conserving its angular momentum about the center, it will be moving faster than its surroundings (which have a smaller angular momentum). Therefore the radial pressure gradient that controls streamline curvature will be too small to direct the displaced element along a streamline of the main flow, and the element will move even further outward. The converse argument holds for inward displacement. These instabilities affect both the transition to turbulence and the eddy viscosity.

Bradshaw<sup>14</sup> has developed an expression for the effect of longitudinal curvature which can be incorporated into the Cebeci-Smith eddy viscosity expression<sup>13</sup>. The inner eddy-viscosity expression is multiplied by  $S^2$  which was obtained by Bradshaw using an analogy between streamline curvature and buoyancy in turbulent shear flow. The expression for  $S$  is given by

$$S = 1/(1 + \beta R_i)$$

$$R_i = 2u/(R_c \partial u/\partial y)$$

where  $R_i$  is analogous to the Richardson number. The parameter  $\beta$  is equal to 7 for convex surfaces and 4 for concave surface according to meteorological data and by Bradshaw's<sup>7</sup> analogy between streamline curvature and buoyancy. According to Bradshaw, the effects of curvature on the mixing length or eddy viscosity are appreciable if the ratio of boundary-layer thickness to radius of curvature,  $\delta/R_c$ , exceeds roughly 1/300.

The interaction of the core flow with the shear layer manifests itself in the application of the boundary conditions for both the shear layer flow and the core flow. For the TSL approximation it is proper to view the system as a singular perturbation problem with the inner flow (i.e., the shear layer) boundary condition being applied at infinity (not  $\delta$ ), and the outer flow (the core flow) boundary condition applied at the wall. The matching condition is:

$$\begin{aligned} \text{Inner Limit of the Outer Expansion (ILOE)} &= \\ \text{Outer Limit of the Inner Expansion (OLIE)} \end{aligned}$$



The two flows are then connected iteratively by displacing the wall by  $\delta^*$  and recomputing the outer flow.

The same procedure of matching the two flows (i.e., ILOE=OLIE) is used for higher order boundary layer theory as discussed earlier (see Van Dyke<sup>7</sup>, p. 91 and pp 134–136, and Schlichting<sup>5</sup> pp 144–147). While higher order boundary layer theory does not lend itself readily to numerical solution, it does give a guide to understanding the interaction between the shear and core flows. Also, second order boundary layer theory contains all of the terms which are of concern here.

As previously noted, for numerical applications the procedure most commonly used to include the effects of curvature is to include all of the second order terms in the equation set which is solved. Examples of this procedure are given in References 11, 12, and 15. Also included in Reference 12, Cebeci et.al., are curvature effects on the eddy–viscosity model.

The correction to the outer inviscid MOC solution is done by displacing the wall by the displacement thickness,  $\delta^*$ , and rerunning the inviscid core solution. Examination of higher order boundary layer theory shows that this procedure is correct through second order. Hence, the deficiency with the current boundary layer matching conditions just concerns modifications to the boundary layer codes.

#### Wall Roughness Effects

Most nozzle boundary layer computer programs calculate wall roughness effects in an uncoupled manner. For example, surface roughness height is used to compute an augmented heat transfer rate. Such an approach is completely unsatisfactory if a purpose of the calculation is to estimate nozzle thrust loss, because the thrust loss calculation requires a rigorous energy balance. The wall roughness height found on liquid rocket wall materials are small enough that a coupled calculation can be performed. A coupled method for analyzing the wall surface roughness is described below.

The effects of a rough wall on the boundary layer can be simulated by the method of Cebeci that is described in Reference 17. In the method developed in Reference 17, the inner region of the Cebeci–Smith eddy viscosity formulation is modified to provide for surface roughness. This is done by modifying the mixing length

$$\ell = 0.4 y [1 - \exp(-y/A)]$$

as described below. First, it is recognized that the velocity profiles for smooth and rough walls are similar, provided that the coordinates are displaced, i.e.,:

$$\ell = 0.4 (y + \Delta y) \{ 1 - \exp[-(y + \Delta y)/A] \}$$

The displacement,  $\Delta y$ , is expressed as a function of an equivalent sand-grain roughness parameter,  $k_s$ , i.e.,:

$$\Delta y = 0.9 (v/U_\tau) [k_s^+ - k_s^+ \exp(-k_s^+/6)]$$

where

$$k_s^+ = k_s U_\tau / \nu.$$

This expression is valid for

$$4.535 < k_s^+ < 2000$$

where the lower limit corresponds to the upper bound for a hydraulically smooth surface. Typical values for equivalent sand roughness,  $k_s$ , are given in Table 1, which has been taken from Reference 4.

Table 1: Equivalent Sand Roughness for Several Types of Surfaces

Type of surface	$k_s, \text{cm}$
Aerodynamically smooth surface	0
Polished metal or wood	$0.05-0.2 \times 10^{-3}$
Natural sheet metal	$0.4 \times 10^{-3}$
Smooth matte paint, carefully applied	$0.6 \times 10^{-3}$
Standard camouflage paint, average application	$1 \times 10^{-3}$
Camouflage paint, mass-production spray	$3 \times 10^{-3}$
Dip-galvanized metal surface	$15 \times 10^{-3}$
Natural surface of cast iron	$25 \times 10^{-3}$

The metallic walls, such as Columbium, of liquid rocket engines fall into the range of  $k_s$  given in the above table. For OTV engine wall boundary layers the  $k_s^+$  parameter should be valid, i.e.,  $<2000$ .

In addition to modifying the eddy viscosity model as described above, it is necessary to discuss the initial boundary layer profile, and the wall boundary conditions. With respect to the former, Cebeci<sup>17</sup> used a modified version of Cole's velocity profile. This method is somewhat complicated and is perhaps unnecessary. A transition from a smooth wall profile by the gradual introduction of roughness should allow the necessary profiles to be generated automatically. With respect to the wall boundary condition, Cebeci uses a displaced wall boundary condition<sup>17</sup>. However, this is not necessary and no modifications to the wall boundary conditions were made.

## Section 2.2 Implementation

The recommendations of Section 2.1 were incorporated into the TDK code<sup>1</sup>. In addition, it was discovered that the standard JANNAF method of computing the boundary layer loss was inadequate for thick boundary layers.

The following lists the major changes to the TDK code. The section numbers refer to the sections in AFAL TR-87-031, Ref 19 which is the report which details the TDK version produced under Phase 1.

- 1) The boundary layer module, BLM, has been modified to include the effects of longitudinal curvature on both the mean flow and turbulent shear stress in the boundary layer. The thrust loss expression has been completely re-derived and three options for computing the thrust loss are included in the code.
- 2) Section 2.6, the BLM analysis section, has been rewritten to include the above modifications and to expand and clarify the numerical procedure.
- 3) Section 4, the program structure documentation has been redone to reflect the code changes.
- 4) Section 5.6, the BLM Subroutine descriptions, has been extended to include the new modifications. Existing documentation has been expanded so that the documentation is more useful.
- 5) Section 6.8, the BLM Input description, has been revised to reflect the changes in the code.
- 6) Section 7, the sample cases, has been redone to reflect the output for the current version of the code.

The TDK Computer Program is designed for engineering use. The FORTRAN IV programming language has been used in an attempt to make the computer program as machine independent as possible. The complete engineering and programming description of the TDK

Computer Program is contained in Ref. 19.

Section 2 of Ref. 19 contains a description of the methods of analysis used in the computer program.

Section 3 contains a description of the numerical methods used to integrate the fluid dynamic and chemical relaxation equations in the computer program.

Section 4 contains a description of the program structure.

Section 5 contains a detailed engineering and programming description of the program subroutines.

### Section 2.3 Phase I. Results and Conclusions

Perhaps the most important result from the Phase I work was the discovery that the standard JANNAF performance methodology was inadequate for thick boundary layers.

The conventional JANNAF method<sup>20,21</sup> for evaluation of the viscous thrust loss in rocket engine nozzle employs both the boundary layer momentum and displacement thickness. This method can be arrived at by two different approaches as shown by Alber<sup>22</sup>. The basis for the approach is to compare the thrust of an inviscid nozzle to a viscous nozzle with the same mass flow rate. In the equation given below, the first term represents the pressure forces acting on an inviscid nozzle and the second and third terms represent the total stress forces acting on the viscous nozzle.

$$\Delta T = \int_0^s (p_c^* - p_\infty) 2\pi r_p \frac{dr_p}{dx} dx - \int_0^s (p_w - p_\infty) 2\pi (r_p + \bar{\delta}^* \cos \phi) \frac{d(r_p + \bar{\delta}^* \cos \phi)}{dx} dx \quad (1)$$

$$+ \int_0^s \tau_w 2\pi (r_p + \bar{\delta}^* \cos \phi) \cos \phi dx$$

where  $r_p$  is the distance from the axis to the potential wall and  $p_c^*$  is the pressure at  $r_p$ , as is shown in Figure 3.

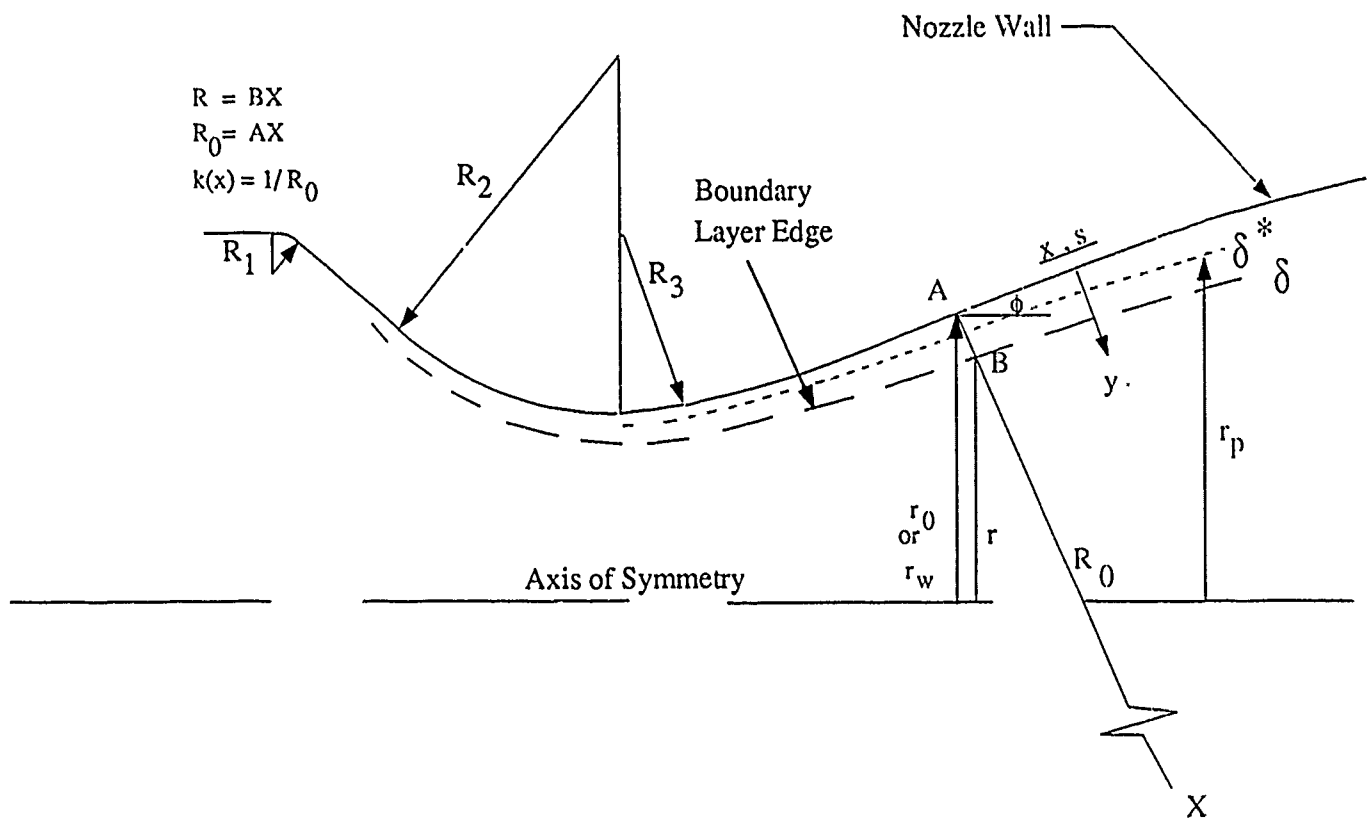


Figure 3. Nozzle Wall Schematic

When the boundary layer characteristics lengths,  $\delta$ ,  $\theta$ , and  $\delta^*$ , are assumed to be small compared to the characteristic nozzle lengths,  $r$  and  $R_c$ , then equation (1) reduces to the standard JANNAF relation<sup>21</sup>

$$\Delta T = 2\pi \cos\phi \left[ \rho_e u_e^2 r_0 \theta - r_0 \delta^* (p_e - p_\infty) \right] \quad (2)$$

If the boundary layer thickness assumption that  $\delta/R_c \ll 1$  is relaxed, then the modified JANNAF relation can be derived<sup>19</sup>, i.e.,

$$\frac{\Delta T}{2\pi} = \rho_e u_e^2 r_0 \bar{\theta} \cos\phi - r_0 \bar{\delta}^* (p_e - p_\infty) \cos\phi \quad (3)$$

using the alternate forms of the momentum and displacement thicknesses for axisymmetric flows shown below

$$\text{(momentum thickness)} \quad \bar{\theta} = \int_0^\delta \frac{r}{r_0} \frac{\rho u}{\rho_e u_e} \left[ 1 - \frac{u}{u_e} \right] dy \quad (4a)$$

$$\text{(displacement thickness)} \quad \bar{\delta}^* = \int_0^\delta \frac{r}{r_0} \left[ 1 - \frac{\rho u}{\rho_e u_e} \right] dy \quad (4b)$$

Table 2 (from Reference 19) shows that the differences in boundary layer loss as computed from Equation 1, 2, and 3 (columns E, A, and B respectively) are significant for nozzles with thick boundary layers.

Table 2: Boundary Layer Thrust Deficit for Variety of Engines in the Absence and Presence of the Longitudinal Curvature. Cold Wall Case

NOZZLE	THRUST DEFICIT, lbf. sec./lbm									
	WITHOUT LONGITUDINAL CURVATURE					WITH LONGITUDINAL CURVATURE				
	EQ. A	EQ. B	EQ. C	EQ. D	EQ. E	EQ. A	EQ. B	EQ. C	EQ. D	EQ. E
SSME	6.8843	6.7730	6.7650	6.2088	6.2233	6.3720	6.3184	6.4758	6.0387	6.5036
ASE	14.1985	13.6977	13.4572	12.3531	11.9394	14.2351	13.7440	13.5000	12.3782	11.7659
RL-10	11.6549	11.0871	10.8094	10.4630	10.4930	11.7732	11.0714	10.8591	10.4517	10.4984
XDELTA	1.8459	1.8160	1.7802	1.7220	1.8132	1.8459	1.8160	1.7870	1.7215	1.8211
BC4515	0.8688	0.8534	0.8481	0.8142	0.8373	0.8688	0.8534	0.8221	0.8141	0.8378
BC1010	1.8578	1.7941	1.7866	1.8000	1.8790	1.8582	1.7942	1.8121	1.8001	1.8788
IUS	1.9864	1.9523	1.9223	1.8381	2.0943	1.9862	1.9521	1.8524	1.8380	2.0328
XLR-134	27.3282	25.8350	25.3452	24.8578	23.2534	27.3525	25.6539	25.2531	24.8322	23.1904

$$\text{Eq. A.} \quad \Delta T = 2\pi \cos\phi [\rho_e u_e^2 r_o \bar{\theta} - r_o \bar{\delta}^*(p_e - p_\infty)]$$

$$\text{Eq. B.} \quad \Delta T = 2\pi [\rho_e u_e^2 r_o \bar{\theta} \cos\phi - r_o \bar{\delta}^*(p_e - p_\infty) \cos\phi]$$

$$\text{Eq. C.} \quad \Delta T = 2\pi [\rho_e u_e^2 r_p \bar{\theta} \cos\phi - r_p \bar{\delta}^*(p_e - p_\infty) \cos\phi]$$

$$\begin{aligned} \text{Eq. D.} \quad \Delta T = & 2\pi [\rho_e u_e^2 r_p \bar{\theta} \cos\phi - r_p \bar{\delta}^*(p_e - p_\infty) \cos\phi \\ & - \int_0^s \rho_e u_e^2 r_o \bar{\theta} \cos\phi \frac{\partial}{\partial x} \left( \frac{r_p}{r_o} \right) dx] \end{aligned}$$

$$\begin{aligned} \text{Eq. E.} \quad \Delta T = & \int_0^s (p_e^* - p_\infty) 2\pi r_p \frac{dr_p}{dx} - \int_0^s (p_w - p_\infty) 2\pi \frac{\partial}{\partial x} (r \bar{\delta}^* \cos\phi) dx \\ & + \int_0^s \tau_w 2\pi (r_p + \bar{\delta}^* \cos\phi) \cos\phi dx \end{aligned}$$

in all the above equations  $\varepsilon(x) = 0$



As can be seen from the above table, the method by which the boundary layer loss is computed is more important than the effect of longitudinal curvatures. Thus, this effect can be ignored for nozzles of current interest.

Appendix A contains 3 published papers which describe different facets of the work performed under Phase I.

### 3.0 Phase 2 Work Effort - Thick Boundary Layer Assessment

The purpose of the Phase 2 Work Effort was to establish, a) when the thin shear layer (TSL) or boundary layer approximations would break down, b) the magnitude of the breakdown in terms of performance, and c) to provide guidance to the new model development done in the Phase III work effort.

In order to determine when the TSL approximation starts to break down, a comparison was made between a traditional Euler Solver/Boundary Layer Code (TDK/BLM)<sup>23</sup>, a full Navier-Stokes solver (VNAP2)<sup>24</sup>, and a parabolized Navier Stokes solver (AXI2DS)<sup>25</sup>. The set of engines examined by these codes is given in Table 3. Also shown in this table is the relative boundary layer thickness for each of the nozzles.

Table 3: Boundary Layer Thickness at the Exit Plane for  
Four Nozzles. Cooled Wall  $T_w = 1000^\circ R$ .

Nozzle	Area Ratio	Transverse Radius at the Exit Plane r exit, inches	Boundary Layer Thickness $\delta_{.995}$ inches	$\delta_{.995}/r$
SSME	77.5:1	45.12	1.80	4%
RL-10	204:1	36.80	4.40	12%
ASE	400:1	25.10	3.25	13%
XLR-134	767:1	10.97	2.08	19%
Hughes 300:1	300:1	1.61	0.45	28%

The results from this comparison are reported in AL-TR-90-041, the Phase II final report<sup>26</sup>, and in Ref. 27, (which also appears in Appendix B). These results were far from conclusive. Perhaps the greatest problem was the disparity in accuracy between the codes at the resolutions we could afford to use them. Since the codes were the best we could obtain after a very significant amount of effort, we concluded that both the NS and PNS solver were not up to the tasks presented them.

However, general trends were observed. These trends were

- 1) When the boundary layer thickness became larger than 10% of the nozzle, the departure between the NS, PNS solutions and the Euler/BL solutions accelerates.
- 2) When compared to data, the Euler/BL solutions are remarkably accurate even for very thick boundary layers.
- 3) In terms of non-performance related parameters, boundary layers thicker than  $\delta/r > .1 \sim .15$  are suspect.
- 4) The subsonic portion of the boundary layer is infinitesimal ( $\delta_{\text{subsonic}} < \delta/1000$ ) in the supersonic portion of large propulsive nozzles.

With respect to objective c), the conclusions reached were that a PNS solver was desired for the Phase III work. The reasons for this decision were

- 1) That a PNS solver was, in terms of computer resources, the only economically viable way that both the viscous layer and invicid core flow could be accurately resolved.
- 2) That coupling a PNS solver to a method of characteristics solution was not desirable due to the differences in numerical accuracy between these two schemes. This rejected approach was what had been originally proposed.

As previously mentioned, Ref. 27, the technical paper reporting this work is in Appendix B.

The purpose of the Phase 3 effort was to develop a new computer model which would extend the state-of-the-art in performance prediction for high area ratio liquid propellant rocket engine nozzles. To this end, a computer code called VIPER (Viscous Interaction Performance Evaluation Routine) was developed. This work is completely documented in AL-TR-90-042. Two technical papers describing this work are given in Appendix C.

Following the recommendations of the Phase 2 Work. The VIPER was based on the Parabolized Navier Stokes equations. The PNS equations are a subset of the Navier-Stokes (NS) equations which are valid for supersonic flows<sup>28,29</sup>. The PNS equations neglect the streamwise diffusion term which, along with special treatment of the subsonic region of the boundary layer, removes the spatial ellipticity from the steady form of the equations and permits a solution using a streamwise marching computational technique. Although the PNS models were developed in the early 1960's<sup>30,31,32</sup>, they were not widely used until the 1970's and 1980's<sup>33-38</sup>.

In the early 1960's the first PNS models were developed by Ferri<sup>30</sup> and Morretti<sup>31</sup>, and Edelman<sup>32</sup>. They introduced their explicit-based numerical techniques to treat coupled wave-mixing-chemical kinetic processes.

The PNS equations are integrated throughout the viscous and inviscid regions of the flow. This procedure eliminates the need to specify the edge conditions in matching boundary layer and inviscid solutions, i.e., the conventional inviscid-viscous interaction. Popular algorithms for solving PNS equations are those by Briley and McDonald<sup>39</sup> and Beam and Warming<sup>40</sup>.

The VIPER code is a PNS solver for supersonic nozzle flow with finite rate chemistry. The Beam-Warming scheme has been employed to solve the governing equations. Richardson Extrapolation for automatic step size control in the marching direction has also been incorporated into the code. This code can treat both laminar and turbulent flows.

The VIPER code is fully documented in AL-TR-90-042, the Phase 3 Report, Ref. 41. The code was verified by running 7 test cases. The characteristics of these nozzles are given in the table below.

Table 4: Nozzle Characteristics for VIPER Verification Test Cases.

Engine Name	Chamber Pressure	Throat Radius(in)	Expansion Ratio	Throat Reynolds Number $Re_{r*}$
1 NASA/LeRC Hi-E	360	0.5	1025.	$1.73 \times 10^5$
2 XLR-134	510	0.396	767.9	$1.80 \times 10^5$
3 STS/RCS	150	1.021	28.46	$1.75 \times 10^5$
4 SSME	3285	5.1527	77.5	$1.18 \times 10^7$
5 RL 10	394.3	2.57	205.03	-
6 ASE	2287	1.254	400.7	$2.20 \times 10^6$
7 HAC-5 lbf	25	0.0935	296.6	$1.10 \times 10^4$

Cases 1,2,5, and 6 were selected because they represent high area ratio nozzles which are the design point of the VIPER. Cases 3 and 7 are small thrusters which have potentially large boundary layers. Lastly, case 4, which is the SSME, was chosen to test the high Reynold's number capability of the code. Results for these engines are tabulated in Table 5. The agreement to measured data (when available) is excellent when it is realized that the effect of combustion or energy release efficiency is not included in these calculations. For example, for the NASA/LeRE hi-expansion ratio engine, the measured value of C\* efficiency was 95.5% (reading 112 of Reference 42). Applying this efficiency to the VIPER prediction gives a value of 466.49 lbf-sec/lbm. Compared with the measured value of  $468.9^{42}$ , the difference is -0.51%.

Table 5: Engine Performance

Engine Name	VIPER $I_{sp}$ Prediction lbf - sec/lbm	TDK/BLM $I_{sp}$ Prediction lbf - sec/lbm	Measured $I_{sp}$ lbf - sec/lbm
NASA/LeRC Hi-E	488.47 (466.49)*	480.31 <sup>1</sup> (458.70)*	468.9 <sup>42</sup>
XLR-134	462.29	468.68 <sup>1</sup>	-
STS/RCS	311.49	-	-
SSME	455.15	457.7 <sup>1</sup>	452.6 <sup>1</sup>
RL 10	462.29	463.03 <sup>1</sup>	458.7 <sup>42</sup>
ASE	470.20	473.58 <sup>1</sup>	477.9 <sup>43</sup>
HAC-5 lbf	218.05	216.65	214.52 <sup>44</sup>

\* corrected for 95.5% measured  $c^*$  efficiency

Comparisons with the JANNAF standard performance prediction code, TDK<sup>1</sup> are also shown in Table 5. The comparison between the two codes are best for the high Reynolds number cases. The lack of a consistent trend between VIPER and TDK/BLM is attributed to the fact that neither code includes combustion efficiency correlations.

Besides the good agreement between VIPER and TDK/BLM-data, another good accuracy check is how well a code conserves mass, momentum, and energy. For finite difference codes such as VIPER, conservation of these quantities is a very good measure of the overall validity of the computational solution (it, of course, does not check the validity of the models used). Table 6 gives a summary of the conservation checks computed by the code. Mass and momentum are conserved very well in all cases. Energy conservation is a much more difficult quantity to achieve. Partly, this is because it requires good mass and momentum conservation, and partly because the reference base for energy is arbitrary. As a case in point, the energy flow  $\dot{m}(h+V^2/2)$  of the E1000 nozzle is only -0.011 BTU/sec across the start line because the chemical enthalpy (negative) balances out the kinetic energy. Hence a small change in total energy can result in a very large percentage difference in energy conservation.

Table 6. Conservation Checks

Nozzle	% Mass Flow Drift	% Momentum Flow Drift	% Energy Flow Drift
NASA/LeRC Hi-E	-1.28	-1.62	very high near zero base
XLR-134	0.02	1.01	-6.3
STS/RCS	- 0.014	0.108	2.9
SSME	0.0126	0.72	- 0.43
RL 10	- 0.085	0.57	-1.67
ASE	-1.18	- 0.31	-5.3
HAC-5 lbf	- 0.88	-1.34	0.76

As is typical of codes using the Beam-Warming difference technique, damping of oscillations caused by compression or shock waves is required. The VIPER code uses explicit 4th order damping to get rid of these high frequency oscillations. The damping term can be written as

$$-\frac{\epsilon_d}{8} [Q^{j+2} - 4 Q^{j+1} + 6 Q^j - 4 Q^{j-1} + Q^{j-2}]$$

where  $\epsilon_d$  is an input number to the code. A value of  $\epsilon_d = 50$  is recommended. To illustrate the effect the damping on the flowfield and computed  $I_{sp}$ , a study was conducted for all 7 of the validation engines. Values of  $\epsilon_d$  of 0 and 50 were used for the comparison. The effect of damping was dramatic on the flowfield in terms of shock location, (see Figure 4), however, the difference in  $I_{sp}$  was less than .07% for all cases, which indicates that the damping has very little effect on the integrated values of wall pressure and shear stress. These results are shown in Table 7. Figure 5 shows a comparison of computed wall shear stress for the SSME nozzle with and without damping. Again the effects are dramatic. However, the difference in integrated wall shear stress was only 17 lbf out of a total of 7824 lbf.

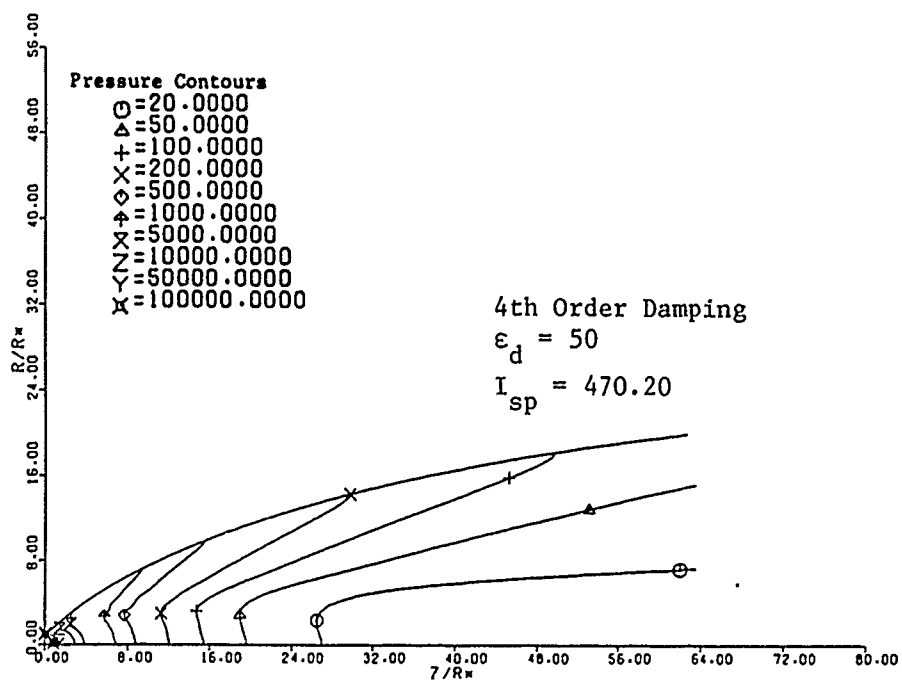
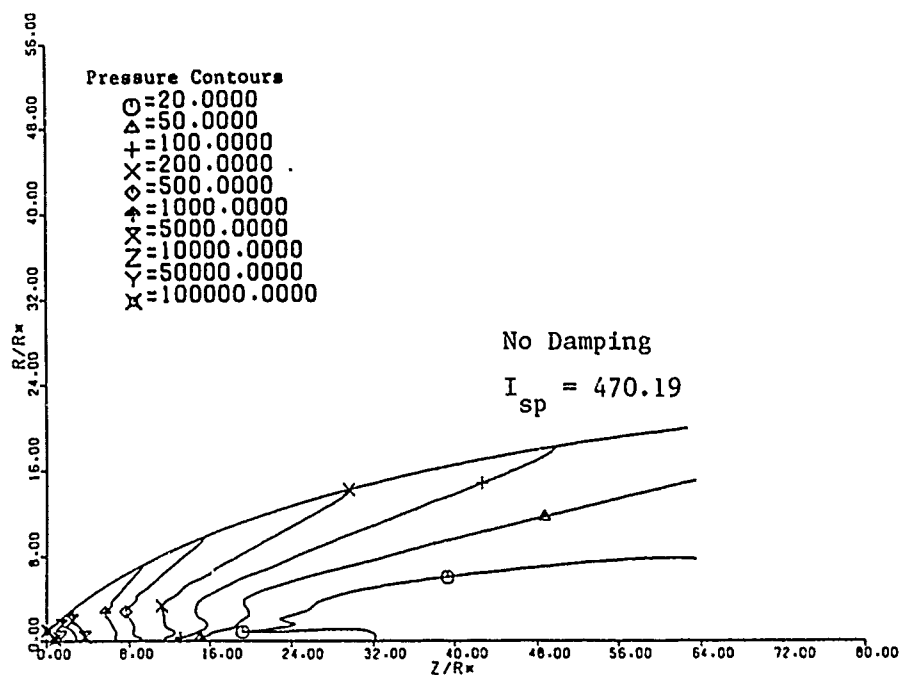


Figure 4. Damping Study, ASE Engine



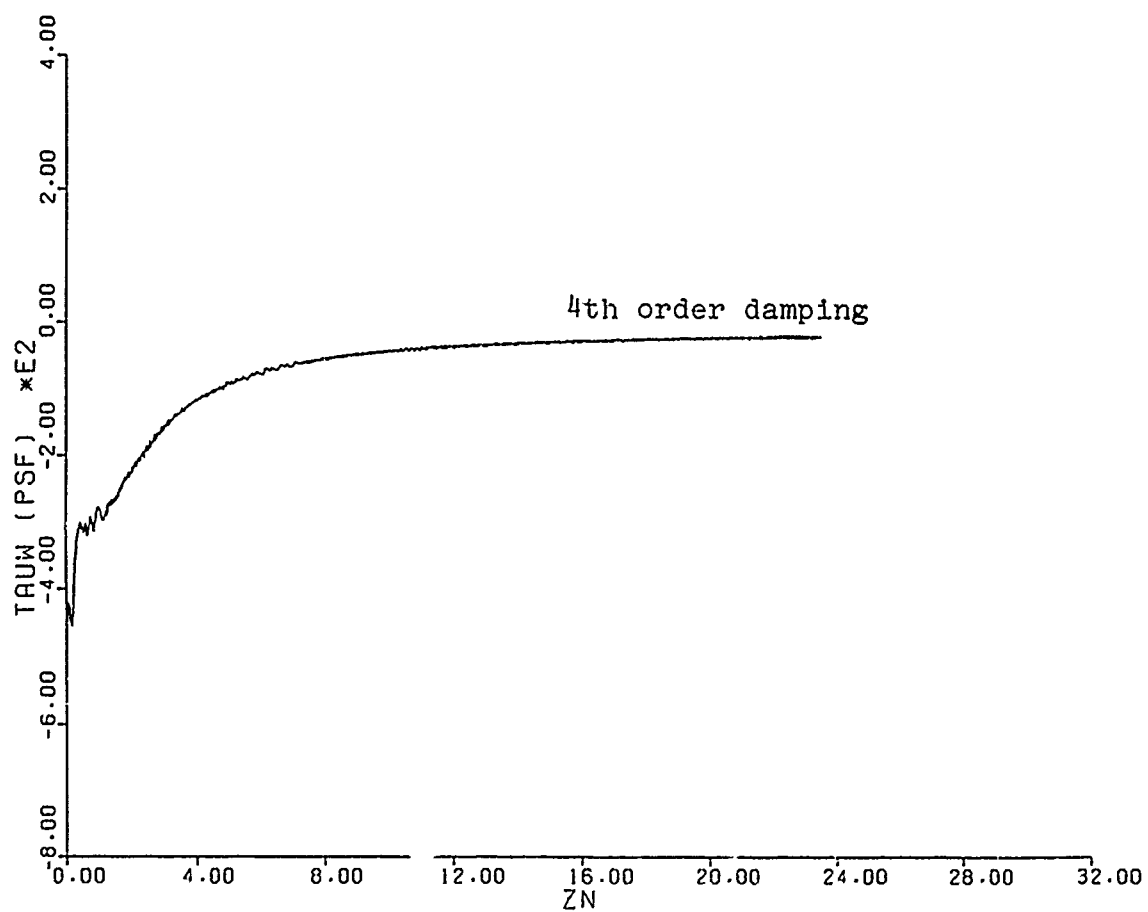
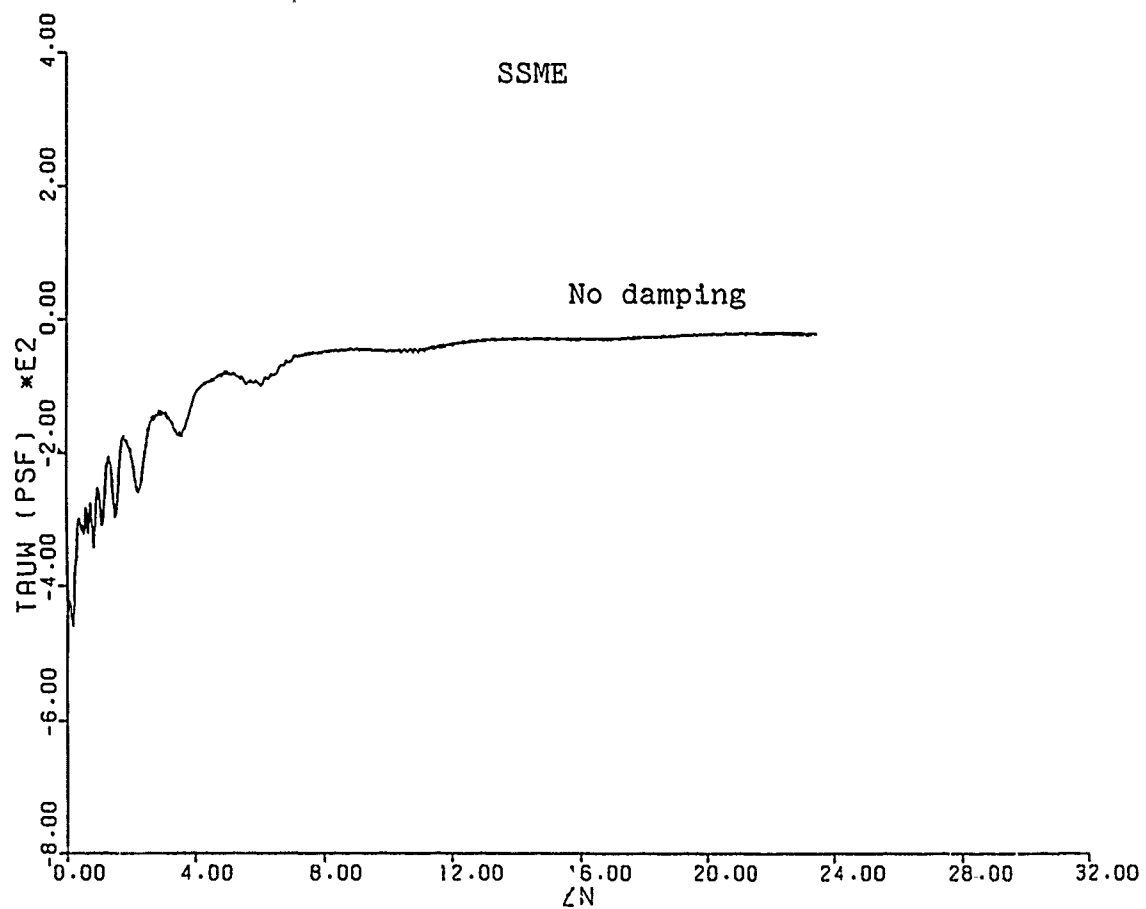


Figure 5. Effect of Damping on Wall Shear Stress

Table 7 Effect of 4th Order Damping

	$I_{sp}$ (lbf - sec/lbm)			
	4th Order Damping	No 4th Order Damping	$\Delta I_{sp}$	% Difference
NASA/Lewis Hi-E	488.47	488.39	0.09	0.018
XLR-134	462.29	462.00	0.29	0.063
STS/RCS	311.49	311.44	0.05	0.016
SSME	455.15	455.18	0.03	0.007
RL 10	462.22	461.99	0.21	0.045
ASE	470.20	470.19	0.01	0.002
HAC-5 lbf	218.05	218.04	0.01	0.005
AIM	304.57	304.64	0.07	0.023

As with any code completing its first state of development, there are deficiencies and unexplained characteristics. The major problem areas are associated with the grid generation, step size control, the  $k-\epsilon$  turbulence model, and the sublayer model.

The deficiency with the mesh generation and step size affects the robustness of the code. Values of the stretching coefficient,  $\alpha$ , must be selected a priori so that there is sufficient mesh to resolve the boundary layer for the entire flow field. The selection of the marching step size is also critical. It can neither be too big nor too small. The step size can be dynamically controlled in the current version of VIPER. However, there is a distinct coupling between the  $\eta$  mesh spacing and the  $\Delta\xi$  step size. The recommendation here is to dynamically modify the mesh spacing so as to automatically resolve the wall shear layer. The step size control logic will then have to be revised so as to properly interact with the dynamic mesh spacing.

In liquid rocket engines, the majority of the vorticity generated in the flow comes from the wall shear layer. Other sources of vorticity are the finite rate chemistry, O/F striations, and

other phenomena which result in total enthalpy variation. Because the wall generates the majority of the vorticity in the flow, the Cebeci-Smith eddy viscosity model used in VIPER is quite adequate. However, there are situations when it would be desirable to use a  $k-\epsilon$  turbulence model. The current  $k-\epsilon$  model in VIPER is not robust and has an inadequate wall treatment. Hence, we recommend that the current model be modified to generate better initial profiles and that the wall sublayer treatment be modified to incorporate the latest models.

The VIPER code currently uses the Vigneron sublayer model to suppress "departure solutions" in the subsonic portion of the boundary layer. As part of that model, there is a safety factor,  $\sigma_s$ , which controls where the sublayer model is turned off. Numerical experiments have shown that the results are quite sensitive to this parameter in contradiction to most of the literature. We recommend that the sublayer model be further investigated and either replaced or modified to control the sensitivity.

Further improvements to VIPER should include the addition of a discrete particulate phase. Such an addition would allow VIPER to analyze both solid and liquid propellant systems. The following is a list of potential particulate micro-models which could be included in the code.

<u>Micro Model</u>	Importance for	
	<u>Liquid Propellant</u>	<u>Solid Propellant</u>
Vaporizing Droplets	✓	
Phase Change		✓
Droplet Super Cooling		✓
Breakup	✓	✓
Aglomeration	✓	✓
Very Small Particles ( $d_p < 1\mu$ )		✓
Condensation/Mass Transfer between Phases	✓	✓

We would recommend that all of the above, except mass transfer between phases, be incorporated into VIPER. The basic particulate model would be a fully coupled model between the gas and discrete phase.

Once particle capability has been added to the VIPER, we recommend that a simple combustion chamber/motor cavity model be added. Such a model would allow the user to run parameteric studies over a rational parameter space in order to assess the impact of each item of interest.

In conclusion, a computer program called VIPER has been developed which accurately predicts the flowfield in liquid propellant rocket engine nozzles. The VIPER code has been developed as a natural extension to the JANNAF standard nozzle performance code, TDK. By incorporating elements of the TDK code in VIPER, the user community knowledge base has been preserved. That is, users familiar with TDK can generate successful VIPER runs in a matter of a few hours.

The purpose of the Phase 4 effort was to devise an experimental test plan which would validate the models developed in the Phase 1 and 3 work efforts.

One of the major problems with predicting the boundary layer loss in rocket exhaust nozzles is that there are no direct measurements of the boundary layer parameters in real nozzle flows to use to refine the analytical models. This observation is especially true for the turbulence models used in boundary layer calculations. Current verification efforts are based on comparison to data in other environments, global heat transfer data for real engines, or backing out the boundary layer loss from thrust measurements by subtracting the other known losses in the system.

The other performance losses are currently evaluated by computer programs, such as TDK<sup>1</sup>, BLM<sup>1</sup>, BLIMPJ<sup>45</sup>, etc using the JANNAF thrust chamber evaluation procedures. These procedures are based upon a physical model that accounts for the processes occurring in the thrust chamber, losses associated with these processes and interactions among the processes<sup>20,21</sup>.

In the model, propellants enter the combustion chamber through the injector, are mixed, vaporized and combusted. Deviation from complete and homogeneous mixing vaporization or combustion to equilibrium are referred to as energy release losses or injector losses. Theoretically, these losses are modeled by the Coaxial Injection Combustion Model (CICM) and the Standard Distributed Energy Release Model (SDER) codes<sup>46</sup>. Experimentally, the energy release loss can be estimated from the characteristic exhaust velocity efficiency,  $\eta_{C*}$ .

The products of the chemical reactions are then expanded in the nozzle. The reactions continue during the expansion. Deviation from the local chemical equilibrium are referred to as the kinetic losses. There are no direct methods of measuring the kinetic losses.

The losses due to non-uniform expansion of the available momentum in the direction of thrust are referred to as two-dimensional or divergence losses. Theoretically, these losses are evaluated from the difference between the ODK (One-Dimensional Kinetics) and MOC (Method of Characteristics) modules of the TDK code.

Graphically, all of the above described losses are shown in Figure 6. The ideal performance is based on ODE calculations.

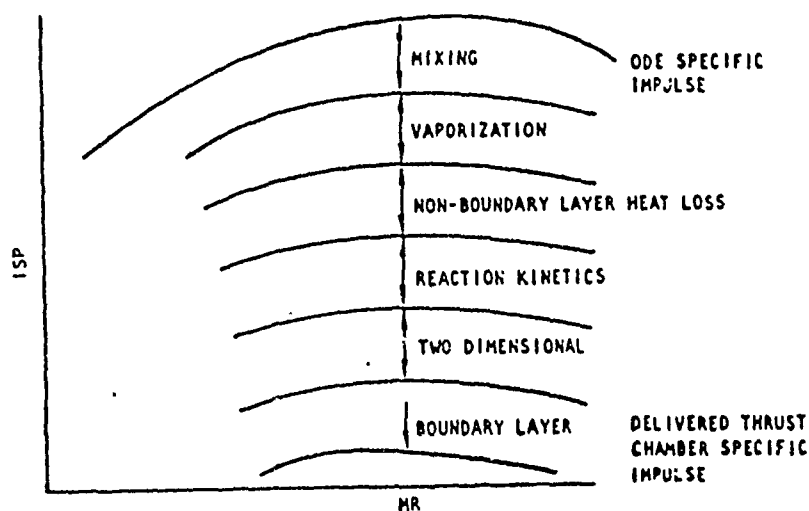


Figure 6. Illustration of thrust chamber losses from ideal performance

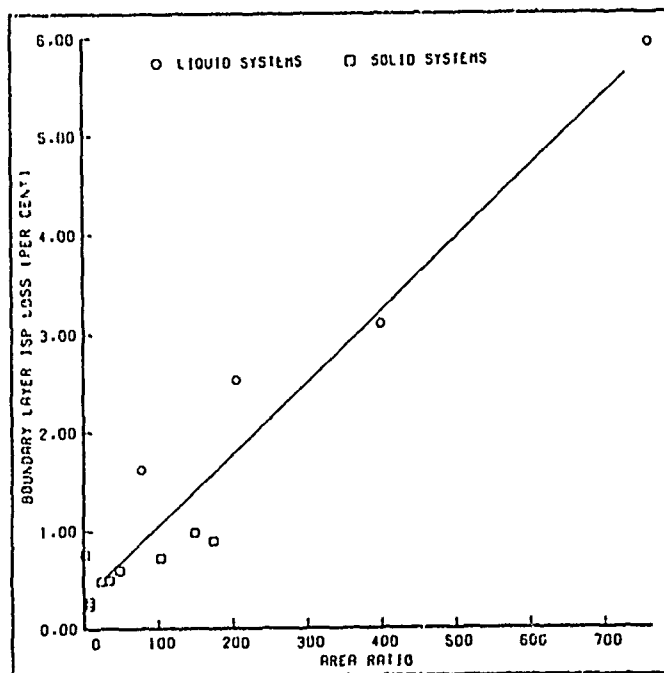


Figure 7. Boundary Layer Isp Losses.

Systematic measurements to verify the predicted magnitude of the aforementioned losses are sparse, and a high degree of uncertainty is associated with the available data. For both the kinetic and boundary layer losses, experimental validation of the predictive techniques for real engines are not available. For low area ratio nozzles, the boundary layer loss has been considered small enough that any errors associated with the predictions were acceptable. The magnitude of the boundary layer loss as a percent of total performance increases with area ratio. Figure 7 shows the boundary layer losses as calculated by the SPP and TDK codes for a variety of motors as a function of area ratio. The dependency of these results on the particular turbulence model used in the calculation are on the order of  $\pm 30\text{-}40\%$ <sup>47</sup>. That is, a predicted 10 second loss could actually be only 7 seconds or could be as high as 13 seconds. Since a 1% change in Isp can result in approximately a 4% change in payload, the accurate knowledge of the boundary layer loss is very important. Hence, the boundary layer calculations must be validated directly using experimental data.

In order to validate or extend analytical methods, the planned experimental effort must include techniques to measure boundary layer parameters that will produce high quality data. Quality data on nozzle wall boundary layers is very limited at present. Perhaps, the best work in this area is that of Back, et al, at JPL<sup>48-51</sup>, which was for cold flow.

As part of the effort to prepare an experimental validation test plan, numerous testing facilities were contacted and visited. Available experimental methods and facility and test requirements were reviewed, and recommendations were made to the Astronautics Laboratory. Results of the study were documented in the Phase 4 final report together with a test plan intended to validate the analytical methods developed during the boundary layer study.

Certain ground rules were used in preparing this test plan. The first ground rule was that we wanted a program which would measure the desired data, we did not want to embark upon a research program to develop improved boundary layer diagnostic techniques. Secondly, we wanted the test environment to simulate as close as feasible the conditions in a real propulsive nozzle. The minimum requirements for this condition are shown in Table 8, below. Last, and most important, we wanted accurate data.

Table 8. Minimum Test Environment Criteria

- o The flow in the boundary layer must be turbulent from before the throat.
- o The boundary layer should encompass between 10% to 40% of the flow at the exit plane.
- o The heat transfer to the wall should be high enough to simulate conditions in a real rocket nozzle.
- c The expansion process should maintain, as realistically as possible, the conditions in a real rocket nozzle. For example, axisymmetric instead of 2D nozzles, ratio of specific heats  $\leq 1.4$ .

Some of the ground rules were found to be mutually exclusive. For example, accurate data taking precluded using a real engine as a test bed. The environment in real engines is too severe for many diagnostic techniques. We also found that off the shelf techniques were not sufficiently accurate for all of the data measurements desired.

#### Parameters to be Measured

The primary interest is computing the boundary layer parameters in propulsive nozzles is in determining the viscous thrust loss and wall heat transfer rate. The most fundamental property in the thrust loss is the wall shear stress. The heat transfer to the wall is determined by the temperature (enthalpy for reacting flows) gradient at the wall. While both the shear stress and temperature gradient can be deduced from other quantities, a direct measurement of these items is definitely preferred. In the absence of direct measurements, diagnostics which require the least amount of assumptions are preferred.

Average velocity and temperature throughout the boundary layer and Reynolds stress terms,  $u'$ ,  $v'$ , are other parameters to be measured. Although the last two are less important, their correct evaluation yields valuable data for validation of turbulence models. Briefly the following measurements are to be made:



1. Local wall shear;
2. Local heat flux at the wall;
3. Average velocity and temperature in the boundary layer;  
and
4. Reynolds stress terms.

### Conclusions

After talking with various organizations, we concluded that two families of techniques are suitable for hypersonic flow velocity measurements: particle scattering and molecular scattering. Particle scattering techniques which include real fringe laser Doppler velocimetry, laser transit anemometry, and Doppler spectrometry, are well developed and velocity measurements in supersonic and hypersonic flow regimes have been demonstrated. However, particle scattering techniques require seeding the flow, which introduces ambiguity due to particle lag in accelerated or decelerated flows. The question of particle lag has been addressed and it is concluded that the measurement uncertainties are small when the particles used are less than  $0.3\text{ }\mu\text{m}$  in shock-free expansion flows.

The uncertainty of the fluctuating components of the velocity within the boundary layer will depend on the density of the flow and the frequency response of the particles.

Molecular techniques which encompass laser induced fluorescence (LIF), Inverse Raman Scattering (IRS) and Coherent Anti-Stokes Raman Scattering CARS, are being developed. These techniques have the potential of yielding more accurate results than particle-based techniques. However, several practical aspects hinder their application to hypersonic flow measurements. LIF of alkalis, which is more accurate than LIF of  $\text{O}_2$ , requires seeding the wind tunnel with highly corrosive materials such as sodium. Seed molecules condense under the low pressure and temperature conditions characteristic of hypersonic wind tunnels. LIF of  $\text{O}_2$  is still under investigation and preliminary analysis shows that the velocity error is about 500 m/sec. IRS and CARS measure the velocity from the spectrum of the coherent Raman scattered signal, and therefore, pressure broadening due to a shock wave can result in large errors. Velocity measurement using IRS is on-axis, and hence the spatial resolution is poor. IRS and CARS, however, have the advantage of yielding the

temperature and pressure simultaneously with the velocity, giving a unified approach to flow field measurement.

Table 9 is a summary of velocity measurement techniques. The table shows the demonstrated velocity range, accuracy, SNR (signal to noise ratio) and other relevant parameters of techniques.

### Recommendation

The primary objective of developing an experimental plan for boundary layer measurements is to obtain accurate and high quality data to compare against the present and future analytical models. During the course of our investigations, no single or set of diagnostic techniques and experimental facilities were found to be capable of achieving this objective. As a result, it was necessary to relax some of the ground rules which we had originally laid out in order to meet the primary goal of obtaining accurate data. As mentioned in the introduction, we concluded that hot engine firings were not compatible with accurate mapping of the boundary layer. This conclusion was based on considerations of available experimental techniques, test times, facility requirements, and cost. We also discovered that there were no diagnostic techniques which were "off the shelf" ready for boundary layer measurements of the required accuracy in simulated rocket nozzles. In addition, facility capabilities for different organizations varied tremendously. Calspan has excellent short duration test facilities, while AEDC has good large scale longer duration capability. However, the selected diagnostic techniques must be mated with the correct facility to insure adequate data acquisition. Because of the developmental nature of the diagnostic techniques and the mating of these techniques with the facilities, the following recommendations are conditional rather than absolute. First, we will cover the recommended diagnostic methods and then discuss recommendations for test facilities.

### Diagnostic Method Recommendations for Velocity Profile Measurements

LDV must be considered the primary candidate for taking velocity measurements in the boundary layer. This conclusion is based on the fact that this method is well developed in comparison to other laser techniques. Alternates and/or backup methods should include LIF and CARS. We strongly recommend that optical techniques should be the cornerstone of these measurements.

Table 9: Summary of Velocity Techniques, Reference 25

TECHNIQUE	PARAMETERS MEASURED	TURBULENCE LEVEL	SNR LIMIT	ACCURACY	MEASURED VELOCITY RANGE	FREQUENCY RESPONSE, HZ	SPACIAL RESOLUTION	COST	STATUS	CONCERNS IN HYPERSONIC FLOWS
Real Fringe (LDV)	$\bar{u}_i, \bar{u}_j$ $u'_i, u'_j, \overline{u'_i u'_j}$	30% & higher	-10 dB 0 to 10 dB	0.1 to 10% 1% and up	1000 m/sec	$10^4$ $10^2$	100 $\mu$ m	Medium	Well Developed	Seeding, Flow Density
Laser Transit Anemometry	$\bar{u}_i, \bar{u}_j$ $u'_i, u'_j, \overline{u'_i u'_j}$	15%	10 dB 10 dB	0.1 to 10% 3 to 15%	1200 m/sec	Steady State	100 $\mu$ m	Medium	Well Developed	Seeding, Flow Density
Doppler Spectrometry	$\bar{u}_i, u'_i$	15%	20 dB	2%	1700 m/sec	$10^6$	100 $\mu$ m	Medium	Used in Shock Tubes	Seeding, Flow Density
Laser Induced Fluorescence	$\bar{u}_i, u'_i$	Experimental	20 dB	1 to 10% Depending on the particles	500 m/sec using Iodine Mach 11 using Sodium(30)	$10^5$	100 $\mu$ m	High	Demonstrated under Laboratory Conditions	Seeding, Flow Density SNR Agent Species, SNR
Inverse Raman	$\bar{u}_i, u'_i$	Have not been demonstrated	20 dB	5 to 10%	Mach 4.6(33)	Steady State	Few cm	High	Demonstrated in Wind Tunnels	SNR, Complexity
CAIRS	$\bar{u}_i, u'_i$	Experimental	20 dB	not established	1000 m/sec(31)	Steady State	Few cm	High	Demonstrated under Laboratory Conditions	SNR, Complexity

We view both LIF and CARS as potentially superior methods of velocity measurement. The trade off between LDV and LIF/CARS is the development time and difficulties associated with particulate seeding for LDV versus moving LIF/CARS from the lab into a test environment. Should the latter be accomplished, then LIF/CARS would be the recommended technique.

#### Static Pressure Measurements

Pressure transducers on the wall are the recommended diagnostic technique for measuring static pressure at the wall. If the selected test conditions are benign enough, pitot measurements can also be used as a backup and to verify calibration of both the wall static pressure and velocity profile.

#### Temperature Profiles

Laser based non-intrusive techniques are recommended. LIF seems to have a slight edge on CARS based techniques, but both methods should perform well theoretically. The final choice should be decided by the selected contractor based on cost and risk factors. Both LIF and CARS are also capable of determining the density profiles in the flow. Information about the chemical composition would thus supply enough information to compute the pressure profile. The redundancy in pressure data will supply a useful accuracy check on the measurements. Total temperature probes are also readily available (see Appendix A). They should be used as a calibration backup if pitot measurements are also taken.

#### Wall Heat Transfer Measurement

There are any number of adequate methods to measure the wall heat transfer rate. However, most of these methods depend on the temperature range of the flow (total and static) and of the wall. The final selection must be based on the test environment selected. However, we do not recommend that the heat transfer rate be deduced solely from backwall temperature measurements. Such methods require operation to steady state to supply the desired accuracy.

### Wall Shear Stress

Direct measurements of the wall shear stress are definitely preferred. If the test environment permits, some sort of the floating element method should be used (see Appendix C and also the description of the Kistler Skin Friction Gauge). Extrapolation of the velocity profile to the wall can also be used if floating elements are not practical. Under no circumstances should the Reynolds Analogy be used as the primary method of determining skin friction. The use of the law of the wall also presupposes the form of the results and hence its use is discouraged.

### Test Facilities

The ideal facilities for these tests would be space based so that practical considerations such as pumping requirements, total pressures, and total temperatures would not be of concern. However, since we are lacking permanent space stations or lunar facilities, we must make due with earth based testing. It is always preferred that the test environment closely simulate the environment to which the data is to be applied. However, in this case, we recommend against real engine firings. Too many of the recommended diagnostic techniques are not well enough established to allow for their extension to such a hostile environment. In fact, some of the test methods suggested would best be done with windows cut into the nozzle wall. Many of the problems associated with facility requirements disappear if the diagnostic techniques can be made to work for short duration test. Calspan has an excellent short duration test capability which would allow good simulation of high area ratio nozzles. However, it is not clear if either LIF or CARS methods can be made to work with test durations in the 50 millisecond range. The Accurex arc tunnel suggested by one of the experimental test plan contributors would only be acceptable if the total enthalpy gradient across the nozzle that is produced by the arc could be eliminated.

In order to simulate a real nozzle as closely as possible, we make the following recommendations.

- 1) The test nozzle should be axisymmetric and have at least an area ratio of 300:1.
- 2) The flow should be fully turbulent before the throat plane.

- 3) The flow should be as hot as is compatible with the diagnostic techniques. Flows in the range of 1500°R are recommended. These types of temperatures will allow for adequate heat transfer rates, density variations, and avoid condensation problems.
- 4) The gas supply system should supply nearly uniform property flow.

In order to assure that the experiments achieve their goal of supplying data to validate analytical models, we also recommend that an organization such as Software and Engineering Associates, Inc. be assigned to monitor the experimental work effort.

## NOMENCLATURE

$c$	speed of light
$d_p$	droplet radius
$g(v)$	line shape function
$h$	enthalpy
$I$	intensity
$M$	Mach number
$n$	normal direction
$P$	pressure
$Pr$	Prandtl number
$r$	radius
$r^*$	throat radius
$Re$	Reynold's number
$s$	entropy
$T$	temperature
$u$	velocity
$U$	velocity
$v$	velocity
$V$	velocity (total)
$y$	distance

### Greek

$\theta$	boundary layer momentum thickness
$\xi$	vorticity
$\rho$	density
$\delta$	boundary layer thickness
$\Delta$	difference
$\tau$	shear stress, characteristic time
$\mu$	coefficient of viscosity
$\nu$	frequency

## NOMENCLATURE (Continued)

### Abbreviations

AL	Astronautics Laboratory
ASE	Rocketdyne Advance Space Engine, area ratio 400:1
BC4515 } BC1010 }	Experimental Nozzles by JPL, conc shaped
BLM	Boundary Layer Module of TDK computer code
CARS	Coherent Anti-Stokes Raman Spectroscopy
CRC	Coherent Raman Spectroscopy
IRS	Inverse Raman Spectroscopy
IUS	Inertial Upper Stage, Space motor, OTV
JANNAF	Joint Army Navy NASA Air Force
LDA	Laser Doppler Anemometry
LDS	Laser Doppler Spectrometry
LDV	Laser Doppler Velocimetry
LIF	Laser Induced Fluorescence
LOX/GH <sub>2</sub>	Liquid Oxygen and Gaseous Hydrogen
LTA	Laser Transit Anemometry
RL-10	Pratt & Whitney Space Engine, area ratio 205:1
SEA	Software and Engineering Associates, Inc.
SRGS	Simulated Raman Spectroscopy
SSME	Space Shuttle Main Engine, area ratio 76:1
TDK	Two Dimensional Kinetic Computer Code
XDELTA	Extended Delta (Solid Propellant Space motor)
XLR134	OTV Engine, Space Storable, area ratio 767:1



## REFERENCES

1. Nickerson, G. R., Coats, D. E., Dang, A. L., Dunn, S. S., and Kehtarnavaz, H., "Two-Dimensional Kinetics Nozzle Performance Computer Program, Volumes I, II, and III, Programming Manual", Software and Engineering Associates, Inc., prepared for GMSFC, contract NAS8-36863, 31 March 1989.
2. Cebeci, T., "Boundary Layer Analysis Module", prepared for Software and Engineering Associates, Inc., January 1982.
3. Nickerson, G. R., Coats, D. E., Hermesen, R. W., and Lamberty, J. T., "A Computer Program for the Prediction of Solid Propellant Rocket Motor Performance (SPP), Vol. 1, AFRPL TR-83-036, Software and Engineering Associates, Inc., Sept. 1984.
4. Cebeci, T., and Bradshaw, P., *Momentum Transfer in Boundary Layers*, McGraw-Hill, New York, 1977.
5. Schlichting, H., *Boundary Layer Theory*, 7th ed., McGraw-Hill, New York, 1979.
6. Landau, L. D., and Lifshitz, E. M., *Fluid Mechanics*, Pergamon Press, London, 1959.
7. Van Dyke, M., *Perturbation Methods in Fluid Mechanics*, Academic Press, New York, 1964.
8. Minutes for the Second Workshop Conference, Improved Solid Performance Program, 7 September 1978, Essex House, Lancaster, CA., available from AFRPL.
9. Finley, P. J., "Static Pressure in Hypersonic Nozzle Boundary Layers", *AIAA J.*, Vol. 15, No. 6, pp. 878-881, June 1977.
10. Van Dyke, M., "Higher Approximations in Boundary-Layer Theory, Part 1. General Analysis", *J. Fluid Mech.*, Vol. 14, Part 1, pp. 161-177, 1962.
11. Schultz-Grunow, F., and Breuer, W., "Laminar Boundary Layers on Cambered Walls", in *Basic Developments in Fluid Mechanics*, Vol. 1, Academic Press, New York, 1965. p. 377.
12. Cebeci, T., Hirsch, R. S., and Whitelaw, J. H., "On the Calculation of Laminar and Turbulent Boundary Layers on Longitudinally Curved Surfaces", *AIAA J.*, Vol. 17, No. 4, pp. 434-436, April 1979.
13. Cebeci, T., and Smith, A.M.O., *Analysis of Turbulent Boundary Layers*, Academic Press, New York, 1974.
14. Bradshaw, P., "The Analogy between Streamline Curvature and Buoyancy in Turbulent Shear Flow", *J. Fluid Mech.*, Vol. 36, Part 1, pp. 177-191, 1969.

## REFERENCES (Continued)

15. Eghlima, A., and Kleinstrewe, C., "Numerical Analysis of Attached Turbulent Boundary Layers Along Strongly Curved Surfaces", *AIAA Journal*, Vol. 23, No. 2, February 1985, pp. 172-184.
16. Kuethe, A. M., and Schetzler, J. D., "*Foundations of Aerodynamics*", John Wiley & Sons, Inc., London, 2nd Ed., 1961.
17. Cebeci, T., and Chang, K. C., "Calculation of Incompressible Rough-Wall Boundary Layer Flows", *AIAA Journal* Vol. 6, No. 7, July 1968, p. 730.
18. Cebeci, T., "Private Communication", January 1984.
19. Kehtarnavaz, H., Coats, D. E., Nickerson, G. R., and Dang, A. L., "Two-Dimensional Kinetics (TDK) Nozzle Performance Program - Thick Boundary Layer Version", AFAL-TR-87-031, Feb. 1988.
20. Pieper, J. L., "ICRPG Liquid Propellant Thrust Chamber Performance Evaluation Manual", CPIA Publication No.178, prepared for the Performance Standardization Working Group, September 1968.
21. "JANNAF Rocket Engine Performance Prediction and Evaluation Manual", CPIA Publication No. 246, April 1975.
22. Alber, E. Irwin, "Comparison and Evaluation of Computer Program Results for Rocket Engine Performance Prediction, Chapter V., Boundary Layer Friction and Heat Transfer", prepared by Dynamic Science for Interagency Chemical Rocket Propulsion Group, Contract No. NAS 7-443 NS-82, 1968.
23. Kehtarnavaz, H., Coats, D. E., Nickerson, G. R., and Dang, A. L., "Two-Dimensional Kinetics (TDK) Nozzle Performance Computer Program-Thick Boundary Layer Version", Software and Engineering Associates, Inc., March 1987, prepared for the AFAL under Contract No. F04611-86-C-0055, AFAL-TR-87-031.
24. Cline, M. C., "'VNAP2" A Computer Program for Computation of Two-Dimensional, Time Dependent, Compressible Turbulent Flow", LASL Report LA-8872, August 1981.
25. Kronzon, Y. "An Euler and PNS Code for Internal Flow of a Perfect Supersonic Gas", AFAL personal communication.
26. Kehtarnavaz, H., and Coats, D. E., "Boundary Layer Study Thick Boundary Layer Assessment", AL-TR-90- , 1990
27. Kehtarnavaz, H., Coats, D. E., and Kronzon, Y., "Thick Boundary Layer Assessment for Nozzle Flow", AIAA Paper 88-3160, 24th Joint Propulsion Conference, Boston, MA., July 1988.

## REFERENCES (Continued)

28. Tannehill, J. C., Venkatapathy, E., and Rakich, J. V., "Numerical Solution of Supersonic Viscous Flow over Blunt Delta Wings", *AIAA Journal*, Vol. 20, 1982, pp. 203-210.
29. Kaul, V. K., and Chaussee, D. S., "AFWAL Parabolized Navier-Stokes Code: 1983 AFWAL/NASA Merged Baseline Versions", U.S. Air Force Wright Aeronautical Lab., AFWAL-TR-83-3118, 1983.
30. Ferri, A., "Review of Problems in Application of Supersonic Combustion", *Journal of the Royal Aeronautical Society*, Vol. 68, Sept. 1964, pp. 575-597.
31. Moretti, G., "Analysis of Two-Dimensional Problems of Supersonic Combustion Controlled by Mixing", *AIAA Journal*, Vol. 3, Feb. 1965, pp. 223-229.
32. Edelman, R., and Weilerstein, G., "A Solution of the Inviscid-Viscid Equations with Applications to Bounded and Unbounded Multicomponent Reacting Flows", AIAA Paper 69-83, Jan. 1969.
33. Ferri, A., "Mixing Controlled Supersonic Combustion", *Annual Review of Fluid Mechanics*, Vol. 5, Annual Reviews, Inc., Palo Alto, CA. 1973, pp. 301-338.
34. Buggeln, R. C., McDonald, H., and Levy, R., "Development of a Three-Dimensional Supersonic Inlet Flow Analysis", NASA Contractor Report 3218, Jan. 1980.
35. Chitsomborn, T., Kumax, A., and Tirvari, S. N., "Numerical Study of Finite-Rate Supersonic Combustion Using Parabolized Equations", AIAA Paper No. 87-0088, Jan. 1987.
36. Sinha, N., and Dash, S. M., "Parabolized Navier-Stokes Analysis of Ducted Turbulent Mixing Problems with Finite-Rate Chemistry", AIAA Paper No. 86-0004, Jan. 1986.
37. Dash, S. M., "An Analysis of Internal Supersonic Flows with Diffusion, Dissipation and Hydrogen-Air Combustion", NASA CR-111783, May 1970.
38. Dash, S. M., and DelGuidice, P. D., "Analysis of Supersonic Combustion Flowfields with Embedded Subsonic Regions", NASA CR-112223, Nov. 1972.
39. Briley, W. R., and McDonald, M., "Solution to the Multi-Dimensional Compressible Navier-Stokes Equations by a Generalized Implicit Method", *Journal of Computational Physics*, Vol. 24, August 1977, pp. 372-397.
40. Beam, R., and Warming, R. F., "An Implicit Factored Scheme for the Compressible Navier-Stokes Equations", *AIAA Journal*, Vol. 16, April 1978, pp. 393-402.
41. Berker, D. R. et al., "Viscous Interaction Performance Evaluation Routine for Nozzle Flows with Finite Rate Kinetic Chemistry", Final Report, AL-TR-90-042, 1990.

## REFERENCES (Continued)

42. Smith, T. A., Pavli, A. J., and Kacynski K. J., "Comparison of Theoretical and Experimental Thrust Performance of a 1030:1 Area Ratio Rocket Nozzle at a Chamber Pressure of 2413 kN/m<sup>2</sup> (350 psia)", NASA Technical Paper 2725, 1987.
43. Nickerson, G. R., and Dang, L.D., "Two-Dimensional Kinetics Computer Program for Orbit Transfer Vehicles". 22nd JANNAF Combustion Meeting, 10 October 1985, JPL, Pasadena, CA.
44. Kushida, R., Hermal, J., Apfel, S., and Zydowicy, M., "Performance of High-Area-Ratio Nozzle for a Small Rocket Thruster", Journal of Propulsion and Power, Vol. 3, No. 4, Pg. 329.
45. Evans, M., "BLIMP-J User's Manual", Aerotherm Division/Acurex Corporation, under Contract NAS8-30930, July 1975.
46. Corliss, L. P., "Liquid Rocket Combustion Computer Model with Distributed Energy Release", Rocketdyne Final Report, Contract NAS7-746, December 1971.
47. Coats, D. E., Berker, D. R., Kawasaki, A. H., "Boundary Layer Loss Models in Nozzle Performance Prediction", 26th JANNAF Combustion Subcommittee Meeting, JPL, Pasadena, CA, October 1989.
48. Back, L. H., Cuffel, R. F., and Massier, P. F., "Laminarization of a Turbulent Boundary Layer in Nozzle Flow-Boundary Layer and Heat Transfer Measurements with Wall Cooling", Journal of Heat Transfer, Trans. ASME, Series C, Vol. 92, No. 3, Aug. 1970, pp. 333-344.
49. Back, L. H., and Cuffel, R. F., "Turbulent Boundary Layer and Heat Transfer Measurements Along a Convergent-Divergent Nozzle," Journal of Heat Transfer, Nov. 1971.
50. Back, L. H., and Cuffel, R. F., "Turbulent Boundary Layer Measurements Along a Supersonic Nozzle with and without Wall Cooling," Transactions of the ASME, May 1972.
51. Cuffel, R. F., Back, L. H., and Massier, P. F., "The Transonic Flowfield in a Supersonic Nozzle with Small Throat Radius of Curvature," AIAA Journal, Vol. 7, No. 7, July 1969, pp. 1364-1366.
52. Modarress, D., and Azzazy, M., "Modern Experimental Techniques for High Speed Flow Measurements," AIAA-88-0420.

APPENDIX A  
TECHNICAL PAPERS FROM THE PHASE 1 WORK EFFORT

<u>Paper Name</u>	<u>Page No.</u>
Effect of Transverse and Longitudinal Curvature on Nozzle Boundary Layer Growth	A-1
Viscous Loss Assessment in Rocket Engines	A-8
Boundary Layer Loss Models in Nozzle Performance Prediction	A-33

(Reprinted with permission)

# AIAA'87

AIAA-87-1821

**Effect of Transverse and Longitudinal Curvature  
on Nozzle Boundary Layer Growth**

**Kehtarnavaz, H. and Coats, D. E.**

**Software and Engineering Associates, Inc.  
Carson City, Nevada 89701**

**AIAA/SAE/ASME/ASEE 23rd Joint  
Propulsion Conference**

**June 29-July 2, 1987/San Diego, California**

A-1

# EFFECT OF TRANSVERSE AND LONGITUDINAL CURVATURE ON NOZZLE BOUNDARY LAYER GROWTH

H. Kehtarnavaz  
Douglas E. Coats  
Software and Engineering Associates, Inc.  
Carson City, Nevada 89701

## ABSTRACT

The performance loss in high expansion ratio nozzles due to the turbulent boundary layer is a critical design parameter in selecting the nozzle geometry. This work studies the effects of transverse and longitudinal curvature on the boundary layer growth and their impact on performance. Curvature effects become important in axisymmetric flows when the curvature radius is of the same order as the boundary layer thickness. The effects of longitudinal curvature manifest themselves as a centrifugal force term on the mean flow in the boundary layer, and also on the turbulent shear stress model. The present Boundary Layer Module (BLM) of the TDK Computer Code has been modified for longitudinal curvature effects by the addition of second order boundary layer terms to the equation set. The normal momentum equation has also been included in the formulation. The edge conditions of the boundary layer have been modified to provide the correct matching with the outer flow expansion. A comparison of results between the modified version of the code and previous version of the code has been made. The modified code has been tested for a variety of nozzles and the results are presented.

## NOMENCLATURE

A	Given by Equation (15a)
b	Given by Equation (15b)
C, c	Given by Equation (15c)
d	Given by Equation (21)
e	Given by Equation (20)
F( $\eta, \zeta$ )	Function in normal momentum equation given by Equation (17)
g( $\eta, \zeta$ )	Nondimensional enthalpy, Equation (18)
H( $\eta, \zeta$ )	Enthalpy
k(x) or k( $\zeta$ )	Transformed longitudinal curvature, absolute value
L	unit length
$m_1 - m_5$	Gradients given by Equations (15d)
p	pressure
Pr	prandtl number
R	Radius of longitudinal curvature
r	Radius of transverse curvature

t	$= y \cos \phi / r$
u, v	velocity components
x, y	Coordinate system

## Greek Letters

$\delta$	Boundary layer thickness
$\delta^*$	Displacement thickness
$\epsilon$	Eddy viscosity term
$\phi$	Wall angle
$\mu$	Viscosity
$\nu$	Kinematic viscosity
$\eta, \zeta$	Transformed coordinates
$\psi$	Stream function
$\rho$	Density
$\theta$	Momentum thickness
$\tau$	Shear stress

## Subscripts

w	at the wall
o	to the wall
u	Refers to velocity
H	Refers to enthalpy

## Superscripts

'	$\partial/\partial \eta$
"	$\partial^2/\partial \eta^2$

## I. INTRODUCTION

The trend toward very large area ratio nozzles, which result in performance gains for space applications, has increased the need for detailed knowledge of the momentum losses due to viscous effects in propulsive nozzles. The traditional approaches (1-8) make use of the Prandtl thin shear layer approximation to compute the losses due to viscous effects, i.e.,  $\delta/l \ll 1$  which eliminates the normal momentum equation or the "centrifugal force". However, it should be noted that the normal pressure gradient vanishes not because the shear layer is thin, but because the surface is relatively flat, i.e., the radius of curvature,  $R$ , is large or more precisely  $R/l \gg 1$ . Van Dyke (9-10) has shown that longitudinal curvature makes a

contribution that is additive to that of transverse curvature and of the same relative order. The perturbation theory applied by Van Dyke demonstrates the importance of second order terms. The metric influence of curvature has been given by Schultz-Grunow and Brewer<sup>(11)</sup> for laminar and incompressible flows. Their approach consists of adoption of a curvilinear coordinate system and taking the arc length along the surface as the coordinate. This brings the longitudinal curvature directly into the problem since any differentiation with respect to  $x$  carries a factor of the ratio of curvature radii (wall position to actual position).

Cebeci, Hirsch, and Whitelaw<sup>(12)</sup> analyzed the turbulent boundary layer on a (convex) longitudinally curved surface using the mean flow equations of Schultz-Grunow and Brewer<sup>(11)</sup> discussed earlier. In their treatment they replaced the laminar viscosity with an effective eddy viscosity. The eddy viscosity was specified to be the standard Cebeci & Smith<sup>(13)</sup> formulation modified by Bradshaw's<sup>(14)</sup> correction for longitudinal curvature. Eghlima

et.al.<sup>(15)</sup> used a similar approach. However, in all these approaches the assumption has been made that the vorticity vanishes along the edge of the boundary layer, i.e., the outer flow is irrotational.

Most of the existing literature is limited to boundary layers in external flows, which have received much more attention than internal flows with thick boundary layers. However, Whitefield and Lewis<sup>(16)</sup> have reported results from experiments on laminar boundary layer development in nozzles. In their experiments the boundary layer thickness were as high as 90% of the nozzle radius.

The purpose of this work is to study the effect of longitudinal curvature on internal flows and specifically nozzles. To do this, the problem has been formulated and the new terms in the resulting equations in similarity form have been added to the BLM Computer Code<sup>(7)</sup> which already accounted for axisymmetric flows with transverse curvature. The modified code has been tested for a variety of rocket engine nozzles and the results have been presented. The code also has been tested for external flows and a comparison with existing literature has been made. For "relatively" thick boundary layers in the nozzles, all second order terms are accounted for and included in the Boundary Layer Module (BLM) of the TDK Computer Code.

## 11. THEORY

For a compressible boundary layer flow in an axisymmetric nozzle, the governing equations including the transverse and longitudinal curvature effects are given as<sup>(12,15,17,18)</sup>

Continuity:

$$\frac{\partial}{\partial x}(\rho u r^n) + \frac{\partial}{\partial y}(\bar{\rho} \bar{v} r^n(1 \pm ky)) = 0 \quad (1)$$

Streamwise Momentum:

$$\begin{aligned} \rho \frac{u}{1 \pm ky} \frac{\partial u}{\partial x} + \bar{\rho} \bar{v} \frac{\partial u}{\partial y} + \frac{\rho k u v}{1 \pm ky} = \\ - \frac{1}{1 \pm ky} \frac{\partial p}{\partial x} + \frac{1}{r^n(1 \pm ky)} \frac{\partial}{\partial y} [r^n(1 \pm ky) \\ \{ \mu \frac{\partial u}{\partial y} - \bar{\rho} \bar{v} \bar{u}' \}]; \quad \bar{\rho} \bar{v} = \rho v + \bar{\rho} \bar{v}' \end{aligned} \quad (2a)$$

Normal Momentum:

$$\frac{k u^2}{1 \pm ky} = \frac{1}{\rho} \frac{\partial p}{\partial y} \quad (2b)$$

Energy:

$$\begin{aligned} \frac{\rho u}{1 \pm ky} \frac{\partial H}{\partial x} + \bar{\rho} \bar{v} \frac{\partial H}{\partial y} = \frac{1}{r^n(1 \pm ky)} \frac{\partial}{\partial y} \\ \{ r^n(1 \pm ky) \cdot [ \frac{\mu}{Pr} \frac{\partial H}{\partial y} \\ + \mu(1 - \frac{1}{Pr}) u \frac{\partial u}{\partial y} - \rho \bar{H} \bar{v}' ] \} \end{aligned} \quad (3)$$

The influence of longitudinal curvature on the mean boundary layer flow is modeled by inclusion of the centrifugal force term in the normal momentum equation<sup>(9,10,11)</sup>. (See Equation 2b).

In these equations  $n$  is the flow index which is zero for two-dimensional flow and one for axisymmetric flows, and  $k=k(x)$  is the longitudinal curvature. Note that the  $-$  sign in  $1 \pm ky$  refers to concave and  $+$  sign refers to convex surfaces. Figure 1 shows the definition of  $r, r_0, R_0$  and  $R$ .

Transverse curvature is defined as:

$$\tau = \frac{y \cos \phi}{r_0} = \frac{r}{r_0} \quad (4a)$$

and the longitudinal curvature as:

$$\frac{1}{R_0} = k(x) \quad (4b)$$

and



$$\frac{H}{R_0} = 1 \pm k(x)y \quad (4c)$$

The boundary conditions for equations (1-3) are:

$$\text{at } y=0, \quad u=0, \quad v=v_w(x), \quad (5a)$$

$$\text{and } T = T_w(x) \text{ or } \dot{q}_w(x) \text{ is known; } (5b)$$

$$\text{at } y = y_{\max}, \quad u = u_e, \quad H = H_e, \quad (5c)$$

$$p = p_e + \frac{\rho_e k}{1 \pm k y} u_e^2 y_{\max}^2.$$

The boundary condition for  $p(y_{\max})$  was taken from Van Dyke (9,10) who matched the "Inner Limit of the Outer Expansion" (j)th iteration to the (j-1)th iteration of the "inner flow" (i.e., the boundary layer). Van Dyke showed that equation (2a) and (5c) include all second order terms caused by longitudinal curvature effect.

In the governing equations the terms for normal stresses have been neglected. After Cebeci-Smith we define:

$$-\rho \bar{v} \bar{v}' = \rho c_m \frac{\partial u}{\partial y} \quad (6a)$$

$$-\rho \bar{H} \bar{v}' = \rho \frac{c_m}{Pr_t} \frac{\partial H}{\partial y} \quad (6b)$$

To obtain the equations in similarity form a stream function  $\psi$  has been defined such that:

$$\rho u r^n = \frac{\partial \psi}{\partial y} \quad (7a)$$

$$\rho \bar{v} r^n = \frac{1}{1 \pm k(x)y} \left[ (\rho v)_w r_0^n - \frac{\partial \psi}{\partial x} \right] \quad (7b)$$

$$\text{where } \psi = [u_e(\zeta) \rho_e u_e \zeta]^{1/2} L^n f(\zeta, \eta); \quad (8)$$

$$f' = u/u_e$$

and  $\zeta$  and  $\eta$  are the similarity coordinates given by:

$$d\zeta = \left( \frac{r_0}{L} \right)^{2n} dx \quad (9a)$$

$$d\eta = \left[ \frac{u_e(\zeta)}{\rho_e u_e \zeta} \right]^{1/2} \rho \left( \frac{r}{L} \right)^n dy \quad (9b)$$

with

$$\frac{1}{1 \pm k(x)y} = w_0(\eta, \zeta) \quad (10)$$

$\Delta - 4$

The streamwise momentum equation, (2a), requires  $\partial p / \partial x$  along lines of constant  $y$ . From Schultz-Grunow(11):

$$\left( \frac{\partial p}{\partial x} \right)_y = \left( \frac{\partial p}{\partial x} \right)_\eta + \left( \frac{\partial p}{\partial y} \right)_x \left( \frac{\partial \eta}{\partial x} \right)_x \left( \frac{\partial \eta}{\partial x} \right)_y \quad (11)$$

Surfaces of constant  $\eta$  are all parallel to the curved wall. At the "edge" the term  $\left( \frac{\partial p}{\partial x} \right)_\eta$  is given by Bernoulli's equation:

$$\left( \frac{\partial p}{\partial x} \right)_y = -\rho_e u_e \frac{du_e}{dx} + \left( \frac{\partial p}{\partial y} \right)_x \quad (12)$$

Replacing the second term on the right hand side in the above equation by using Equations (2b) and (9b) gives:

$$\frac{\partial p}{\partial x} = -\rho_e u_e \frac{du_e}{dx} - \frac{\rho k(x)}{1 \pm k(x)y} u_e^2 r^{n,2} \quad (13)$$

$$\frac{1 - (1-t)^{n+1}}{(1-t)^{n(n+1)}} \left( \frac{r_0}{L} \right)^n \cdot L^n \frac{(m_1 - m_2)}{\zeta}$$

The second term on the right hand side is of second order and is included in the streamwise momentum equation in the  $m_5$  coefficient.  $m_1$  and  $m_2$  are given by Eq. (15d).

In terms of new variables the continuity and streamwise momentum equations, 1-2a can be rewritten as:

$$\begin{aligned} (b f'')' + m_1 f f'' + m_2 (c - m_5 f')^2 - m_3 f'' - A(m_3 - m_1 f) f' \\ = \zeta \left[ f' \frac{\partial f'}{\partial \zeta} - f'' \frac{\partial f}{\partial \zeta} - A f' \frac{\partial f}{\partial \zeta} \right] \end{aligned} \quad (14)$$

where ' represents  $\frac{\partial}{\partial \eta}$  and

$$A = k(\zeta) w_0(\eta, \zeta) \left( \frac{r_0}{L} \right)^{-n} \frac{c}{(1-t)^n} \zeta Re_\zeta^{-1/2} \quad (15a)$$

$$b = \frac{c}{w_0(\eta, \zeta)} (1 + \epsilon_m^+) (1-t)^{2n} \quad (15b)$$

$$c = \frac{\rho_e u_e}{\rho_e u_e}, \quad c = \frac{\rho_e}{\rho} \quad (15c)$$

$$m_2 = \frac{\zeta}{u_e} \frac{du_e}{d\zeta}, \quad m_4 = \frac{\zeta}{\rho_e u_e} \frac{d}{d\zeta} (\rho_e u_e)$$

the boundary layer for ASE nozzle at the exit plane. A pressure difference of about 15% is observed across the boundary layer with a negative slope (concave surface), i.e., the pressure at the wall is 15% higher than the pressure at the edge of boundary layer.

For nozzles with "higher" curvature, the pressure gradient across the boundary layer may vary significantly. For SSME nozzle a pressure difference of about 35% is observed from Figure 6 across the boundary layer with  $(\delta/R_o)_{\text{exit}} = 0.016$ .

The boundary layer is considerably thicker for SSME<sup>(22)</sup>.

#### IV. CONCLUDING REMARKS

The results in this work indicate that the longitudinal curvature is of importance in high expansion area ratio and/or strongly curved nozzle contours. The primary effect is on the velocity profile which results in thicker boundary layer. The magnitude of  $\delta/R_o$  specifies the importance of longitudinal curvature. Also, it is found out that generally the inclusion of longitudinal curvature decreases the thrust deficit and consequently increases the performance for rocket engine nozzles. The method used to obtain the curvature seems to be adequate and more stable and more accurate than methods which lead to calculation of the second derivative.

#### ACKNOWLEDGMENT

This work was supported by the Air Force Astronautics Laboratory (AFAL) under Contract No. F0411-86-C-0055. The authors wish to thank the contract monitor, Mrs. Elizabeth Slimak, at AFAL, for her support.

#### REFERENCES

1. Pieper, J. L., "Performance Evaluation Methods for Liquid Propellant Rocket Thrust Chambers", CPIA Publication No. 132, prepared for the Performance Standardization Working Group, November 1966.
2. "JANNAF Rocket Engine Performance Prediction and Evaluation Manual", CPIA NO. 246, April 1975.
3. Nickerson, G. R., Dang, L. D., and Coats, D. E., "Two-Dimensional Kinetics (TDK) Reference Computer Program", Final Report, Software and Engineering Associates, Inc., under NASA Contract NAS8-35931, April 1985.

4. Nickerson, G. R., Coats, D. E., Hermesen, R. W., and Lamberty, J. T., "A Computer Program for the Prediction of Solid Propellant Rocket Motor Performance (SPP)", Vol. 1, AFRPL TR-83-036, Software and Engineering Associates, Inc., Sept. 1984.
5. Weingold, H. D., "The ICRPG Turbulent Boundary Layer (TBL) Reference Program", prepared for ICRPG Perf. Std. Working Group, July 1968.
6. BLIMP-J Users Manual, prepared by M. Evans, Aerotherm Division/Acurex Corporation, July 1975 under Contract NAS8-30930.
7. Cebeci, T., "Boundary Layer Analysis Module", prepared for Software and Engineering Associates, Inc., January 1982.
8. Landau, L. D., and Lifshitz, E. M., Fluid Mechanics, Pergamon Press, London, 1959.
9. Van Dyke, M., "Higher Approximation in Boundary Layer Theory, Part 1, General Analysis", J. of Fluid Mechanics, 1962, page 161.
10. Van Dyke, M., "Higher-Order-Boundary-Layer Theory", Annual Review of Fluid Mechanics, 1969, page 265.
11. Schultz-Grunow, F., and Breuer, W., "Laminar Boundary Layers on Cambered Walls", in Basic Developments in Fluid Mechanics, Vol. 1, Academic Press, NY, 1965, page 377.
12. Cebeci, T., Hirsh, R. S., and Whitelaw, J. H., "On the Calculation of Laminar and Turbulent Boundary Layers on Longitudinally Curved Surfaces", AIAA, J., Vol. 17, No. 4, page 434.
13. Cebeci, T., and Smith, A. M. O., Analysis of Turbulent Boundary Layers, Academic Press, NY, 1974.
14. Bradshaw, P., "The Analogy Between Streamline Curvature and Buoyancy in Turbulent Shear Flow", J. Fluid Mech. Vol. 36, Part 1, pages 177-191, 1969.
15. Eghlima, A., and Kleinstreuer, C., "Numerical Analysis of Attached Turbulent Boundary Layers Along Strongly Curved Surfaces", AIAA, J., Vol. 23, No. 2, Feb. 1985, page 177.
16. Whitefield, D. L., and Lewis, C. H., "Boundary Layer Analysis of Low Density Nozzles, Including Displacement Slip, and Transverse Curvature", J. of Spacecraft and Rockets, Vol. 7, No. 4, pages 462-468, April 1970.

- 
- Figure 1: Schematic of a Nozzle

A line graph comparing two methods of determining curvature. The vertical axis is labeled 'CURVATURE' and has a scale from 0.00 to 0.05 in increments of 0.01. The horizontal axis is labeled 'X, FT.' and has a scale from 0.00 to 3.00 in increments of 0.50. Two data series are plotted: a solid line representing the 'Method used in this work' and a dashed line representing the 'Circular Arc Nozzle'. The solid line starts at approximately 0.020 at X=0.00, remains relatively flat with minor fluctuations, peaks at about 0.023 near X=2.10, and then drops to approximately 0.015 at X=2.80. The dashed line is a straight horizontal line at a curvature of approximately 0.018, extending from X=0.00 to X=2.80.

X, FT.	Method used in this work (Curvature)	Circular Arc Nozzle (Curvature)
0.00	0.020	0.018
0.50	0.020	0.018
1.00	0.021	0.018
1.50	0.020	0.018
2.00	0.021	0.018
2.10	0.023	0.018
2.50	0.020	0.018
2.80	0.015	0.018

ASE NOZZLE

X, FT	CURVATURE (E-2)
0.00	0.40
0.50	0.30
1.00	0.20
1.50	0.14
2.00	0.10
2.50	0.07
3.00	0.05
3.50	0.04
4.00	0.035
4.50	0.03
5.00	0.025
5.50	0.02
6.00	0.015

(a)

SSME Nozzle

Curvature (inverted) vs. X, FT

X, FT	Curvature (inverted)
0.00	0.14
4.00	0.08
8.00	0.05
10.50	0.00

A-6

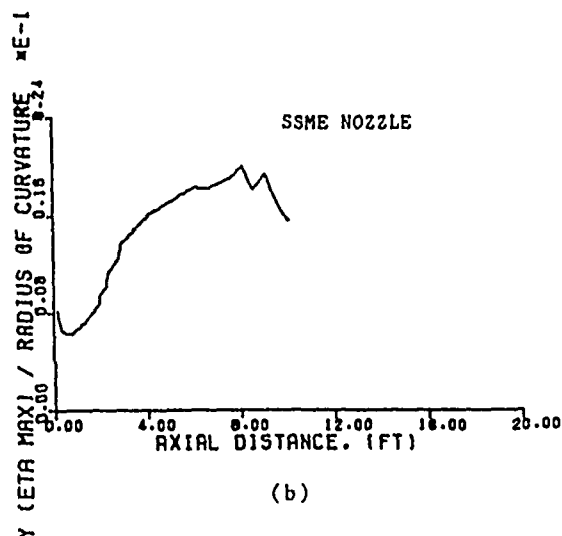
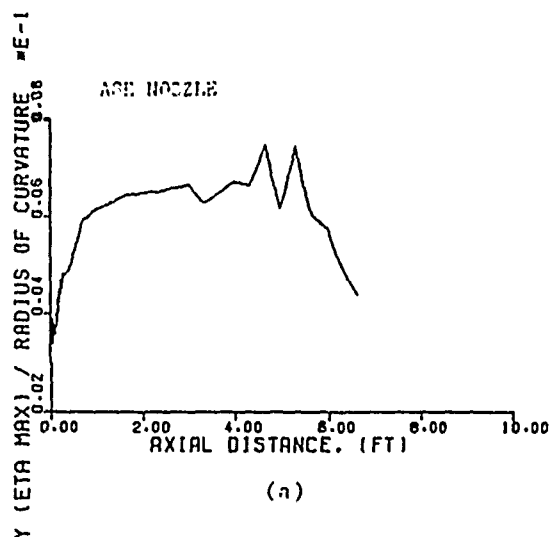


Figure 4:  $\delta/R_0$  for ASE and SSME Nozzles

X PRESSURE PROFILE  
 VELOCITY PROFILE  
 EPS = 400.00  
 R, FT = 2.090  
 Z, FT = 6.626  
 UE (ETA MAX), FT/SEC. = 15045.0  
 YE (ETA MAX), FT = 0.2696031  
 PE (ETA MAX), LBF/FT2 = 65.6  
 ASE LCRVOP=1

TEMPERATURE PROFILE  
 TE (ETA MAX), DEG(R) = 1747.4  
 TH DEG(R) = 818.0

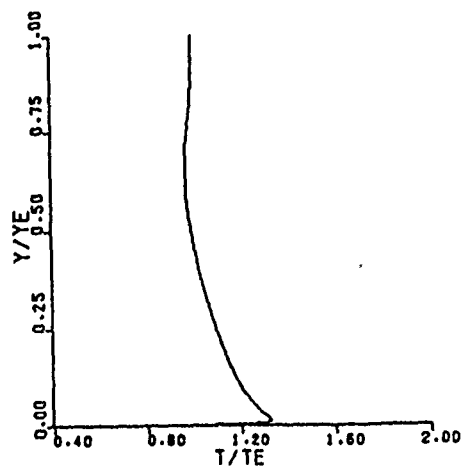
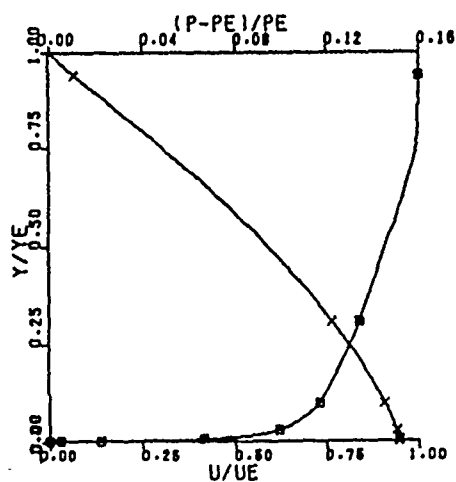
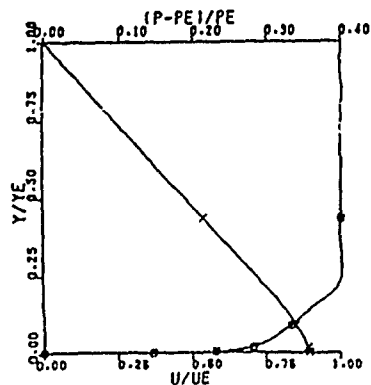


Figure 5: Velocity, Temperature and Pressure Profiles Across the Boundary Layer for ASE Nozzle.



X PRESSURE PROFILE  
 VELOCITY PROFILE  
 EPS = 77.60  
 R, FT = 9.780  
 Z, FT = 10.101  
 UE (ETA MAX), FT/SEC. = 13944.3  
 YE (ETA MAX), FT = 0.6672226  
 PE (ETA MAX), LBF/FT2 = 732.4  
 SSME LCRVOP=1

Figure 6: Velocity and Pressure Profiles Across the Boundary Layer for SSME Nozzle.

# VISCOUS LOSS ASSESSMENT IN ROCKET ENGINES

By

Homayun Kehtarnavaz †  
Douglas E. Coats \*  
Anthony L. Dang \*\*

Software and Engineering Associates, Inc.  
Carson City, Nevada 89701

- † Senior Research Scientist, Member AIAA  
Currently at Physical Research, Inc., Irvine, CA 92718
- \* Vice President, Senior Member AIAA
- \*\* Principal Research Scientist  
Currently at Physical Research, Inc., Irvine, CA 92718

## ABSTRACT

The performance losses in rocket nozzles due to the viscous effects have been studied. Special consideration was given to nozzles with high expansion ratios. The formulation of the boundary layer equations used in this study includes the effects of transverse and longitudinal curvatures. The effects of longitudinal curvature manifest themselves as a centrifugal force term on the mean flow in the boundary layer, and also on the turbulent shear stress model. The results indicate that although the longitudinal curvature creates a fairly strong pressure difference across the boundary layer, the effects on the performance is minimal. The results also show that in high expansion ratio nozzles, the viscous layer becomes very "thick" and the traditional boundary layer assumptions cause significant error in the viscous loss calculations. Improvements to the method of evaluating thrust loss are presented.

## NOMENCLATURE

$H(\eta, \zeta)$	Enthalpy
$k(x)$ or $k(\zeta)$	Transformed longitudinal curvature, positive for convex and negative for concave surfaces
$L$	Length scale
$p$	Pressure
$pr$	Prandtl number
$R$	Radius of longitudinal curvature
$r$	Radius of transverse curvature
$Re$	Reynolds number
$t$	$= y \cos\phi/r_o$
$T$	Thrust
$u, v$	Velocity components
$x, y$	Coordinate system

### Greek Letters

$\delta$	Boundary layer thickness
$\delta^*$	Displacement thickness
$\epsilon$	Eddy viscosity term
$\bar{\epsilon}(x)$	Given by eg.
$\phi$	Wall angle
$\mu$	Viscosity
$\nu$	Kinematic viscosity
$\eta, \zeta$	Transformed coordinates
$\psi$	Stream function
$\rho$	Density
$\theta$	Momentum thickness
$\tau$	Shear stress

### Superscripts

'	$\partial/\partial\eta$
"	$\partial^2/\partial\eta^2$
*	Potential Flow (at distance $\delta^*$ from the wall)
—	Modified Value

### Subscripts

w	At the wall
o	To the wall
u	Refers to velocity
H	Refers to enthalpy
e	At the edge of boundary layer
p	At the edge of potential flow

### Abbreviations

ASE	Rocketdyne Advance Space Engine, area ratio 400:1
BC4515	Experimental Nozzles by JPL, cone shaped
BC1010	
BLM	Boundary Layer Module of TDK computer code
IUS	Inertial Upper Stage, Space motor, OTV
JANNAF	Joint Army Navy NASA Air Force
Lox/GH <sub>2</sub>	Liquid Oxygen and Gaseous Hydrogen
RL-10	Pratt & Whitney Space Engine, area ratio 205:1
SSME	Space Shuttle Main Engine, area ratio 76:1
TDK	Two Dimensional Kinetic Computer Code
XDELTA	Extended Delta (Solid Propellant Space motor)
XLR134	OTV Engine, Space storable, area ratio 767:1



## INTRODUCTION

The trend toward very large area ratio nozzles, which result in performance gains for space applications, has increased the need for detailed knowledge of the momentum losses due to nozzle viscous effects (i.e., boundary layer) in propulsion systems. These losses degrade overall system performance by increasing system weight, decreasing useful payload weight, and/or decreasing effective system range. The traditional approaches<sup>1-8</sup> use the Prandtl thin shear layer approximation i.e.,  $\delta/L \ll 1$ , to compute the losses due to viscous effects. These assumptions eliminate the normal momentum equation or the "centrifugal force balance". The normal pressure gradient vanishes not because the shear layer is thin, but because the surface is relatively flat, i.e., the radius of curvature is large.

Van Dyke<sup>9-10</sup> has shown that longitudinal curvature makes a contribution that is additive to that of transverse curvature and is of the same relative order of magnitude. The perturbation theory applied by Van Dyke demonstrates the importance of second order terms. The metric influence of curvature has been given by Schultz-Grunow and Brewer<sup>11</sup> for laminar and incompressible flows.

Cebeci, Hirsch, and Whitelaw<sup>12</sup> analyzed the turbulent boundary layer on a (convex) longitudinally curved surface. In their treatment they replaced the laminar viscosity with an effective eddy viscosity. The eddy viscosity was specified to be the standard Cebeci & Smith<sup>13</sup> formulation modified by Bradshaw's<sup>14</sup> correction for longitudinal curvature. Eghlima et.al.<sup>15</sup> used a similar approach. However in all these approaches, the assumption has been made that the vorticity vanishes along the edge of the boundary layer, i.e., the outer flow is irrotational.

It has been found that the standard JANNAF method<sup>2</sup> for predicting boundary layer losses is not sufficiently accurate for computing boundary layer losses for space engines. These engines exhibit substantial boundary layer growth due to their very high expansion ratios. For small engines, a major portion of the nozzle flow can be completely enveloped by the wall shear layer (up to 90%).

The two major deficiencies of the JANNAF boundary layer thrust loss calculation method<sup>2</sup> are that the effects of both transverse and longitudinal curvature are assumed to be

small. Since in highly expanded flows, the boundary layer thickness can become a significant fraction of either the transverse or longitudinal curvature, this effect should not be ignored.

The objective of this paper is (1) to assess the significance of nozzle wall curvature effects, and (2) to assess performance losses due to viscous effects using a more complete description of the viscous shear layer within the boundary layer equations for a wide range of space applications engines.

## THEORY

For a compressible boundary layer flow in an axisymmetric nozzle, the governing equations including the transverse and longitudinal curvature effects are given as<sup>12,15,17,18</sup>.

Continuity:

$$\frac{\partial}{\partial x} (\rho u r^n) + \frac{\partial}{\partial y} [\bar{\rho} \bar{v} r^n (1+ky)] = 0 \quad (1)$$

Streamwise Momentum:

$$\begin{aligned} \rho \frac{u}{1+ky} \frac{\partial u}{\partial x} + \bar{\rho} \bar{v} \frac{\partial u}{\partial y} + \frac{\rho k u v}{1+ky} = - \frac{1}{1+ky} \frac{\partial p}{\partial x} + \frac{1}{r^n(1+ky)} \cdot \\ \frac{\partial}{\partial y} \left[ r^n(1+ky) \left[ \mu \frac{\partial u}{\partial y} - \bar{\rho} \bar{v} u' \right] \right]; \bar{\rho} \bar{v} = \rho v + \bar{\rho} \bar{v}' \end{aligned} \quad (2a)$$

Normal Momentum:

$$\frac{k u^2}{1+ky} = \frac{1}{\bar{\rho}} \frac{\partial p}{\partial y} \quad (2b)$$

Energy:

$$\begin{aligned} \frac{\rho u}{1+ky} \frac{\partial H}{\partial x} + \bar{\rho} \bar{v} \frac{\partial H}{\partial y} = \frac{1}{r^n(1+ky)} \cdot \frac{\partial}{\partial y} \left[ r^n(1+ky) \cdot \right. \\ \left. \left[ \frac{\mu}{Pr} \frac{\partial H}{\partial y} + \mu \left( 1 - \frac{1}{Pr} \right) u \frac{\partial u}{\partial y} - \rho H \bar{v}' \right] \right] \end{aligned} \quad (3)$$

The influence of longitudinal curvature on the mean boundary layer flow is modeled by inclusion of the centrifugal force term in the normal momentum equation<sup>9-11</sup>. (See equation 2b).

Figure 1 shows the definition of  $r$ ,  $r_o$ ,  $R_o$  and  $R$ .

Transverse curvature is defined as:

$$t = \frac{y \cos \phi}{r_o} = \frac{r}{r_o} \quad (4a)$$

and the longitudinal curvature as:

$$\frac{1}{R_o} = k(x) \quad (4b)$$

and

$$\frac{R}{R_o} = 1 + k(x)y \quad (4c)$$

The boundary conditions for equations (1-3) are:

$$\text{at } y = 0, \quad u = 0, \quad v = v_w(x), \quad (5a)$$

$$\text{and } T = T_w(x) \text{ or } q_w(x) \text{ is known;} \quad (5b)$$

$$\text{at } y = y_{max}, \quad u = u_e, \quad H = H_e, \quad p = p_e + \frac{\rho_e k}{1+ky} u_e^2 y_{max}. \quad (5c)$$

The boundary condition for  $p(y_{max})$  was taken from Van Dyke<sup>9-10</sup> who matched the "Inner Limit of the Outer Expansion" (j)<sup>th</sup> iteration to the (j-1)<sup>th</sup> iteration of the "inner flow" (i.e., the boundary layer). Van Dyke showed that equations (2a) and (5c) include all second order terms caused by longitudinal curvature effect.

To include the longitudinal curvature effect in the eddy viscosity model, the Bradshaw's<sup>19,20</sup> expression has been employed to correct the inner eddy viscosity term by multiplying this expression by  $S^2$  where:

$$S = \frac{1}{1+R_i \beta} \quad R_i = 2u k(x) \left[ \frac{\partial u}{\partial y} \right]^{-1} \quad (6)$$

where  $R_i$  is analogous to Richardson number and  $\beta$  is reported to be 7 for convex and 4 for concave surfaces<sup>19,20</sup>.

The streamwise momentum equation, (2a), requires  $\partial p/\partial x$  along lines of constant  $y$ .

Surfaces of constant  $\eta$  are all parallel to the curved wall. At the boundary layer "edge", the term  $\left[\frac{\partial p}{\partial x}\right]_y$  is given by:

$$\left[\frac{\partial p}{\partial x}\right]_y = -\rho_e u_e \frac{du_e}{dx} + \left[\frac{\partial p}{\partial y}\right]_x \left[\frac{\partial y}{\partial \eta}\right]_x \left[\frac{\partial \eta}{\partial x}\right]_y \quad (7)$$

The conventional JANNAF method<sup>2</sup> for evaluation of the viscous thrust loss in rocket engine nozzle employs both the boundary layer momentum and displacement thicknesses. This method can be arrived at by two different approaches as shown by Alber<sup>21</sup>. The basis for the approach is to compare the thrust of an inviscid nozzle to a viscous nozzle with the same mass flow rate. In the equation given below, the first term represents the pressure forces acting on an inviscid nozzle and the second and third terms represent the total stress forces acting on the viscous nozzle.

$$\Delta T = \int_0^s (p_e^* - p_\infty) 2\pi r_p \frac{dr_p}{dx} dx - \int_0^s (p_w - p_\infty) 2\pi (r_p + \delta^* \cos\phi) \quad (8)$$

$$\frac{d(r_p + \delta^* \cos\phi)}{dx} dx + \int_0^s \tau_w 2\pi (r_p + \delta^* \cos\phi) \cos\phi dx$$

where  $r_p$  is the distance from the axis to the potential wall and  $p_e^*$  is the pressure at  $r_p$ , as is shown in Figure 1. For thin boundary layers, the conventional assumption is to let  $r_p = r_o$ . However, to maintain generality, Equation (8) distinguishes between the potential and real wall. The integral form of the momentum equation (with transverse and longitudinal curvature effects) can be derived as:

$$\begin{aligned} \frac{\partial}{\partial x} \left[ \rho_e u_e^2 r_o \int_0^\delta \frac{r}{r_o} \frac{\rho u}{\rho_e u_e} \left[ 1 - \frac{u}{u_e} \right] dy \right] + \rho_e u_e r_o \frac{\partial u_e}{\partial x} \int_0^\delta \left[ 1 - \frac{\rho u}{\rho_e u_e} \right] \frac{r}{r_o} dy \\ - r_o \int_0^\delta \frac{r}{r_o} \rho k u v dy - \epsilon(x) r_o \left[ \delta - \frac{\delta^2}{2r_o} \right] = \tau_w r_o \end{aligned} \quad (9a)$$

where:  $\frac{\partial p_e}{\partial x} + \rho_e u_e \frac{\partial u_e}{\partial x} = \epsilon(x)$  (9b)

The details of the derivation can be found in Reference 16. Alternate forms of the momentum and displacement thicknesses for axisymmetric flows are defined as:

(momentum thickness)  $\bar{\theta} = \int_0^{\delta} \frac{r}{r_o} \frac{\rho u}{\rho_e u_e} \left[ 1 - \frac{u}{u_e} \right] dy$  (10a)

(displacement thickness)  $\bar{\delta}^* = \int_0^{\delta} \frac{r}{r_o} \left[ 1 - \frac{\rho u}{\rho_e u_e} \right] dy$  (10b)

Implementing Eqs. (10) in Eq. (9) yields

$$\begin{aligned} \frac{\partial}{\partial x} (\rho_e u_e^2 r_o \bar{\theta}) - r_o \bar{\delta}^* \frac{\partial p_e}{\partial x} - r_o \int_0^{\delta} \frac{r}{r_o} \rho k u v dy \\ + \epsilon(x) r_o \left[ \bar{\delta}^* - \delta + \frac{\delta^2}{2 r_o} \right] = \tau_w r_o \end{aligned} \quad (11)$$

Inserting Eq. (11) in Equation (8) and neglecting terms of order  $\bar{\delta}^{2*}$ , the thrust deficit is:

$$\begin{aligned} \frac{\Delta T}{2\pi} = \int_0^s [p_e^* - p_w] r_p \frac{dr_p}{dx} dx - \int_0^s [p_w - p_\infty] \frac{d}{dx} (r_p \bar{\delta}^* \cos \phi) dx \\ + \int_0^s r_o \left[ -k(x) \int_0^{\delta} \frac{r}{r_o} \rho u v dy + \epsilon(x) (\bar{\delta}^* - \delta + \delta^2/2r_o) \right] \cos \phi dx \\ + \int_0^s \cos \phi \cdot \left[ \frac{\partial}{\partial x} (\rho_e u_e^2 r_o \bar{\theta}) - r_o \bar{\delta}^* \frac{\partial}{\partial x} (p_e - p_\infty) \right] dx \end{aligned} \quad (12)$$

Here  $p_e^*$  is the pressure at the edge of the potential flow and  $p_e$  is the pressure at the edge of the boundary layer, i.e., at  $r_w - \delta \cos \phi$ .

To this point, the thrust loss equation has been derived with very few of the traditional boundary layer assumptions being made. To examine the effects of these assumptions, they will be applied one at a time.

- 1) Non-dissipative edge condition, i.e.,  $\epsilon(x) \neq 0$ . In the absence of dissipative or applied forces on the core flow, Bernoulli's equation is satisfied and  $\epsilon(x) = 0$  (see eq. 9b). Examples of flows where  $\epsilon(x) \neq 0$  would be two phase core flow or MHD flow. The second term of the third integral in Eq. (12) disappears when  $\epsilon(x) = 0$ .
- 2) The boundary layer is thin compared to the local radius of curvature, i.e.,  $\delta/\bar{R}_0 \ll 1$ . This assumption leads to the following:

$$\partial p / \partial y = 0 \quad \text{or} \quad p = p_w = p_c^* = p_e$$

$$\text{and} \quad \frac{\partial \phi}{\partial x} = 0$$

$$\begin{aligned} \frac{\Delta T}{2\pi} = & \int_0^s \cos \phi \cdot \frac{\partial}{\partial x} \left[ \rho_c u_c^2 r_0 \bar{\theta} - r_0 \delta^* (p_e - p_\infty) \right] dx \\ & - \int_0^s (p_e - p_\infty) \cos \phi \frac{d}{dx} (r_p \delta^*) dx \end{aligned} \quad (13)$$

Integrating the first term in Eq. (13) by parts and assuming that  $\delta^*(s=0) = \bar{\theta}(s=0) = 0$  yields

$$\begin{aligned} \frac{\Delta T}{2\pi} = & \rho_c u_c^2 r_p \bar{\theta} \cos \phi - r_p \delta^* (p_e - p_\infty) \cos \phi \\ & - \int_0^s \rho_c u_c^2 r_0 \bar{\theta} \cos \phi \frac{\partial}{\partial x} \left[ \frac{r_p}{r_0} \right] dx \end{aligned} \quad (14)$$

- 3) For adiabatic and cooled wall flows, the displacement thickness,  $\delta^*$ , is usually less than the boundary layer thickness,  $\delta$ . The assumption applied here is that  $\delta^* \cos \phi / r_p \ll 1$  which is less restrictive than  $\delta / r_p \ll 1$ .

The remaining integral in eq. (14) vanishes by noting that

$$r_p/r_o = 1 - \frac{\delta^*}{r_o} \cos\phi = 1$$

To the same order of accuracy, Eq. (14) can be rewritten as

$$\frac{\Delta T}{2\pi} = \rho_c u_c^2 r_o \bar{\theta} \cos\phi - r_o \delta^* (p_c - p_\infty) \cos\phi \quad (15)$$

- 4) The above equation reduces to the standard JANNAF<sup>2</sup> relationship for thrust loss with the additional assumption  $\delta \cos\phi / r_o \ll 1$ . That is

$$\frac{r}{r_o} = 1 - \frac{\delta \cos\phi}{r_o} \approx 1$$

which leads to

$$\theta = \bar{\theta} \text{ and } \delta^* = \bar{\delta}^*$$

and (15) becomes:

$$\Delta T = 2\pi \cos\phi \left[ \rho_c u_c^2 r_o \bar{\theta} - r_o \bar{\delta}^* (p_c - p_\infty) \right] \quad (16)$$

In conclusion, it can be seen that in order to reduce the general form of the thrust loss Eq. (8) to the standard JANNAF form<sup>2</sup>, i.e., Eq. 16, requires four assumptions. The first assumption, i.e., that Bernoulli's equation is satisfied at the edge of the boundary layer is met in most liquid rocket engines of interest.

The other three assumptions deal with varying degrees of how thin the boundary layer is compared to a given length scale. The "thin" assumptions are:

- o The boundary layer is thin compared to the local longitudinal radius of curvature, i.e.,  $\delta/R_o \ll 1$ .



- o The displacement between the viscous and potential walls is small compared to the local wall radius, i.e.,  $\delta^* \cos \phi / r_0 \ll 1$ , which leads to  $r_p \approx r_0$ .
- o The boundary layer thickness is small compared to the local wall radius, i.e.,  $\delta \cos \phi / r_0 \ll 1$ , which leads to  $r \approx r_p \approx r_0$ .

## RESULTS AND DISCUSSION

The BLM (Boundary Layer Module) within the TDK (Two-Dimensional Kinetics) code was modified to include the normal momentum equation together with longitudinal curvature terms.

Solutions to the momentum and energy equations can be obtained in a very efficient manner by using the block elimination method as discussed by Keller. The implicit finite difference scheme that has been developed by Keller and Cebeci<sup>22</sup> was implemented to obtain numerical solution to these equations<sup>16</sup>. The BLM Code was validated by comparison to another boundary layer code, MABL<sup>23</sup>. The code was also verified for flow over a flat plate and available experimental data for flow over a convex surface. These results are presented in Ref. 16.

The nozzle wall is not generally known analytically, and is often obtained from tabular input data by spline fitting. Calculation of longitudinal curvature which requires the second derivative of a nozzle wall creates "severe" fluctuations of the second derivative which in turn can cause numerical instabilities. It was decided to divide the nozzle wall into numbers of equally spaced intervals and let a circle pass through every three points. The radius of the circle is taken to be the radius of the curvature at the middle point. This method has been verified against an analytical wall and the results are satisfactory<sup>16,24</sup>.

The importance of longitudinal curvature is determined by the magnitude of  $\delta/R_0$ , i.e., the ratio of the boundary layer thickness to the radius of curvature. Figs. 2a and 2b indicate this value for ASE and SSME nozzles, respectively. The magnitude of  $\delta/R_0$  for SSME is larger than ASE nozzle and thus a larger pressure gradient across the boundary layer is expected. This can be observed from a comparison of velocity profiles in Figs. 3 and 4.

The effect of longitudinal curvature on performance is depicted in Table 1. It can be seen that although the longitudinal curvature affects the mean flow velocity, temperature and

pressure profiles in the boundary layer, it has insignificant impact on nozzle performance. However, the methodology being used to evaluate viscous loss has to distinguish between a thin and thick boundary layer.

Essentially, Eq. (A) in this table which is the standard JANNAF method is not valid for thick boundary layers, because of the magnitude of term  $r/r_o$  where  $r$  is the distance from the axis of symmetry to the edge of the boundary layer. As the value of  $r/r_o$  increases, the thin shear layer assumption yields erroneous results for boundary layer losses, i.e., Eq. (A). Eq. (B) was developed for axisymmetric flows, and for the thick boundary layers is expected to yield quite different values from Eq. (A) and it can be seen that for nozzles with high area ratio such as ASE, RL-10 and XLR134, the difference between these equations is more significant. This difference is due to a thick boundary layer when  $r/r_o$  is significantly less than unity. To be more exact  $r_p$  should be replaced for  $r_o$  in Eq. (B) as shown in the analysis and upon doing that in fact the effects are more severe on the high area ratio nozzles, Eq. (C). The results of adding another higher order term to Eq.(C) has been indicated in Eq. (D). It can be seen that addition of this term makes a change of up to about 8% in the thrust loss for high area ratio nozzles. Using the integrated wall shear method i.e., Eq. (E) yields results quite different (up to 16%) from Eq. (A) for ASE nozzle, (area ratio= 400), RL-10 (area ratio 205) and XLR134, (area ratio 767:1). However, as the higher order terms are added to Equation (D), the results become closer to values of Eq. (E). This is expected because of mathematical equivalency of both equations. The overall results indicate that the standard JANNAF method for performance prediction is not adequate and can produce fairly large error performance predictions for high expansion nozzles.

The results indicated in this table justifies the usage of Eq. (E) for the thrust Calculations and Eq. (E) should be used to obtain the thrust loss. Furthermore, the inclusion of longitudinal curvature is not crucial to performance prediction in contoured wall of a rocket engine nozzle.

### CONCLUDING REMARKS

The results in this work indicated that although the effects of the longitudinal curvature are of importance on the mean flow velocity, pressure and temperature profiles in the boundary layer in strongly curved nozzle contours, it does not have a significant impact on the overall prediction of nozzle performance. However, for nozzles with a thick viscous layer, the

standard JANNAF method which is formulated for thin shear layers "over-estimates" the boundary layer thrust deficit and it should be replaced by the equation (E) in Table 1 which will be referred to as "wall shear method".

#### ACKNOWLEDGMENT

This work was performed at Software and Engineering Associates, Inc. under Astronautics Laboratory (AFAL) Contract No. F0411-86-C-0055. The authors wish to thank Dr. Phillip Kessel and Mrs. Elizabeth Slimak, at AFAL, for their support.

## REFERENCES

- 1 Pieper, J. L., "Performance Evaluation Methods for Liquid Propellant Rocket Thrust Chambers", CPIA Publication No. 132, prepared for the Performance Standardization Working Group, November 1966.
- 2 "JANNAF Rocket Engine Performance Prediction and Evaluation Manual", CPIA Publication No. 246, April 1975.
- 3 Nickerson, G. R., Dang, L. D., and Coats, D. E., "Two-Dimensional Kinetics (TDK) Reference Computer Program", Final Report, Software and Engineering Associates, Inc., under NASA Contract NAS8-35931, April 1985.
- 4 Nickerson, G. R., Coats, D. E., Hermisen, R. W., and Lamberty, J. T., "A Computer Program for the Prediction of Solid Propellant Rocket Motor Performance (SPP)", Vol. 1, AFRPL TR-83-036, Software and Engineering Associates, Inc., Sept. 1984.
- 5 Weingold, H. D., "The ICRPG Turbulent Boundary Layer (TBL) Reference Program", prepared for ICRPG Perf. Std. Working Group, July 1968.
- 6 BLIMP-J User's Manual, prepared by M. Evans, Aerotherm Division/Acurex Corporation, under Contract NAS8-30930, July 1975.
- 7 Cebeci, T., "Boundary Layer Analysis Module", prepared for Software and Engineering Associates, Inc., January 1982.
- 8 Landau, L. D., and Lifshitz, E. M., *Fluid Mechanics*, Pergomon Press, London, 1959.
- 9 Van Dyke, M., "Higher Approximation in Boundary Layer Theory, Part 1, General Analysis", J. of Fluid Mechanics, 1962, page 161.
- 10 Van Dyke, M., "Higher-Order-Boundary-Layer Theory", Annual Review of Fluid Mechanics, 1969, page 265.
- 11 Schultz-Grunow, F., and Breuer, W., "Laminar Boundary Layers on Cambered Walls", *Basic Developments in Fluid Mechanics*, Vol. 1, Academic Press, NY, 1965, page 377.

- 12     Cebeci, T., Hirsh, R. S., and Whitelaw, J. H., "On the Calculation of Laminar and Turbulent Boundary Layers on Longitudinally Curved Surfaces", AIAA J., Vol. 17, No. 4, April 1979, page 434.
- 13     Cebeci, T., and Smith, A. M. O., *Analysis of Turbulent Boundary Layers*, Academic Press, NY, 1974.
- 14     Bradshaw, P., "The Analogy Between Streamline Curvature and Buoyancy in Turbulent Shear Flow", J. of Fluid Mech., Vol. 36, Part 1, 1969, pages 177-191.
- 15     Eghlima, A., and Kleinstreuer, C., "Numerical Analysis of Attached Turbulent Boundary Layers Along Strongly Curved Surfaces", AIAA J., Vol. 23, No. 2, Feb. 1985, page 177.
- 16     Kehtarnavaz, H., Coats, D. E., Nickerson, G. R., and Dang, A. L., "Two-Dimensional Kinetics (TDK) Nozzle Performance Computer Program-Thick Boundary Layer Version", Software and Engineering Associates, Inc., Report No. AFAL-TR-87-031, March 1987.
- 17     Cebeci, T., "Eddy-Viscosity Distribution in Thick Axisymmetric Turbulent Boundary Layers", J. of Fluid Engineering, June 1973, page 319.
- 18     So, R. M. C., "Momentum Integral for Curved Shear Layers", J. of Fluid Engineering, June 1975, page 253.
- 19     Van Dyke, M., *Perturbation Methods in Fluid Mechanics*, Academic Press, N.Y., 1964.
- 20     Bradshaw, P., "The Analogy Between Streamline Curvature and Buoyancy in Turbulent Shear Flow", J. of Fluid Mech., Vol. 36, Part 1, 1969, pp. 177-191.
- 21     Alber, E. Irwin, "Comparison and Evaluation of Computer Program Results for Rocket Engine Performance Prediction. Chapter V, Boundary Layer Friction and Heat Transfer", prepared by Dynamic Science for Interagency Chemical Rocket Propulsion Group, Contract No. NAS 7-443 NS-82, 1968.

- 22 Keller, H. B., and Cebeci, T., "Accurate Numerical Methods for Boundary Layer Flows, Part II, Two-Dimensional Turbulent Flows", AIAA J., Vol. 10, 1972, page 1193.
- 23 Dang, A. L., Kehtarnavaz, H., and Nickerson, G. R., "Solution of the Boundary Layer Equations with Non-Equilibrium Reacting Chemistry in Rocket Nozzles", 25th JANNAF Combustion Meeting NASA/MSFC, Huntsville, AL, October 1988.

## LIST OF FIGURES

- Figure 1: Schematic of a Nozzle  
Figure 2a: Magnitude of  $\delta/R_0$  for ASE Nozzle  
Figure 2b: Magnitude of  $\delta/R_0$  for SSME Nozzle  
Figure 3: Velocity and Pressure Profiles for ASE Nozzle at the Exit Plane  
Figure 4: Velocity and Pressure Profiles for SSME Nozzle at the Exit Plane

## LIST OF TABLES

- Table 1: Boundary Layer Thrust Deficit for Variety of Engines in the Absence and Presence of the Longitudinal Curvature. Cold Wall Case.

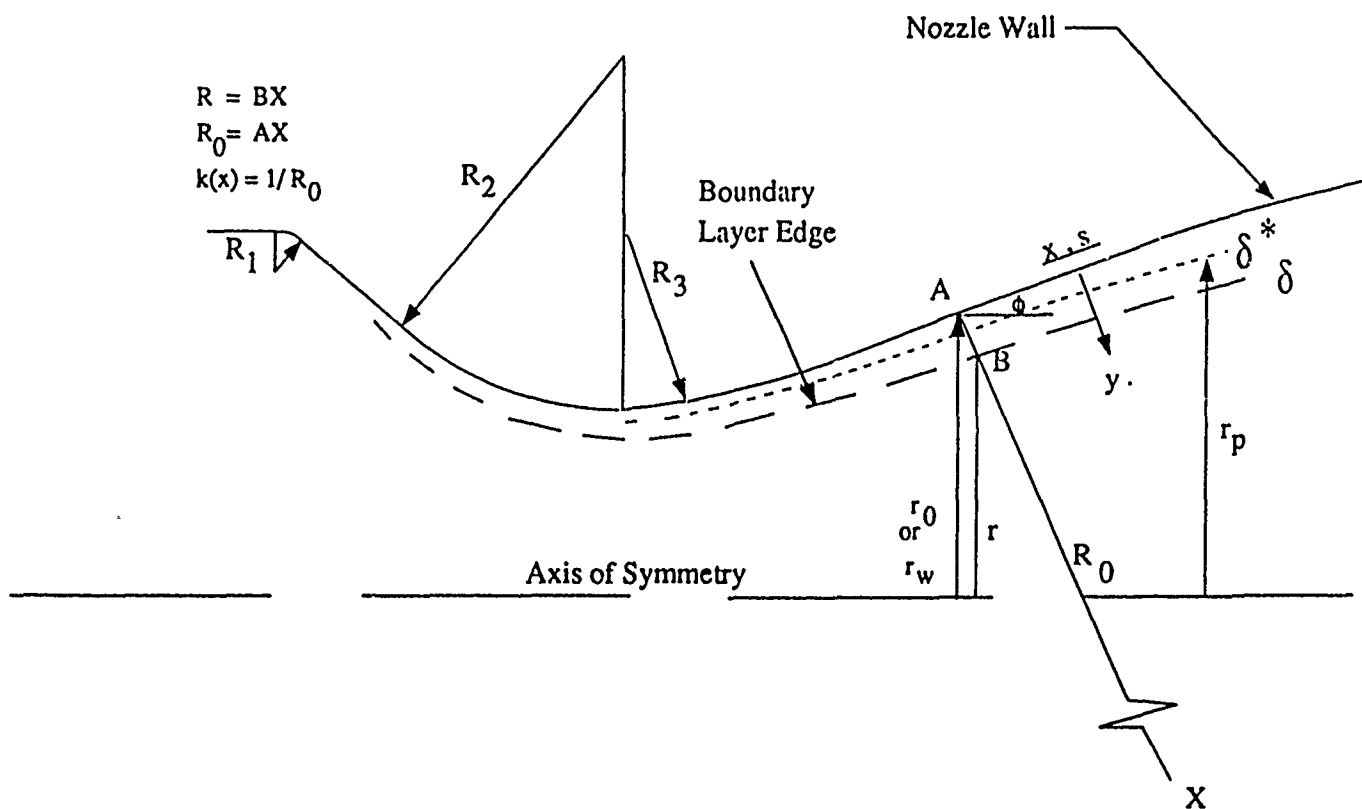


Figure 1: Schematic of a Nozzle



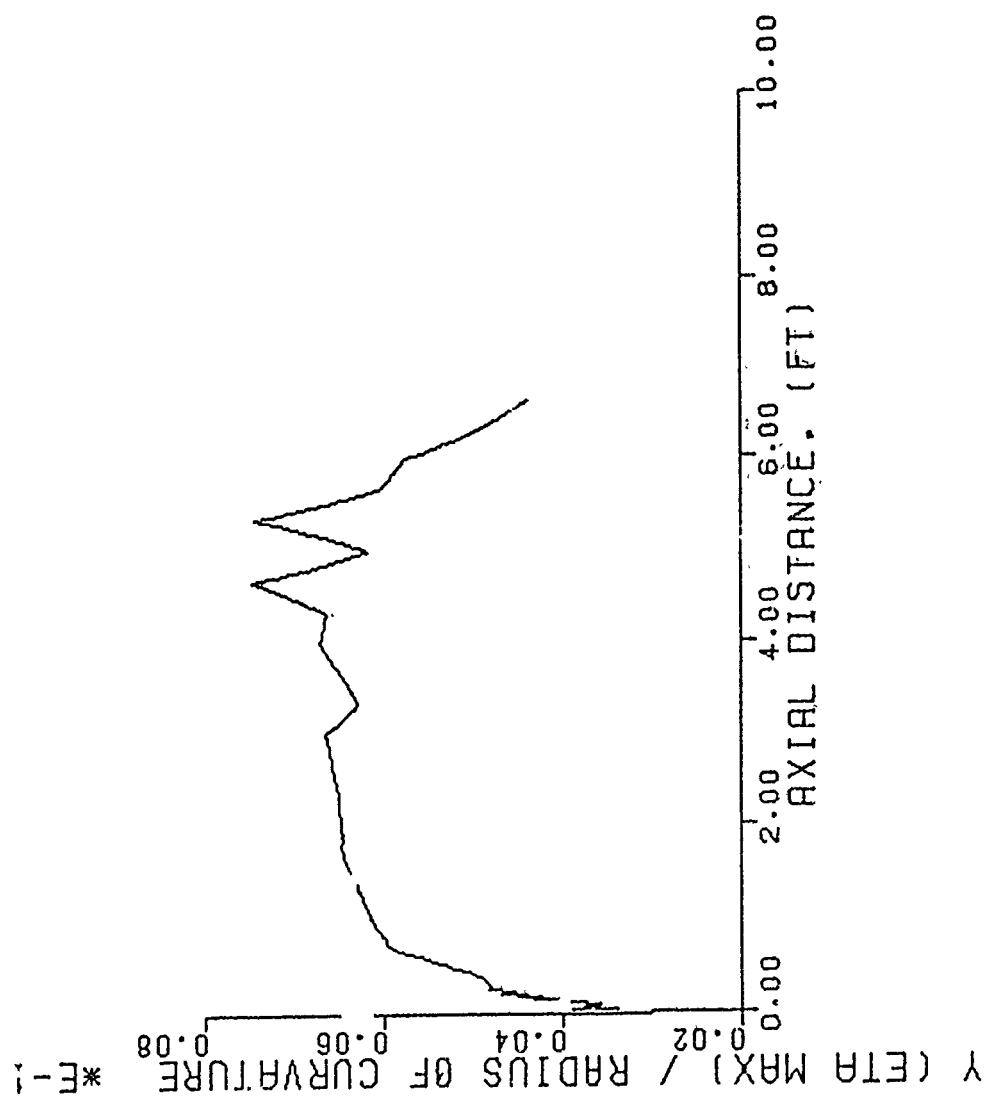


Figure 2a: Magnitude of  $\delta/R_0$  for ASE Nozzle

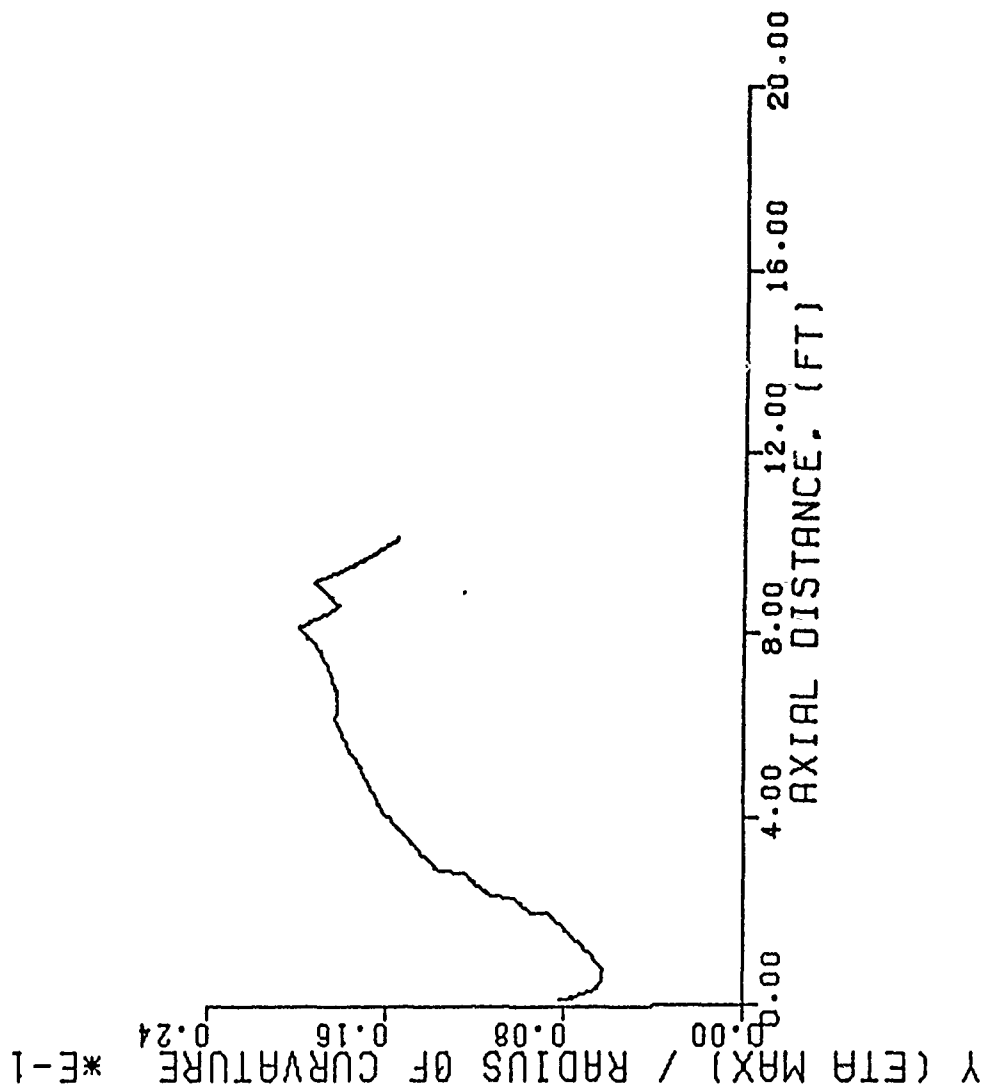


Figure 2b: Magnitude of  $\delta/R_0$  for SSME Nozzle

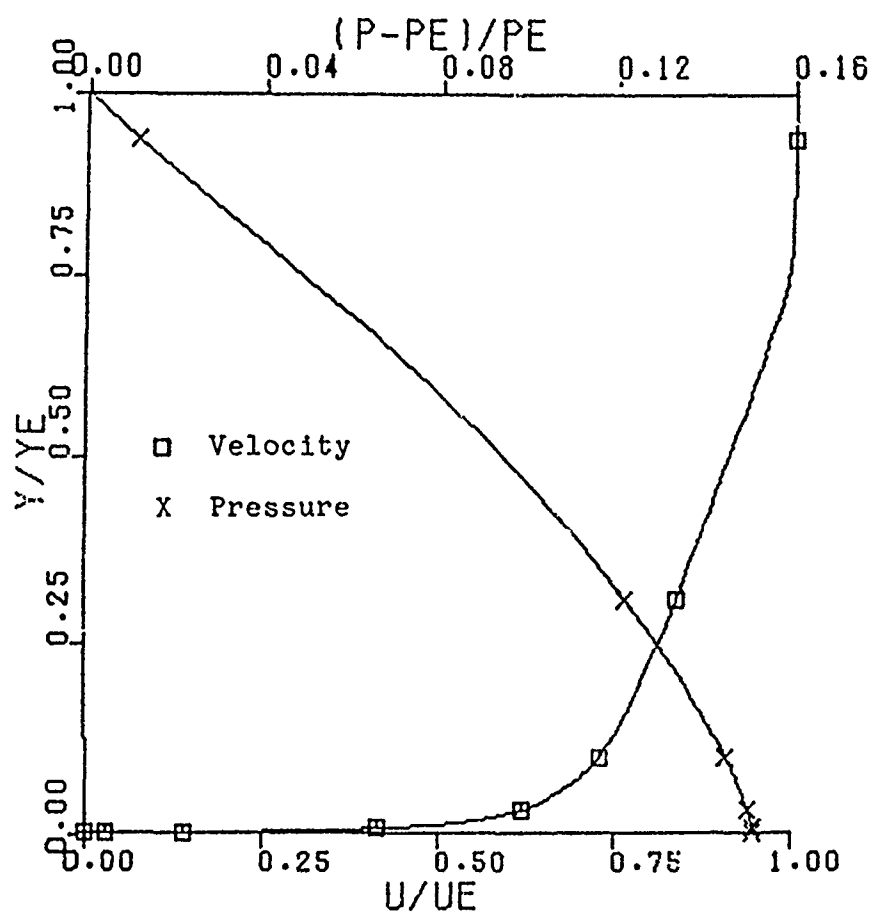


Figure 3: Velocity and Pressure Profiles  
at the nozzle exit plane

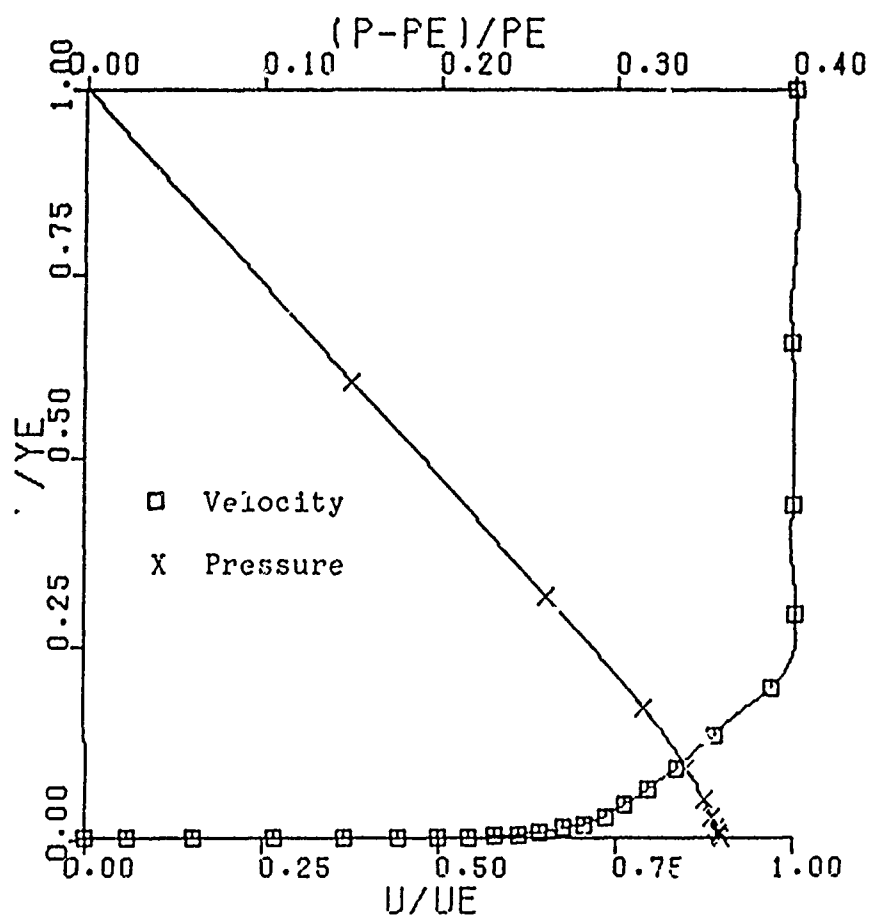


Figure 4: Velocity and Pressure Profiles  
for SSME Nozzle at the Exit Plane

Table 1 Boundary Layer Thrust Deficit for Variety of Engines in the Absence and Presence of the Longitudinal Curvature. Cold Wall Case

NOZZLE	THRUST DEFICIT, lbf. sec./lbm									
	WITHOUT LONGITUDINAL CURVATURE					WITH LONGITUDINAL CURVATURE				
	EQ. A	EQ. B	EQ. C	EQ. D	EQ. E	EQ. A	EQ. B	EQ. C	EQ. D	EQ. E
SS. 5	6.8843	6.7730	6.7650	6.2088	6.2233	6.3720	6.3184	6.4758	6.0387	6.5036
ASE	14.1985	13.6977	13.4572	12.3531	11.9394	14.2351	13.7440	13.5000	12.3782	11.7659
RL-10	11.6549	11.0871	10.8094	10.4630	10.4830	11.7734	11.0714	10.8591	10.4517	10.4964
XDELTA	1.8459	1.8160	1.7902	1.7220	1.8132	1.8459	1.8160	1.7870	1.7215	1.8211
BC4515	0.8688	0.8534	0.8481	0.8142	0.8373	0.8686	0.8534	0.8221	0.8141	0.8378
BC1010	1.8578	1.7941	1.7866	1.8000	1.8790	1.8582	1.7942	1.8121	1.8001	1.8788
IUS	1.9864	1.9523	1.9223	1.8381	2.0943	1.9862	1.9521	1.8524	1.8380	2.0828
XLR-134	27.3282	25.6350	25.3452	24.8578	23.2534	27.3525	25.6539	25.2531	24.6322	23.1904

$$\text{Eq. A } \Delta T = 2\pi \cos\phi [\rho_0 u_0^2 r_0 \bar{\theta} - r_0 \delta^* (p_0 - p_\infty)]$$

$$\text{Eq. B. } \Delta T = 2\pi [\rho_0 u_0^2 r_0 \bar{\theta} \cos\phi - r_0 \delta^* (p_0 - p_\infty) \cos\phi]$$

$$\text{Eq. C. } \Delta T = 2\pi [\rho_0 u_0^2 r_0 \bar{\theta} \cos\phi - r_p \delta^* (p_0 - p_\infty) \cos\phi]$$

$$\text{Eq. D. } \Delta T = 2\pi [\rho_0 u_0^2 r_0 \bar{\theta} \cos\phi - r_p \delta^* (p_0 - p_\infty) \cos\phi] - \int_0^s \rho_0 u_0^2 r_0 \bar{\theta} \cos\phi \frac{\partial}{\partial x} \left( \frac{r}{r_0} \right) dx$$

$$\text{Eq. E. } \Delta T = \int_0^s (p_0 - p_\infty) 2\pi r_p \frac{dr}{dx} dx - \int_0^s (p_w - p_\infty) 2\pi \frac{\partial}{\partial x} (r \delta^* \cos\phi) dx + \int_0^s r_w 2\pi (r_p + \delta^* \cos\phi) \cos\phi dx$$

In all the above equations  $\tau(x) = 0$

# BOUNDARY LAYER LOSS MODELS IN NOZZLE IN PERFORMANCE PREDICTION

Douglas E. Coats, Daniel R. Berker, Alan Kawasaki

Software and Engineering Associates, Inc.  
Carson City, Nevada

## ABSTRACT

This paper details the importance of boundary layer shear stress models in predicting the boundary layer parameters of interest. Laminar and turbulent boundary layers are investigated. Different shear stress models are considered for a wide range of liquid and solid propellant systems and over a range of nozzle expansion ratios. Simple empirical fits to the computed results models for solid and liquid systems are also given.

## INTRODUCTION

The trend toward very large area ratio nozzles, which result in performance gains for space propulsion applications, has increased the need for detailed knowledge of the momentum losses due to nozzle viscous effects (i.e., boundary layer). These losses degrade overall system performance, such as increasing system weight, decreasing useful payload weight, and/or decreasing effective system range. Another important factor in the designing of propulsive nozzles is the detailed knowledge of heat transfer at the wall for regeneratively cooled walls and/or material performance.

Because of the importance to rocket propulsion, the Astronautics Laboratory at Edwards Air Force Base has sponsored the Boundary Layer Study Contract to improve the understanding and computational predictive capabilities for boundary layers in rocket nozzles with high area ratios. As part of this study, the sensitivity of the computed boundary layer loss to various parameters was investigated. The effects of both longitudinal and transverse curvature were reported in Reference 1 and 2. Interactions between the viscous wall shear layer and the inviscid core have been reported in Reference 3. This paper discusses the importance of validating the turbulent shear stress model.

The methods used to calculate the boundary layer performance loss are presented first. The magnitude of the differences between methods of computing  $\Delta I_{spBL}$  are not small<sup>2,4</sup> and should be addressed by the propulsion community.

Results of boundary layer losses are then presented for a variety of liquid and solid systems. Computations are for both laminar and turbulent flows (eddy viscosity model) using the TDK<sup>5</sup>, SPP<sup>6</sup>, and VIPER<sup>7-8</sup> codes. Results comparing eddy viscosity and  $\bar{k}-\epsilon$  turbulence models are presented for one case.

## NOMENCLATURE

$I_{sp}$	Specific impulse	<u>Greek Letters</u>	
$\bar{K}$	Kinetic energy of turbulence	$\delta$	Boundary layer thickness
$L$	Unit length	$\delta^*$	Displacement thickness
$p$	Pressure	$\epsilon$	Turbulence dissipation rate also expansion ratio
$Pr$	Prandtl number	$\phi$	Wall angle
$R_C$	Radius of longitudinal curvature	$\mu$	Viscosity
$r$	Radius of transverse curvature	$\nu$	Kinematic viscosity
$Re$	Reynolds number	$\rho$	Density
$t$	$= y \cos \phi / r_0$	$\theta$	Momentum thickness
$T$	Thrust	$\tau$	Shear stress
$u, v$	Velocity components		
$x, y$	Coordinate system		

### Subscripts

BL	Boundary layer
D	Delivered

Approved for public release; distribution is unlimited.

## CALCULATION OF THE BOUNDARY LAYER LOSS IN NOZZLE FLOWS

The conventional JANNAF method 9-10 for evaluation of the viscous thrust loss in rocket engine nozzle employs both the boundary layer momentum and displacement thickness. This method can be arrived at by two different approaches as shown by Alber<sup>11</sup>. The basis for the approach is to compare the thrust of an inviscid nozzle to a viscous nozzle with the same mass flow rate. In the equation given below, the first term represents the pressure forces acting on an inviscid nozzle and the second and third terms represent the total stress forces acting on the viscous nozzle.

$$\Delta T = \int_0^s (p_e^* - p_\infty) 2\pi r_p \frac{dr_p}{dx} dx - \int_0^s (p_w - p_\infty) 2\pi (r_p + \bar{\delta}^* \cos \phi) \frac{d(r_p + \bar{\delta}^* \cos \phi)}{dx} dx \quad (1)$$

$$+ \int_0^s \tau_w 2\pi (r_p + \bar{\delta}^* \cos \phi) \cos \phi dx$$

where  $r_p$  is the distance from the axis to the potential wall and  $p^*$  is the pressure at  $r_p$ , as is shown in Figure 1.

When the boundary layer characteristics lengths,  $\delta$ ,  $\theta$ , and  $\delta^*$ , are assumed to be small compared to the characteristic nozzle lengths,  $r$  and  $R_0$ , then equation (1) reduces to the standard JANNAF relation<sup>10</sup>

$$\Delta T = 2\pi \cos \phi \left[ \rho_e u_e^2 r_0 \theta - r_0 \delta^* (p_e - p_\infty) \right] \quad (2)$$

If the boundary layer thickness assumption that  $\delta/R_0 \ll 1$  is relaxed, then the modified JANNAF relation can be derived<sup>4</sup>, i.e.,

$$\frac{\Delta T}{2\pi} = \rho_e u_e^2 r_0 \bar{\theta} \cos \phi - r_0 \bar{\delta}^* (p_e - p_\infty) \cos \phi \quad (3)$$

using the alternate forms of the momentum and displacement thicknesses for axisymmetric flows shown below

$$(\text{momentum thickness}) \quad \bar{\theta} = \int_0^{\delta} \frac{r}{r_0} \frac{\rho u}{\rho_e u_e} \left[ 1 - \frac{u}{u_e} \right] dy \quad (4a)$$

$$(\text{displacement thickness}) \quad \bar{\delta}^* = \int_0^{\delta} \frac{r}{r_0} \left[ 1 - \frac{\rho u}{\rho_e u_e} \right] dy \quad (4b)$$

Table 1 (from Reference 2) shows that the differences in boundary layer loss as computed from Equation 1, 2, and 3 (columns E, A, and B respectively) are significant for nozzles with thick boundary layers.

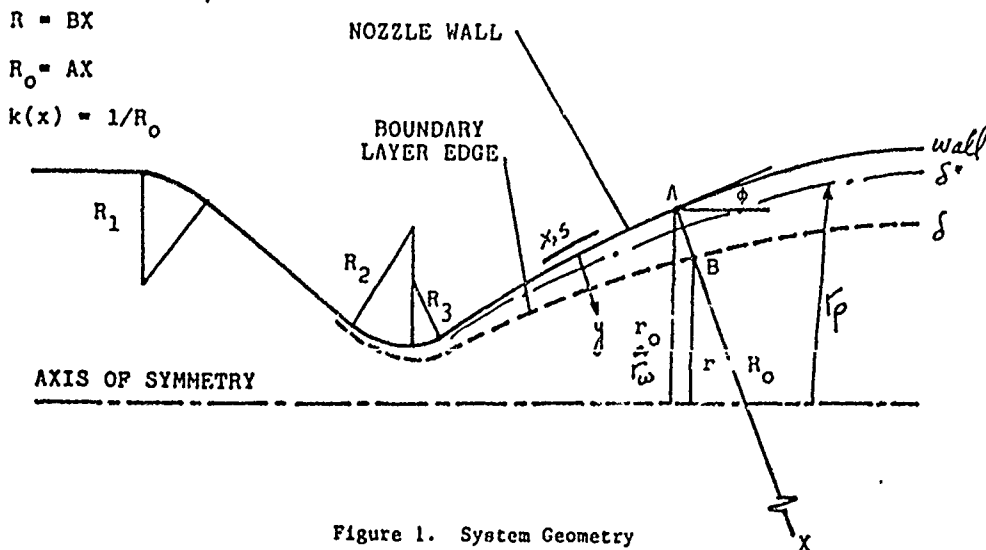


Figure 1. System Geometry

Table 1 Boundary Layer Thrust Deficit for Variety of Engines in the Absence and Presence of the Longitudinal Curvature. Cold Wall Case

NOZZLE	THRUST DEFICIT, lbf. sec./lbm									
	WITHOUT LONGITUDINAL CURVATURE					WITH LONGITUDINAL CURVATURE				
	EQ. A	EQ. B	EQ. C	EQ. D	EQ. E	EQ. A	EQ. B	EQ. C	EQ. D	EQ. E
SSME	6.8843	6.7730	6.7650	6.2088	6.2733	6.3720	6.3184	6.4758	6.0387	6.5036
ASE	14.1985	13.6977	13.4572	12.3531	11.9394	14.2351	13.7440	13.5000	12.3782	11.7659
RL-10	11.6349	11.0871	10.8094	10.4630	10.4930	11.7732	11.0714	10.8591	10.4517	10.4964
XDELTA	1.8459	1.8160	1.7902	1.7220	1.8132	1.8450	1.8160	1.7870	1.7215	1.8211
BC4515	0.8688	0.8534	0.8481	0.8142	0.8373	0.8686	0.8534	0.8221	0.8141	0.8378
BC1010	1.8578	1.7941	1.7866	1.8000	1.8790	1.8582	1.7942	1.8121	1.8001	1.8788
IUS	1.9864	1.9523	1.9223	1.8381	2.0843	1.9862	1.9521	1.8524	1.8380	2.0828
XLR-134	27.3282	25.6350	25.3452	24.8578	23.2534	27.3525	25.6539	25.2531	24.6322	23.1904

$$\text{Eq. A. } \Delta T = 2\pi \cos\phi \left\{ \rho_0 u_0^2 r_0 \bar{\theta} - r_0 \delta^* (p_0 - p_\infty) \right\}$$

$$\text{Eq. B. } \Delta T = 2\pi \left\{ \rho_0 u_0^2 r_0 \bar{\theta} \cos\phi - r_0 \delta^* (p_0 - p_\infty) \cos\phi \right\}$$

$$\text{Eq. C. } \Delta T = 2\pi \left\{ \rho_0 u_0^2 r_0 \bar{\theta} \cos\phi - r_0 \delta^* (p_0 - p_\infty) \cos\phi \right\}$$

$$\text{Eq. D. } \Delta T = 2\pi \left\{ \rho_0 u_0^2 r_0 \bar{\theta} \cos\phi - r_0 \delta^* (p_0 - p_\infty) \cos\phi - \int_0^s \rho_0 u_0^2 r_0 \bar{\theta} \cos\phi \frac{\partial}{\partial x} \left( \frac{r}{r_0} \right) dx \right\}$$

$$\text{Eq. E. } \Delta T = \int_0^s (p_0 - p_\infty) 2\pi r_p \frac{dr}{dx} dx - \int_0^s (p_w - p_\infty) 2\pi \frac{\partial}{\partial x} (r \delta^* \cos\phi) dx + \int_0^s r_w 2\pi (r_p + \delta^* \cos\phi) \cos\phi dx$$

in all the above equations  $\tau(x) = 0$



## ROLE OF TURBULENCE MODELS

The unsteady Navier-Stokes equations are generally recognized as being capable of accurately describing both laminar and turbulent flows. However, the difficulties associated with resolving the various length scales in turbulent flows has removed direct solution of these equations from practical engineering usage. Instead, the time or Reynold's averaged Navier-Stokes equations are solved for cases of engineering interest. The time averaging of the equation generates "apparent" stresses and heat fluxes which are modeled empirically. This empiricism relates mean flow variables to the apparent stresses.

Two classes of turbulence modeling are currently popular. The first class is the eddy viscosity or mixing length methods which trace their origins to Boussinesq and Prandtl. These methods are also referred to as simple algebraic or zero equation models. The second class uses transport equations to evaluate the turbulent Reynolds stress terms. A frequently used two-equation model is the  $\bar{k}$ - $\epsilon$  method which was first proposed by Harlow and Nakayama<sup>12</sup>. Some popular  $\bar{k}$ - $\epsilon$  methods follow the work of Jones and Launder<sup>13</sup> and Launder and Spalding<sup>14</sup>.

The JANNAP standard codes for evaluating boundary layer losses, i.e., SPP-BLM<sup>6</sup>, TDK-BLM/MABL<sup>5</sup>, and BLIMP-J<sup>15</sup> all use the Cebeci-Smith eddy viscosity model<sup>16</sup>. The VIPER code being developed under this effort includes both the Cebeci-Smith eddy viscosity model and a  $\bar{k}$ - $\epsilon$  model, see Reference 7 and 8.

With the success of viscous flow calculations it is easy to forget the origin and amount of empiricisms that go into these calculations. All of these turbulence models were developed for air and pressure gradients which seem very modest by rocket nozzle standards. A study conducted by Evans<sup>17</sup> comparing 3 similar eddy viscosity models (Kendall, Bushnell, and Cebeci-Smith) concluded that large differences in heat transfer could occur between these models. The main culprit was assumed to be the way which these models handle density and temperature gradients across the boundary layer, especially in the law of the wall region.

### Baseline Computations

To establish a baseline for the computations, a series of four liquid engines (RL10, SSME, XLR134, and ASE) were run on the TDK/BLM codes and eight solid motor cases on SPP/BLM. The results of these computations are shown in Figure 2. The major reason for higher losses on liquid systems is that these systems tend to have cooled walls and hence higher boundary losses. No attempt was made to correct for the effects of regen heat addition to the core flow on the overall boundary layer loss. As a result of these computations, we found the following expressions to be reasonable fits of the data.

solid propellant systems

$$\Delta I_{spBL} / I_{spD} \times 100 = 0.32 + 3.887 \times 10^{-3} \epsilon$$

liquid propellant systems

$$\Delta I_{spBL} / I_{spD} \times 100 = 1.065 + 6.192 \times 10^{-3} \epsilon$$

where  $\epsilon$  is the nozzle area ratio

While the above can be used for estimates of the boundary layer loss, care should be exercised for liquid systems since the amount of heat extracted from the flow (and hence  $\Delta I_{spBL}$ ) varies greatly from engine to engine and is not a function of area ratio.

### PNS Results

Computations were performed for six liquid propellant rocket engines using the VIPER<sup>7-8</sup> code. The VIPER code was selected for this study because it contains all of the models to do a complete and consistent set of calculations. It can

treat both laminar and turbulent flow with reacting chemistry. It has two turbulence models, Cebeci-Smith and  $\bar{k}$ - $\epsilon$ , and can handle very thick boundary layers since the core flow and wall shear layer are directly coupled. The boundary layer loss was computed as the integral of the shear stress along the wall (last term in equation 1).

Laminar and turbulent (eddy viscosity) results were obtained for all six nozzles. The characteristics of these engines are given in Table 2 and the results are shown in Figure 3. While there is a significant amount of scatter in the computed results, it is clear that the turbulent losses are from 2 to 4 times larger than the laminar losses.

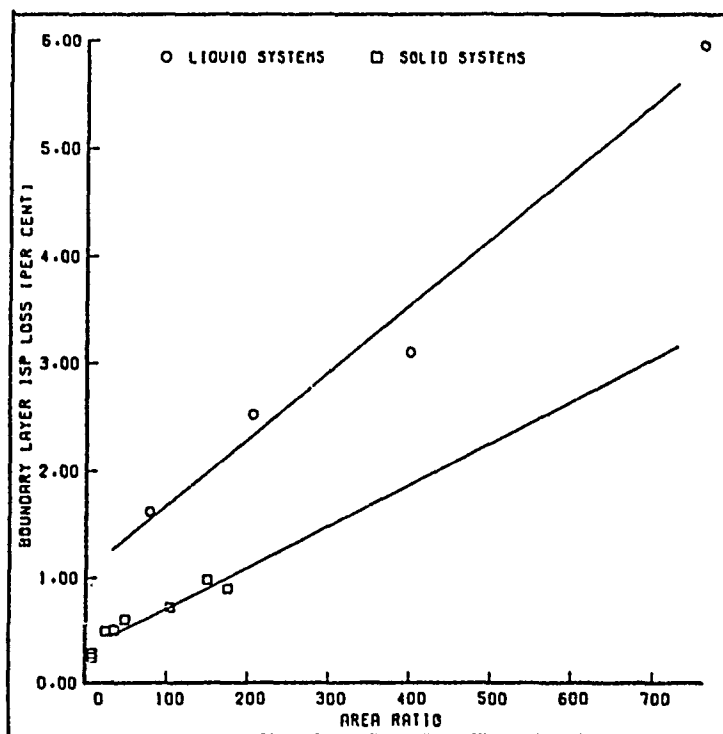


Figure 2. Boundary Layer Loss as a Function of Area Ratio

Table 2. Engine Characteristics

Engine Name	Chamber Pressure	Throat Radius(in)	Expansion Ratio
NASA/Lewis Hi-E	360	.5	1025.
XLR-134	510	.396	767.9
RCS	150	1.021	28.46
SSME	3285	5.1527	77.5
RL 10	394.3	2.57	209.03
ASE	228	1.254	400.7

Unfortunately the  $\bar{k}-\epsilon$  turbulence model incorporated in VIPER turned out not to be as robust as we had hoped and we were able to obtain reasonable results for only one case. That case was the XLR-134 high expansion ratio nozzle. The following table shows the results for this nozzle using frozen chemistry.

Table 3. XLR 134 Boundary Layer Loss Results

Turbulence Model	Delivered $I_{sp}$	$\Delta I_{sp_{BL}}$	$\Delta I_{sp}/I_{sp} \%$
Cebeci Smith	456.377	17.839	3.909
$\bar{k}-\epsilon$	452.833	23.688	5.231

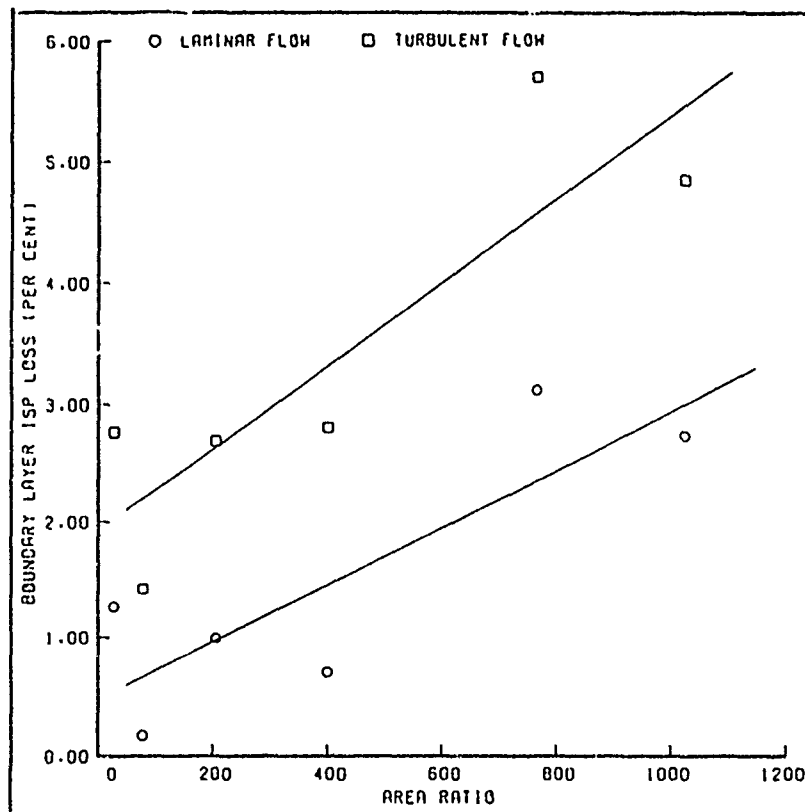


Figure 3. Laminar and Turbulent Boundary Layer Loss Comparison

No matter how the comparison of the above is made, a one percent difference in delivered  $I_{sp}$  has to be considered significant.

The magnitude of the boundary layer loss and the discrepancy between turbulence models can only be resolved by very careful boundary layer measurements in an environment similar to a rocket engine.

It is obvious from the results presented here that experimental validation of boundary layer loss models is required if the design margins on future high area ratio space systems are to be lowered. To put this statement in perspective, the rule of thumb is that a loss of 1% in  $I_{sp}$  results in a 2% loss in payload.

### CONCLUSIONS

The magnitude of the boundary layer performance loss has been shown to range 1 to 6% of the total delivered  $I_{sp}$  for liquid propellant rocket engines with moderate to high area ratios. The effect of turbulence has been shown to increase the performance loss over a laminar boundary layer by factors of 2 to 6 making the onset of turbulence a critical factor for small high area ratio nozzles.

The uncertainty in turbulence models had been previously estimated to be in the 10 - 25% range on predicted  $I_{sp}$  loss. The calculations presented here showed a range of 25 - 33% depending on the selected base.

## REFERENCES

1. Kehtamavaz, H. and Coats, D.E., "Effects of Transverse and Longitudinal Curvature on Nozzle Boundary Layer Growth", AIAA-87-1821, 23rd Joint Propulsion Meeting, San Diego, CA, June 1987.
2. Kehtamavaz, H., Coats, D.E., Nickerson, G.R., and Dang, A.L., "Two-Dimensional Kinetics (TDK) Nozzle Performance Computer Program-Thick Boundary Layer Version", Software and Engineering Associates, Inc., Report no AFAL-TR-87-031, March 1987.
3. Kehtamavaz, H., Coats, D.E., and Kronyon, Y., "Thick Boundary Layer Assessment For Nozzle Flow", AIAA-88-3160, 24th Joint Propulsion Meeting, Boston, MA, 1988.
4. Kehtamavaz, H., Coats, D.E., and Dang, A.L., "Viscous Loss Assessment In Rocket Engines", to be published in the Journal of Propulsion and Power.
5. Nickerson, G.R., Coats, D.E., Dang, A.L., Dunn, S.S., and Kehtamavaz, H., "Two-Dimensional Kinetics Nozzle Performance Computer Program, Volumes I, II, and III, Programing Manual", Software and Engineering Associates, Inc., prepared for GMSFC, Contract NAS8-36863, 31 March 1989.
6. Nickerson, G.R., Coats, D.E., Dang, A.L., Dunn, S.S., "The Solid Propellant Rocket Motor Performance Computer Program (SPP), Version 6.0", Vol. I, II, IV, AFRPL TR-87-078, December 1987.
7. Dang, A.L., Kehtamavaz, H., and Coats, D.E., "PNS Solution of Non-Equilibrium Reacting Flow in Rocket Nozzles", 25th JANNAF Combustion Meeting, Vol. II, pp103-116, NASA/MSFC, Huntsville, AL, October 1988.
8. Dang, A.L., Kehtamavaz, H., and Coats, D.E., "The Use of Richardson Extrapolation in PNS Solutions of Rocket Nozzle Flow", AIAA Paper 89- 2895, 25th AIAA/ASME/SAE/ASEE Joint Propulsion Conference, Monterey, CA, July 10-22, 1989.
9. Pieper, J.L., "Performance Evaluation Methods for Liquid Propellant Rocket Thrust Chamber", CPIA Publication No. 132, prepared for the Performance Standardization Working Group, November 1966.
10. "JANNAF Rocket Engine Performance Prediction and Evaluation Manual", CPIA Publication No. 246, April 1975.
11. Alber, E. Irwin, "Comparison and Evaluation of Computer Program Results for Rocket Engine Performance Prediction, Chapter V., Boundary Layer Friction and Heat Transfer", prepared by Dynamic Science for Interagency Chemical Rocket Propulsion Group, Contract No. NAS 7-443 NS-82, 1968.
12. Harlow, F.H. and Nakayama, P.I., (1968). Transport of Turbulence Energy Decay Rate, Los Alamos Scientific Laboratory Report LA-3854, Los Alamos, New Mexico.
13. Jones, W.P. and Launder, B.E., (1972). The Prediction of Laminarization with a Two-Equation Model of Turbulence, *Int. J. Heat Mass Transfer*, vol. 15, pp. 301-314.
14. Launder, B.E. and Spalding, D.B. (1974). The Numerical Computation of Turbulent Flows, *Comput. Methods Appl. Mech. Eng.*, vol 3, pp. 269-289.
15. *3LIMP-J User's Manual*, prepared by M. Evans, Aerotherm Division/Acurex Corporation, under Contract NAS8-30930, July 1975.
16. Cebeci, T., and Smith, A.M.O., "Analysis of Turbulent Boundary Layers, Academic Press, NY, 1974.
17. Evans, M., "JANNAF Boundary Layer Integral Matrix Procedure", Aerotherm Report 75-152, NAS8-30930, July 1975.

APPENDIX B  
TECHNICAL PAPERS FROM THE PHASE 2 WORK EFFORT

<u>Paper Name</u>	<u>Page No.</u>
Thick Boundary Layer Assessment for Nozzle Flow	B-1

(Reprinted with permission)

# AIAA'88

**AIAA-88-3160**

**Thick Boundary Layer Assessment  
for Nozzle Flow**

H. Kehtarnavaz and D.E. Coats,  
Software Engineering Associates,  
Inc., Carson City, NV; and Y.  
Kronzon, Pennsylvania State Univ.,  
Mechanical Engineering Department,  
University Park, PA

**AIAA/ASME/SAE/ASEE 24th JOINT  
PROPULSION CONFERENCE**

July 11-13, 1988/Boston, Massachusetts

For permission to copy or republish, contact the American Institute of Aeronautics and Astronautics  
370 L'Enfant Promenade, S.W., Washington, D.C. 20024

# THICK BOUNDARY LAYER ASSESSMENT FOR NOZZLE FLOW

H. Kehtarnavaz\* and D. E. Coats\*\*  
Software and Engineering Associates, Inc.  
Carson City, Nevada

Y. Kronzon†  
Pennsylvania State University  
Mechanical Engineering Department  
University Park, Pennsylvania

## ABSTRACT

The effects of thick boundary layers on nozzle flow performance has been investigated. The relationship between the boundary layer and the core flow for a variety of real engine parameters has been established. Euler/boundary layer solutions are compared against the full Navier-Stokes solver and PNS solver. These solutions have been compared to the standard JANNAF TDK/BLM computer code.

The interaction between the viscous layer and the core flow has been studied for a thick boundary layer where the "thin" shear layer equations are not valid. This study is for perfect gas with constant  $\gamma$ .

The validity and restrictions for "thin" shear layer assumption for thick boundary layers has been studied.

## ABBREVIATIONS

ASE	Rocketdyne Advanced Space Engine
BLM	Boundary Layer Module of the TDK/BLM Computer Program
CFL	Courant, Levy, and Friedrichs (Number)
$I_{sp}$	Specific Impulse
OTV	Orbital Transfer Vehicle
SBS-1A	Hughes Spacecraft Engine
SSME	Space Shuttle Main Engine
TDK	Two-Dimensional Kinetic Computer Code
XLR-134	Low Thrust Cryogenic Engine, OTV

\* Research Scientist, Member AIAA  
\*\* Vice President, SEA, Inc., Member AIAA  
† Research Associate, Presently at AFAL

## I. INTRODUCTION

The trend towards very large area ratio nozzles, which result in performance gains for space applications, has increased the need for detailed knowledge of the momentum losses due to nozzle viscous effects (i.e., boundary layer) and the flowfield parameters in propulsion systems. These losses degrade overall system performance as it directly affects payload efficiencies such as increasing system weight, decreasing useful payload weight, and decreasing effective system range.

As the interest in understanding of high speed flows and performance of propulsive nozzles increases, there is need for the development of more precise computational techniques. The performance loss in high expansion ratio nozzles due to the viscous layer is a critical design parameter in selecting the nozzle geometry. Recent studies<sup>(1-3)</sup> indicate that for high area ratio nozzles, the viscous layer can become quite thick such that the evaluation of losses due to this layer based upon the traditional Prandtl thin shear layer approximation could be insufficient for its application. Although the second order boundary layer equations could be utilized for obtaining improved results, there is still a need for superior techniques to treat "thick" viscous layers.

Very powerful computational capabilities have been developed in the application of finite difference techniques to the solution of the fluid dynamic equations governing compressible flows.

The most notable algorithm was introduced by McCormack in his classic 1969 paper on the effect of viscosity on hypervelocity impact cratering<sup>(4)</sup>. His explicit solution technique, which is a variation on the Lax-Wendroff second order method, uses a predictor-corrector operator to achieve second order accuracy while using a first order accurate finite difference approach. Since this method is easily applied to complex flowfield problems, it is widely used in the CFD community today<sup>(5)</sup>.

To resolve the viscous layer portion of the flow in Navier-Stokes solvers, a fine mesh should be considered near the wall region. This will result in increasing the computation time considerably. To some extent, this difficulty has been overcome by the development of PNS (parabolized Navier-Stokes) equations and PNS-based computer programs.

The parabolized Navier-Stokes equations neglect the streamwise diffusion term, which along with special treatment of the subsonic region of the boundary layer removes the spatial ellipticity from the steady form of the equations and permits a solution by streamwise marching computational techniques. The major advantage of the PNS codes, in general, is that they solve a steady form of the governing equations and are much more efficient than time-dependent codes for solution of the unsteady Navier-Stokes equations. Due to these attributes, PNS codes are widely used today to analyze fluid dynamics of compressible flow.

Our goal in this work was to establish a fundamental understanding of thick viscous layers. Supersonic flows in propulsive nozzles have been considered in this work. Three codes (NS, PNS, and boundary layer solvers) were selected and exercised on the candidate engines embracing laminar to fully turbulent boundary layer flows.

## II. TEST CASES AND CODES

A list of candidate engines and their specifications is shown in Table 1. The test cases cover the whole range of laminar (300:1 nozzle) to completely turbulent nozzle flows (ASE and SSME). The software selected to perform this study were the TDK/BLM code<sup>(1)</sup>, a PNS code<sup>(20)</sup>, the AXI2DS (Euler) code<sup>(28)</sup>, and the VNAP2 (NS) code<sup>(21)</sup>.

Some of the computer programs had to be modified to increase the resolution and/or computation accuracy. Both the inviscid and viscous solutions are obtained and compared.

## III. INVISCID SOLUTION

A comparison between the TDK, VNAP2, and AXI2DS code results for the nozzle mass flow rate, thrust, and  $I_{sp}$  are presented in Table 2. The VNAP2 Code (NS Solver) was modified to separate the subsonic/transonic and supersonic portion of the flow. The validity of "segmentation" of the nozzle has been discussed elsewhere<sup>(6)</sup> and it has been shown that this method results in accurate solutions in a fairly reasonable amount of computation time.

There is excellent agreement between VNAP2 in the Euler mode and TDK. AXI2DS yields comparable results; however, due to the poor grid resolution in AXI2DS, the results are slightly different from the other two. From this table it can be concluded that for low thrust engines, such as the Hughes 300:1 engine,  $I_{sp}$  is very sensitive to the nozzle mass flow rate due to the small mass flow rates.

So, for low thrust engines, it is necessary that the methodology being used must conserve mass as much as possible. Also, from Table 2, it can be observed that poor grids have significant effect on the higher area ratio nozzles, i.e., for high expansion ratio nozzles, such as the XLR-134, an enormous number of grid points is necessary to solve the flowfield correctly.

## IV. VISCOUS SOLUTIONS

The results of the thrust and  $I_{sp}$  calculations for all the test cases and for the viscous flows are tabulated in Table 3. The initial line properties for the PNS Code were taken from the VNAP2 solution. For the low thrust engine, the flow is laminar and the viscous layer occupies about 30% of the nozzle ( $\delta_{995}/r = .30$ ), and disagreement between TDK/BLM and VNAP2 is basically due to the

Table 1: Candidate Engines for Thick Boundary Layer Study

ENGINE	APPLICATION	PROPELLANT	THRUST (lb <sub>f</sub> )	CHAMBER PRESSURE (psia)	THROAT RADIUS, R <sub>t</sub> (inches)	REYNOLDS NUMBER $Re_{R_t}$	EXPANSION RATIO
SSME (Space Shuttle Main Engine)	SSTO	LOX/O <sub>2</sub>	163,000	2935.7	5.1527	$1.18 \times 10^7$	77.5:1
ASE (Rocketdyne, Advanced Space Engine)	OTV	LOX/O <sub>2</sub>	22,600	2287	1.254	$2.20 \times 10^6$	400:1
SSS-1A (Hughes Spacecraft Engine)	Spacecraft	H <sub>2</sub> /N <sub>2</sub>	5.45	100	.0925	$3.90 \times 10^4$	300:1
XLR-134	OTV	LOX/CH <sub>4</sub>	511	510	.396	$1.80 \times 10^5$	761:1



Table 2: Comparison of Thrust Calculations for TDK, VNAP2 and AX120S for an inviscid flow of a Perfect Gas, Adiabatic Wall

NOZZLE	TDK			VNAP2 (Euler Mode)					AX120S (Euler Mode)				
	MASS FLOW RATE, lbm/sec	THRUST, lbf	ISP, sec. lbf/lbm	GRIDS		MASS FLOW RATE lbm/sec	THRUST, lbf	ISP, sec. lbf/lbm	% ISP DIFFERENCE WITH TDK	GRIDS		% ISP DIFFERENCE WITH TDK	
				AXIAL x RADIAL	CFL					2D (AXIAL) x 4C (RADIAL)	X ISP		
													TRANSONIC SUPERSONIC
BSME	1058.95	450690.9	425.60	71 x 31	.8	1059.96	450764.6	425.26	.07	1059.96	427552.7	403.36	5.22
				151 x 41	.6								
ASE	49.35	22535.13	456.66	141 x 31	.6	49.2101	22484.48	456.90	-.05	49.21	22195.73	451.03	1.23
				151 x 51	.7								
HUGHES 300:1	0.02193	5.455	248.76	91 x 41	.6	.02212	5.441	246.00	1.11	.02212	5.346	241.67	2.85
				131 x 45	.8								
XLR-134	1.11455	511.49	458.92	121 x 31	.6	1.13193	520.94	460.22	-.28	1.13193	481.03	424.96	7.40
				141 x 51	.6								

resolution of the viscous layer, particularly near the wall. These results are obtained for variable grid spacing with more gridlines close to the wall. However, in TDK/BLM about 120 points are assumed in the viscous layer as opposed to about 20 points in the NS or PNS solvers. So, it can be concluded that the discrepancy between these results is due to the resolution of the viscous layer.

There are still fundamental questions that have to be answered; that is how thick is the subsonic layer and how accurate can an NS or PNS solver predict the thickness of this sublayer? Two of the candidate engines, ASE and XLR-134, were chosen to answer these questions for further studies.

In ASE, the viscous layer occupies about 15% of the nozzle and in the XLR-134 nozzle, this value is about 20% ( $\delta_{995}/r$ ). Both adiabatic and cooled walls are considered; and subsonic layer thickness, together with a number of points across the viscous layer and subsonic layer are depicted in Table 4. From this table, it can be observed that generally, if an NS solver is applied to supersonic nozzle flow to resolve the viscous layer, an enormous number of points will be needed which makes the computational time prohibitively large. This table also indicates that the subsonic layer thickness is about 1% of the boundary layer and the mass travelling in this sublayer is so small such that it cannot have any major effect on the performance. The thickness of the subsonic layer is very small compared to the viscous layer and the flowfield, and does not establish a concern about the information travelling backward in the nozzle in this sublayer due to the elliptic nature of the governing equations.

#### V. SHEAR LAYER CORE FLOW INTERACTION

In the nozzle expansion, at some point, the Reynold's number can become low enough that the thin shear layer (TSL) or boundary layer equations no longer yield acceptable accuracy for performance prediction. There is no simple way to detect when the TSL equations are no longer adequate.

There are several studies in the area of the inviscid-viscous interaction. Among these are the methods of Carter<sup>(11,12)</sup>, Le Bailly<sup>(13,14)</sup>, Wigton<sup>(15)</sup>, Veldman<sup>(16)</sup> and Moses<sup>(17,18)</sup>. All of these schemes consist of coupling a system of elliptic equations for the inviscid flow to parabolic equations for the boundary layer. However, all of these studies neglect the fact that the parabolic boundary layer equations will not give accurate results for a thick viscous layer in internal flows<sup>(19)</sup>. Higher order boundary layer equations are treated in reference 1 and 2 in a more complete manner than found in most of the literature on viscous-inviscid interaction. However, there is no doubt that for "thick boundary layers," full Navier-Stokes or parabolized Navier-Stokes equations are far better tools for treating the viscous layer. It is our goal in this section to clarify the viscous-inviscid interaction.

For the purpose of this study, the XLR-134 nozzle, which we computed to have a fairly thick boundary layer, was chosen. At each axial station flow values were obtained in a direction perpendicular to the wall (boundary layer coordinate) using the VNAP2 code. Both viscous

Table 3: Comparison of Thrust Calculations for TDK, VNAP2(NS) and PNS Codes for Viscous Flow of a Perfect Gas, Adiabatic Wall

	TDK/BLM			VNAP2					PNS				
NOZZLE	MASS FLOW RATE, lbm/sec	THRUST, lbf	ISP, sec./lbm	GRIDS		MASS FLOW RATE lbm/sec	THRUST, lbf	ISP, sec./lbm	% ISP DIFFERENCE WITH TDK	GRIDS		% ISP DIFFERENCE WITH TDK	
				AXIAL x RADIAL	CFL					70 (AXIAL) x 44 (RADIAL)			
				TRANSONIC	TRANSONIC					MASS FLOW RATE, lbm/sec	THRUST, lbf	ISP, sec./lbm	
				SUPERSONIC	SUPERSONIC								
SSME	1058.95	448512.0	423.54	161 x 81	.6	1042.60	452348.2	433.86	-2.43	1042.60	427930.4	410.44	3.10
				210 x 81	.6								
ASE	49.34	22298.8	451.87	204 x 95	.7	49.54	22123.1	446.58	1.17	49.54	22757.7	459.38	-1.66
				181 x 95	.7								
MUGHES 300:1	0.02193	5.3156	242.39	165 x 55	.6	.02244	5.8914	262.54	-8.31	.02244	5.1682	230.31	4.98
				181 x 81	.7								
XLR-134	1.11455	505.85	453.86	161 x 81	.7	1.21826	537.50	441.20	2.79	1.21826	473.45	388.63	14.37
				161 x 81	.7								

Table 4: Subsonic Layer Thickness Predicted by VNAP2, BLM and PNS Codes

Engine	COOLED WALL ( $T_w = 1000 \text{ R}$ )							ADIABATIC WALL						
	$\delta_{0.995}$ (BLM)	Points Across the Subsonic Layer/ Points Across the Boundary Layer			$\delta_{\text{Subsonic}}$ (inches)			$\delta_{0.995}$ (BLM)	Points Across the Subsonic Layer/ Points across the Boundary Layer			$\delta_{\text{Subsonic}}$ (inches)		
		VNAP2*	BLM	PNS*	VNAP2	BLM	PNS		VNAP2*	BLM	PNS*	VNAP2	BLM	PNS
ASE	2.13	3/14	45/142	5/16	.0178	.0072	.155	2.43	5/15	53/132	4/15	.0527	.0513	.2362
XLR134	2.02	1/5	58/126	3/15	.0071	.0347	.0551	2.22	4/18	63/140	5/14	.0560	.0424	.1561

\* Number of points in the radial direction for ASE is 95 and for XLR134 is 81 with more points close to the wall. This is an approximation for VNAP2 and PNS Codes.

and inviscid solutions were obtained for comparison. The difference between the axial and total velocities for the inviscid and viscous solutions are depicted in Figure 1. Also shown on Figure 1 is the displacement thickness,  $\delta^*$ , as computed by the TDK/BLM code. In classical TSL theory, the effect of the boundary layer on the outer or core flow is taken into account by displacing the wall in the normal direction by  $\delta^*$ . The outer flow is then recomputed using the displaced wall and thus reflects the interaction of the TSL on the core flow. The difference between these two inviscid calculations (from TDK) divided by the original inviscid velocity are shown on Figure 1 and labeled as the TSL asymptote. As is clearly evident in Figure 1, the fractional velocity differences approach a higher asymptote than predicted by TSL theory and at a much farther distance from the wall.

The same results for ASE nozzle are shown in Figure 2. From the boundary layer code  $\delta_{0.995} = 1.5$  inches at  $X = 60$  inches (this is about 7% of the flowfield, i.e.,  $\delta/r = .07$ ). The boundary layer thickness relative to the local transverse curvature ( $\delta/r$ ) is about half of the XLR134 value. So it is anticipated that the boundary layer equations yield more accurate results for the ASE nozzle. From Figure 2, it can be seen that at  $\delta = 1.5$  inches the value of  $(U_{\text{inv}} - U_{\text{vis}})/U_{\text{inv}}$  is changing very slowly as opposed to the region closer to the wall, meaning that the viscous effects are almost dissipated at the 1.5 inches outward from the wall. However, there is still some viscous effects or interaction for distances larger than 1.5 inches.

The VNAP2 and TDK code solutions for inviscid flow of a perfect gas yield the edge condition for solving the boundary layer equations.

Boundary layer equations were solved for all cases using the two sets of edge conditions and the results are indicated in Table 5. This table reveals that for the boundary layer losses, the agreement between the two calculations are not good. Since the boundary layer code used for both calculations was the same, the differences are attributed to the inviscid edge conditions. Both the mesh resolution and accuracy of the Method of Characteristic calculation are considered superior to those of the VNAP2 code.

To examine the magnitude of the streamwise diffusion terms in Navier-Stokes equations, the full NS equations are compared against NS equations without the streamwise diffusion terms for one engine, the ASE. Table 6 compares the thrust and mass flow rate for both cases, and Figure 3 indicates the Mach number and pressure at the exit plane for both cases. Excellent agreement is observed. Figure 3 indicates a severe pressure gradient at the wall throughout the boundary layer and mild pressure gradient for the inviscid portion of the flow. This is compatible with the results in Reference 1 and 2 where the second order boundary layer solution reveals this pressure gradient across the shear layer. These sample results indicate that the magnitude of streamwise diffusion terms in Navier-Stokes equations for supersonic flows, compared to other terms, are very small, and that they can be eliminated from the NS equations. The performance results with axial diffusion term is closer to the TDK/BLM results (see Table 3). However, the difference between the  $I_{sp}$ 's in Table 6 can be due to the numerical scheme rather

than the axial diffusion terms. This has been a conclusion of studies presently being performed at Software and Engineering Associates Inc.

Table 5: Comparison of the Boundary Layer Losses Between TDK/BLM and VNAP2/BLM for Adiabatic Wall

Engine	$I_{sp}$ , lbf. sec./lbm.		
	TDK/BLM	VNAP2/BLM	% Difference (TDK-VNAP2)/TDK
SSHE	2.057	2.184	- 6.17
Hughes 300:1	3.43	2.896	15.57
ASE	4.789	5.614	-17.227
XLR-134	5.635	6.854	-21.633

Table 6: Mass Flow Rate, Thrust and  $I_{sp}$  for the ASE in the Presence and Absence of Axial Diffusion Terms

WITH AXIAL DIFFUSION			WITHOUT AXIAL DIFFUSION		
Mass Flow Rate lbm/sec	Thrust, lbf	$I_{sp}$ , lbf - sec / lbm	Mass Flow Rate lbm/sec	Thrust, lbf	$I_{sp}$ , lbf - sec / lbm
49.54	22,123	446.58	49.63	22,103	445.35

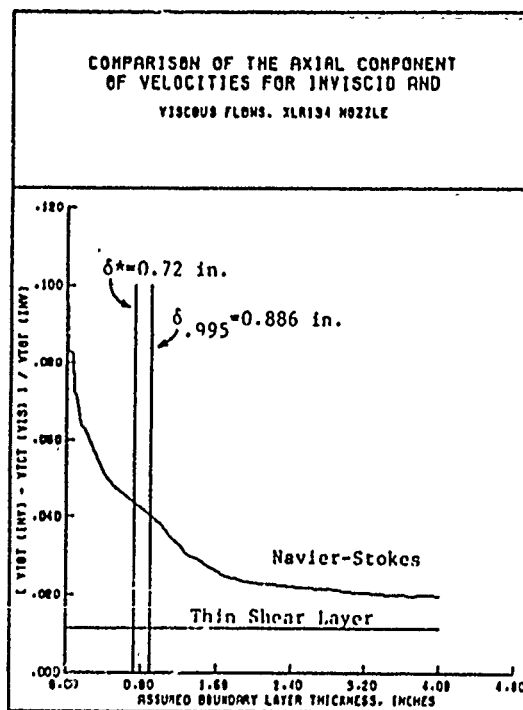
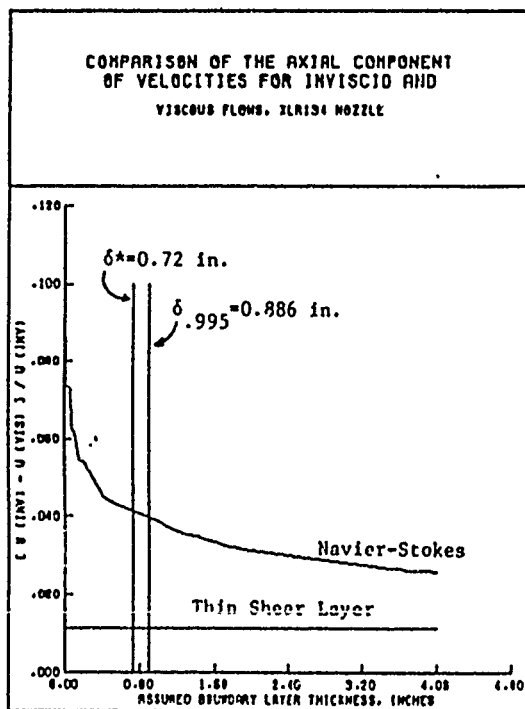


Figure 1. Interaction between the core flow and the viscous layer predicted by the full NS and Thin Shear Layer approximation for XLR-134 Nozzle.

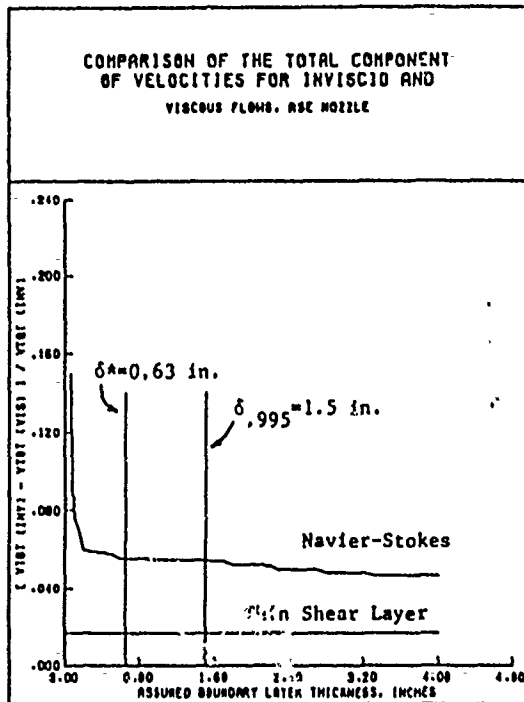
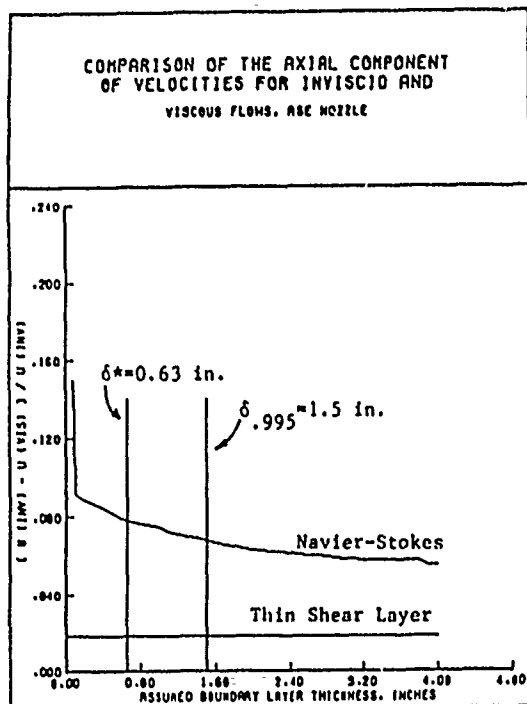


Figure 2. Interaction between the core flow and the viscous layer predicted by the full NS and Thin Shear Layer approximation for ASE Nozzle.

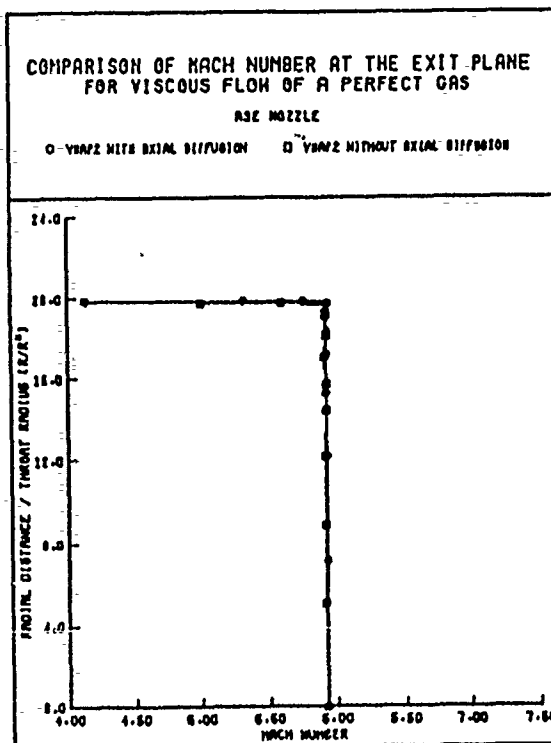
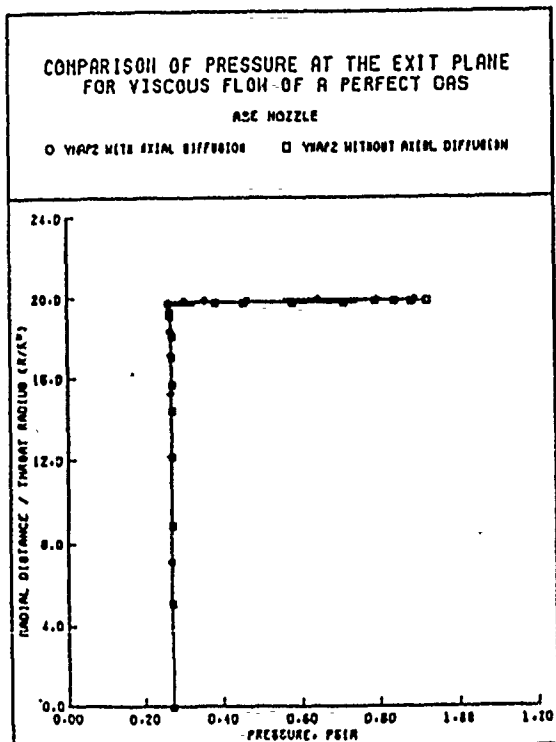


Figure 3. Comparisons of exit plane Mach number and pressure profiles between NS solutions with and without streamwise diffusion for ASE Nozzle.

## VI. CONCLUSION

The effects of various methods of computing the wall shear layer in propulsive nozzles has been studied for relatively thick boundary layers. It was found that for nozzle flows where the computed boundary layer thickness exceeds 10% of the local nozzle radius that calculations based on the traditional Prandtl thin boundary layer assumptions are not of sufficient accuracy for detailed propulsion studies. No firm criteria or methods have been developed to estimate the magnitude of the error associated with the use of the thin shear layer assumptions. The work that this report is based on is still in progress and it is hoped that more definitive results will be generated.

## VII. ACKNOWLEDGMENT

This work was supported by the Air Force Astronautics Laboratory (AFAL) under Contract No. F04611-86-C-0055. The authors wish to thank the contract monitor, Mrs. Elizabeth Slimak, at AFAL, for her support, and also Dr. Phil Kessel for his helpful suggestions.

## REFERENCES

1. Kehtarnavaz, H., Coats, D. E., Nickerson, G. R., and Dang, A. L., "Two-Dimensional Kinetics (TDK) Nozzle Performance Computer Program - Thick Boundary Layer Version," Software and Engineering Associates Inc., AFAL Report No. AFAL-TR-87-031, March 1987.
2. Kehtarnavaz, H., and Coats, D. E., "Effect of Transverse and Longitudinal Curvature on Nozzle Boundary Layer Growth," AIAA Paper No. AIAA-87-1821, 1987.
3. Kehtarnavaz, H., and Coats, D. E., "Thrust Loss in a Rocket Engine Due to Boundary Layer Effects," Submitted to Journal of Propulsion and Power, 1988.
4. MacCormack, R. W., "The Effect of Viscosity on Hypervelocity Impact Cratering," AIAA Paper 69-354, April 1969.
5. Desnoyer, D., "A Two-Schemes Method for Chamber and Nozzle Flows," AIAA Paper No. AIAA-86-0106, 24th Aerospace Sciences Meeting, Reno, NV, January 1986.
6. Buggein, R. C., McDonald, H., and Levy, R., "Development of a Three-Dimensional Supersonic Inlet Flow Analysis," NASA Contractor Report 3218, January 1980.
7. Shirazi, S. A., and Truman, C. R., "Comparison of Algebraic Turbulence Models for PNS Predictions of Supersonic Flow Past a Sphere-Cone," AIAA Paper No. 87-0544, January 1987.
8. Chitsomborn, T., Kumax, A., and Tirvari, S. N., "Numerical Study of Finite-Rate Supersonic Combustion Using Parabolized Equations," AIAA Paper No. 87-0088, January 1987.
9. Sinha, N., and Dash, S. M., "Parabolized Navier-Stokes Analysis of Ducted Turbulent Mixing Problems with Finite-Rate Chemistry," AIAA Paper No. 86-0004, January 1986.
10. Kehtarnavaz, H., and Coats, D. E., "Thick Boundary Layer Assessment," AFAL Report, Contract No. F04611-86-C-0055, 1988.
11. Carter, J. E., "A New Boundary Layer Interaction Technique for Separated Flow," NASA-TM-78690, 1978.
12. Carter, J. E., "Viscous-Inviscid Interaction of Transonic Turbulent Separated Flow," AIAA 81-1241, Presented at AIAA 14th Fluid and Plasma Dynamics Conference, Palo Alto, CA, June 1981.
13. Le Balleur, J. C., "Couplage Visqueux Non Visqueux: Methode Numerique et Applications Aux Ecoulements Bidimensionnels Transoniques et Supersoniques," La Recherche Aerospaciale, No. 1978-2, March-April 1978, pp. 67-76.
14. Le Balleur, J. C., "Calcul des Ecoulements a Forte Interaction Visqueuse au Moyen de Methodes de Couplage," Paper No. 1, AGARD Conference Proceedings No. 291, February 1981.
15. Wigton, L. B., "Viscous-Inviscid Interaction in Transonic Flow," Ph.D. thesis, Dept. of Applied Mathematics, University of California, Berkeley, CA, May 1981.
16. Veldman, A. E. P., "Calculation of Incompressible Boundary Layers with Strong Viscous-Inviscid Interaction," Paper No. 12, AGARD Conference Proceedings No. 291, February 1981.
17. Moses, H. L., Jones, R. R., O'Brien, W. F., and Peterson, R. S., "Simultaneous Solution of the Boundary Layer and Freestream with Separated Flow," AIAA Journal, Vol. 16, No. 1, January 1978, pp. 61-66.
18. Moses, H. L., Thomason, S. B., and Jones, R. R., "Simultaneous Solution of the Inviscid Flow and Boundary Layers for Compressor Cascades," AIAA Journal, Vol. 20, No. 10, Oct. 1982, pp. 1466-1468.
19. Strawn, R. C., Ferziger, J. H., and Kline, S. J., "A New Technique for Computing Viscous-Inviscid Interactions in Internal Flows," AIAA Paper No. A85-11637, 1985.
20. Kronzon, Y., "An Euler and PNS Code for Internal Flow of a Perfect Supersonic Gas," AFAL Personal Communication.
21. Gline, M. C., "VNAP2, A Computer Program for Computation of Two-Dimensional, Time Dependent, Compressible Turbulent Flow," LASL Report LA-8872, August 1981.

APPENDIX C  
TECHNICAL PAPERS FROM THE PHASE 3 WORK EFFORT

<u>Paper Name</u>	<u>Page No.</u>
The Use of Richardson Extrapolation in PNS Solutions of Rocket Nozzle Flow	C-1
PNS Solution of Non-Equilibrium Reacting Flow in Rocket Nozzles	C-14

(Reprinted with permission)



AIAA- 89- 2895

**THE USE OF RICHARDSON EXTRAPOLATION  
IN PNS SOLUTIONS OF ROCKET NOZZLE FLOW**

A.L. Dang and H. Kehtarnavaz  
Physical Research, Inc.  
Irvine, CA

D.E. Coats  
Software & Engineering Associates, Inc.  
Carson City, NV

**AIAA/ASME/SAE/ASEE  
25th Joint Propulsion Conference**  
Monterey, CA / July 10-12, 1989

For permission to copy or republish, contact the American Institute of Aeronautics and Astronautics  
370 L'Enfant Promenade, S.W., Washington, D.C. 20024

# THE USE OF RICHARDSON EXTRAPOLATION IN PNS SOLUTIONS OF ROCKET NOZZLE FLOW

A. L. Dang\*, H. Keshmavaz\*\*  
Physical Research Inc.,  
Irvine, California

D. E. Coats†  
Software & Engineering Associates, Inc.  
Carson City, Nevada

## ABSTRACT

A Parabolized Navier-Stokes Code, VISPER (Viscous Performance Code for Nozzle Flow with Finite Rate Chemistry) has been developed which calculates the internal flow of turbulent and non-equilibrium reacting gases. The technique of Richardson Extrapolation is applied to the 1st order Beam-Warming scheme to provide (i) estimates for the local error at each marching step, (ii) automatic step size variation, and, (iii) extension to second order. The resulting numerical procedure is more stable than the second order Beam-Warming method and has the efficiency of an automatic step size control method. Two turbulence models, mixing length and  $k-\epsilon$ , are used to resolve the wall shear layer. The results from this code are compared against existing experimental data for supersonic combustion and rocket nozzle flows. For the latter, comparisons are also made to predictions from classical inviscid/boundary layer methods. A measure of the interaction between the core flow/boundary layer is obtained and, at the same time, the extent of the validity of the classical method of calculation is revealed.

## NOMENCLATURE

c	mass fraction
$C_p$	specific heat
h	species enthalpy
H	total enthalpy ( $h + V^2/2$ )
J	Jacobian
p	pressure
$P_r$	prandtl number
q	heat flux
R	gas constant
r	transverse curvature
T	temperature
V	velocity
$u, v$	axial and normal components of velocity
x	axial direction
y	normal direction

## Greek Symbols

$\xi, \eta$	transformed coordinates for x and y
$\omega_i$	species production term
$\omega$	Vigneron pressure splitting term
$\mu$	viscosity
$\rho$	density
$\tau$	shear stress

## Superscripts

*	reference value
~	contravariant
i	index in $\xi$ direction (axial)
-	dimensional quantity

## Subscripts

i	species
j	index in $\eta$ direction (radial)
L	laminar
r	reference value
T, t	turbulent
x, $\xi$	in axial or transformed axial direction
y, $\eta$	in normal or transformed normal direction

\* Principal Research Scientist  
Director of CFD

\*\* Senior Research Scientist,  
AIAA Member

† Vice President,  
Senior AIAA Member



## INTRODUCTION

In recent years, there has been a substantial amount of research in computing steady, viscous, internal flow, due to its importance in the design of components such as gas turbine and ramjet combustors, turbo-machinery, inlet ducts, and rocket engine nozzles. The equations that govern such flows are the Navier-Stokes equations. Under certain conditions these flowfields can be accurately predicted with a simplified version of the full Navier-Stokes equations. The Parabolized Navier-Stokes equations represent one such class of simplifications.

Parabolized Navier-Stokes (PNS) equations are a subset of the Navier-Stokes (NS) equations which are valid for predominantly supersonic flow with subsonic shear layers, provided no streamwise separation occurs<sup>1,2</sup>. The PNS equations neglect the streamwise diffusion term which, along with special treatment of the subsonic region of the boundary layer, removes the spatial ellipticity from the steady form of the equations and permits a solution using a streamwise marching computational technique. Although the PNS models were developed in the early 1960's, they were not widely used until the 1970's and 1980's<sup>3-9</sup>.

As the interest in understanding of high speed flows and performance of propulsive nozzles increases, there is need for development of more precise computational techniques. It has been shown that the adequacy of the standard JANNAF (Joint Army, Navy, NASA, Air Force) liquid rocket performance prediction methodology<sup>10</sup> is questionable for high expansion ratio nozzles and/or nozzles with thick viscous layer. The JANNAF procedure uncouples the inviscid flow and viscous layer and loses validity when there are extensive interactions between the viscous layer and the core flow.

The PNS equations are integrated throughout the viscous and inviscid regions of the flow. This procedure eliminates the need to specify the edge conditions in matching boundary layer and inviscid solutions, i.e. the conventional inviscid-viscous interaction. Popular algorithms for solving PNS equations are those by Briley and McDonald<sup>11</sup> and Beam and Warming<sup>12</sup>, and more recently, upwind algorithms<sup>41-44</sup>.

Richardson Extrapolation is a generic numerical procedure that can be applied to any computational scheme for which there is an asymptotic expansion of the local truncation error as the mesh is infinitely refined<sup>27</sup>. This extrapolation technique can be used to provide estimates for local error as well as a way to extend a numerical scheme to higher order. Richardson Extrapolation has been used successfully in the numerical solution of ordinary differential equation, and numerical quadrature, to name a few<sup>27</sup>. For fluid dynamic applications this technique has been

applied extensively to boundary layer equations by Keller and Cebeci<sup>36</sup>, Blottner<sup>37</sup>, and others<sup>39</sup>, either to raise the order of the numerical scheme or to do accuracy study. More recently, Richardson Extrapolation has been applied to Multigrid Methods<sup>38,40</sup>, to provide local error estimates and extension to higher order. The use of Richardson Extrapolation here differs from that of references 36,37 in two ways. Firstly, the technique is applied to the marching direction and not the radial direction, to obtain the local error and extension to second order. Secondly, the information from the local error is utilized to provide automatic step size control in the marching direction.

The resulting algorithm has been implemented in a production code for liquid rocket performance, called VISPER, developed for AFAL. The predictions from VISPER are compared to experimental data as well as to the established JANNAF code, TDK/BLM/MABL<sup>29</sup>. For nozzles known to have a thick viscous layer, comparing VISPER results to classical inviscid/boundary layer calculations yields a measure of the interaction between the core flow and the boundary layer.

## GOVERNING EQUATIONS

For body fitted coordinates  $(\xi, \eta)$ , with  $\xi = \xi(x, r)$  and  $\eta = \eta(x, r)$ , the PNS equations for axisymmetric flow in conservation form are:

$$\frac{\partial}{\partial \xi} \left[ r \frac{\xi_x E + \xi_r F}{J} \right] + \frac{\partial}{\partial \eta} \left[ r \frac{\eta_x (E + E_v) + \eta_r (F + F_v)}{J} \right] + \frac{G}{J} = 0 \quad (1)$$

where

$$E = (\rho u, \rho u^2 + p, \rho uv, \rho Hu)$$

$$E_v = (0, \tau_{xx}, \tau_{xr}, u\tau_{xx} + v\tau_{xr} + q_x)$$

$$F = (\rho v, \rho uv, \rho v^2 + p, \rho Hv)$$

$$F_v = (0, \tau_{xr}, \tau_{rr}, u\tau_{xr} + v\tau_{rr} + q_r)$$

$$G = (0, 0, -p, -u\tau_{xr} - v\tau_{rr})$$

$$J = \begin{vmatrix} \xi_x & \xi_r \\ \eta_x & \eta_r \end{vmatrix}$$

$$\tau_{xx} = -\mu \left[ \frac{4}{3} u_{\eta\eta} \eta_x - \frac{2}{3} v_{\eta\eta} \eta_r \right]$$

$$\tau_{xr} = -\mu (u_{\eta\eta} \eta_r + v_{\eta\eta} \eta_x)$$

$$\tau_{rr} = -\mu \left[ \frac{4}{3} v_{\eta} \eta_r - \frac{2}{3} u_{\eta} \eta_x \right]$$

$$q_x = -\frac{\mu}{Pr} h_{\eta} \eta_x$$

$$q_r = \frac{\mu}{Pr} h_{\eta} \eta_r$$

For planar flow, simply remove  $r$  and  $G$  from equation (1). In the above equations, the viscosity,  $\mu$ , represents the effective viscosity, i.e., for laminar flow,  $\mu$  is the laminar viscosity, while for turbulent flow,  $\mu$  is the sum of the laminar and turbulent viscosity. Similarly, for turbulent flow, the effective thermal conductivity is represented by

$$\frac{\mu}{Pr} = \frac{\mu_L}{Pr_L} + \frac{\mu_T}{Pr_T}$$

The thermodynamic properties are related to the species mass fractions,  $c_i$ , as follows:

$$h = \sum c_i h_i(T)$$

$$c_p = \sum c_i c_{p_i}(T)$$

$$R_G = \sum c_i R_{G_i}(T),$$

the summation is taken over the number of species.

The species continuity equations for axisymmetric flow in transformed coordinates are:

$$\begin{aligned} \rho \tilde{u} \frac{\partial c_i}{\partial \xi} + \rho \tilde{v} \frac{\partial c_i}{\partial \eta} &= \frac{\partial}{\partial \eta} \left( \frac{\mu}{Pr} \frac{\partial c_i}{\partial \eta} \eta_x \right) \eta_x \\ &+ \frac{\partial}{\partial \eta} \left( \frac{\mu}{Pr} \frac{\partial c_i}{\partial \eta} \eta_r \right) \eta_r \\ &+ \omega_i + \frac{1}{r} \frac{\mu}{Pr} \frac{\partial c_i}{\partial \eta} \eta_r \end{aligned} \quad (2)$$

Unity Lewis number is assumed in equation (2) to simplify the coding and should not significantly affect the accuracy of the results for the problems considered here.

For planar flow, simply remove the  $\frac{1}{r}$  term in equation (2). In equation (2),  $\tilde{u}$  and  $\tilde{v}$  denote the contravariant velocities,

$$\tilde{u} = u \xi_x + v \xi_r$$

$$\tilde{v} = u \eta_x + v \eta_r$$

$$\omega = \text{species production terms.}$$

The following non-dimensionalization is implemented

$$x = \bar{x}/r^*$$

$$h = \bar{h}/u^2$$

$$r = \bar{r}/x^*$$

$$P = \bar{P}/\rho_r u_r^2$$

$$u = \bar{u}/u_r$$

$$\mu = \bar{\mu}/r^* \rho_r u_r$$

$$v = \bar{v}/u_r$$

$$\omega_i = \bar{\omega}_i r^* / \rho_r u_r$$

$$T = \bar{T}/T_r$$

and consequently the form of equations (1) and (2) remains unchanged.

### FINITE DIFFERENCE EQUATIONS

The numerical scheme used for equation (1) is basically the linearized block implicit method of Briley-McDonald<sup>11</sup> or Beam-Warming<sup>12</sup>. The present implementation of the finite difference scheme differs from previous PNS solvers in two major ways. First, the vector ( $p, u, v, h$ ) is used as dependent variables, instead of the more common vector ( $p, \rho u, \rho v, \rho h$ ). Second, the diffusion terms are treated using second derivatives explicitly. The advantages of the present approach are that the tridiagonal block matrices do not need conditioning and no artificial damping, either implicit or explicit, is necessary. The geometric conservation law<sup>15</sup> is observed in differencing the fluxes.

The species continuity equations, equation (2), are finite-difference using the implicit Euler method at the forward station, once a solution for the fluid equations is obtained there. This decoupled approach between the fluid and the chemistry cuts down on the bandwidth of the block tridiagonal matrices, while does not seem to affect the accuracy of the scheme.

The Vigneron sublayer model<sup>13,14</sup> is used to suppress the ellipticity of the subsonic region of the boundary layer. More details on the numerics are available in reference 35, as this paper is oriented toward applications.

Equation (1) is rewritten as:

$$\begin{aligned} \frac{\partial}{\partial \xi} (\hat{E}) + \frac{\partial}{\partial \xi} (\hat{P}) + \frac{\partial}{\partial \eta} (\hat{F}) \\ + \hat{G} = 0 \end{aligned} \quad (3)$$

where

$$\hat{E} = r \frac{\xi_x E + \xi_r F}{J} - \hat{p}$$

$$\hat{p} = r(0, \xi_x(1-\omega)p, \xi_r(1-\omega)p, 0)$$

$$\omega = \text{parameter in Vigneron Sublayer model,}$$

$$\omega = \min \left[ \frac{\sigma M_\xi^2}{1 + (\gamma-1)M_\xi^2}, 1 \right],$$

$$0.7 \leq \sigma \leq 0.85$$

$$M_\xi = \text{Mach Number in the } \xi \text{ direction}$$

$$F = r \frac{\eta_x(E+E_v) + \eta_r(F+F_v)}{J}$$

$$\hat{G} = \frac{G}{J},$$

In the Beam-Warming scheme, the flux vectors  $\hat{E}$ ,  $\hat{F}$ ,  $\hat{G}$  need to be linearized about the present station. Each of the flux vectors can be represented as of the sum of terms of the form  $fW$ , where  $f$  is a grid related quantity such as  $\xi_x r/J$ ,  $\eta_x r/J$ , or  $1/J$ , and  $W$  is a flux vector, such as  $E$ ,  $F$ , or  $G$ . Denoting by  $j$  the index for  $\eta$ , and  $i$  the index for  $\xi$ , then,

$$\Delta(fW) = (fW)_j^{i+1} - (fW)_j^i \quad (4)$$

$$= \Delta f_j^i W_j^{i+1} + f_j^{i+1} \Delta W_j^i$$

Using Taylor's expansion to first order:

$$\Delta W_j^i = W_j^{i+1} - W_j^i$$

$$= \frac{\partial W}{\partial Q} \Delta Q_j$$

$$+ \frac{\partial W}{\partial Q_\eta} \Delta Q_{\eta j} \quad (5)$$

$$= \frac{\partial W}{\partial Q} \Delta Q_j$$

$$+ \frac{\partial W}{\partial Q_\eta} \frac{\partial}{\partial \eta} (\Delta Q)_j$$

where

$$Q = (p, u, v, h)$$

$$Q_\eta = \frac{\partial Q}{\partial \eta}.$$

Differences in the  $\eta$  direction are evaluated as central differences at the forward point. When linearization of the form (4) and (5) are applied to equation (3), a tridiagonal block structure results which can be solved efficiently for the increment,

$$\Delta Q_j = Q_j^{i+1} - Q_j^i.$$

Once a solution for the fluid dynamic equations (1) is obtained at the forward station, the species continuity equations can be solved at the same station, using the implicit Euler scheme.

## BOUNDARY CONDITIONS

At the solid wall, the following boundary conditions are implemented:

$$u = 0 \quad v = 0$$

$$\partial p / \partial n = 0, \quad (\partial h / \partial r = 0 \text{ or } T = T_w).$$

At the centerline, symmetric conditions are implemented:

$$\frac{\partial u}{\partial n} = 0 = \frac{\partial \rho}{\partial n} = \frac{\partial h}{\partial n}, \quad v = 0,$$

where  $n$  is the normal vector to the wall and/or axis.

## TURBULENT MODELS

Mixing length<sup>16,17</sup> and  $k-\epsilon$  models<sup>18,19</sup> for the effective viscosity have been incorporated into the VISPER code. An extensive discussion about the  $k-\epsilon$  model can be found in Ref. 20. The method used to obtain the starting conditions for the  $k-\epsilon$  model were based on the philosophy that the starting solution must at least satisfy the approximate governing equations for  $k$  and  $\epsilon$ . To obtain profiles for  $k$  and  $\epsilon$  a local similarity solution of the mean-flow governing equations was obtained using the mixing length model at the starting marching step<sup>21</sup>.

This similarity solution included approximate profiles for the eddy viscosity and the Reynolds shear stresses. The initial profiles for  $k$  and  $\epsilon$  could then be evaluated.

Some uncertainty regarding the nature of turbulent flow for low values of the local Reynolds number still exists. For example, the no-slip boundary condition for flow over a solid surface ensures that viscous effects will be dominant in the immediate vicinity of the surface, leading to low local Reynolds numbers. Jones & Launder<sup>19</sup> extended the  $k-\epsilon$  model to the wall region without using a near wall analysis. However, their model has not yet been thoroughly verified.

Patankar and Spalding<sup>22</sup> have applied the k- $\epsilon$  model, incorporating a Couette flow analysis for the near wall region and using a modified van Driest formula<sup>23</sup>. Arora, et al<sup>24,25</sup> have compared boundary layer solutions obtained with near wall models to several sets of experimental data, including planar and axisymmetric, incompressible and compressible, laminar and turbulent, reacting and non-reacting and both subsonic and supersonic flows. Their results indicate that the modified van Driest formula suggested by Cebeci and Chang<sup>26</sup> is suitable for a wide range of boundary layer flows. Thus, this methodology was adopted for the present effort.

### ARTIFICIAL DISSIPATION

In all the test cases presented in this paper, no artificial damping is used. This added stability is attributed to the way the numerics are implemented, as explained in the section on Finite Difference Equations. Although the usual 4th order explicit and 2nd order implicit smoothing terms for PNS solvers<sup>8</sup> have been included into the code, it has been found that activating either of them is detrimental to the accuracy of the code. This fact is especially noteworthy since the 4th order smoothing term does not affect the formal accuracy of a lower order method.

### STEP CONTROL AND RICHARDSON EXTRAPOLATION VERIFIED

The technique of Richardson extrapolation<sup>27</sup> has been applied to provide an elaborate step size control, and at the same time, extend the numerical scheme to second order in the marching direction. Briefly speaking, the procedure works as follows. At each marching step from  $\xi$  to  $\xi + \Delta\xi$ , the solutions at  $\xi + \Delta\xi$  are obtained two ways. The first way takes a step of size  $\Delta\xi$  and, the second takes 2 steps of size  $\Delta\xi/2$ . The results at  $\xi + \Delta\xi$  obtained with one step and 2 steps are then compared to obtain the local error. If the local error exceeds a preset limit, then the step is halved and the procedure repeated. If the local error is within the accepted limit, then the solution at  $\xi + \Delta\xi$  is extrapolated to second order in the marching direction as

$$f = 2f^{**} - f^*$$

where  $f$  denotes any dependent variables, and  $f^*$ ,  $f^{**}$  denote the solution at  $\xi + \Delta\xi$  obtained in one, 2 steps, respectively.

The procedure works quite well for this PNS application. Figure 1 shows a typical step size variation as a function of axial distance for nozzle flows. In this flow situation, the region of highest gradient is near the throat, which requires a small step size, and as the flow expands through the nozzle, a larger step size can be used.

### GRID

A simple algebraic grid, based on transfinite interpolation<sup>28</sup>, is used in all the test cases presented in this paper. A sample grid is shown in Figure 2.

### FINITE RATE CHEMISTRY

The basic finite rate chemical kinetics capability was taken from the TDK<sup>29</sup> code. This includes the reaction rate processor and the species net production rate evaluator. Capabilities for both Arrhenius and Landau-Celler rate data forms are allowed. Both second and third order reactions are treated for the latter, specific 3rd body reaction rate ratios can be input to the code.

### TRANSONIC SOLUTION

The initial start line for the PNS is obtained by taking the inviscid transonic analysis from the Two-Dimensional Kinetics Code (TDK)<sup>29</sup> and attaching a boundary layer next to the wall. The above transonic solution is approximate and based on the perturbation method. This approach is justifiable in view of the very thin boundary layer at the throat. One other advantage in using a TDK based transonic solution is that a direct comparison with TDK/BLM<sup>29</sup> (TDK/Boundary Layer Module) and/or TDK/MABL (TDK/Mass Addition Boundary Layer) codes can be made.

### RESULTS AND DISCUSSION

Three test cases were selected to verify the code. The first test case is for verification of the combustion and turbulence models and the other two test cases deal with the reacting flow in nozzles where the viscous layers are known to be thick.

1. Burrows & Kurlov<sup>30</sup> supersonic combustion to verify the combustion and turbulence models in the code.
2. SBS-1A spacecraft engine.
3. XLR-134 engine.

The specifications of the two liquid rocket engines are given in Tables 1 and 2, together with the boundary layer thickness computed using a classical thin boundary layer approach. It can be seen that the viscous layer is fairly thick in these nozzles as predicted by the boundary layer equations and for these cases the extent of the interaction is rather significant<sup>10</sup>. In these cases the equations should be integrated through the entire flowfield rather than conventional inviscid-viscous interaction. So, these two test cases seem to be suitable for these studies.

Test Case 1: Burrows & Kurlov  
Supersonic Combustion<sup>30</sup>

This test case was employed to verify the validity of the combustion and turbulence models within the PNS code. Figure 3 is the schematic of the test case and Figure 4 compares the experimental data for the mass fraction of  $H_2O$  with what is predicted by the PNS code using mixing length and  $k-\epsilon$  turbulence models. From these results it can be concluded that accurate predictions of species mass fractions are obtained with VISPER, and that little difference is seen between the two turbulence models.

Test Case 2: SBS-1A Spacecraft Engine

A Hughes Aircraft Corporation (HAC) small thruster, HIE-54, was used to validate the theoretical performance prediction of the PNS code. This engine was selected for our study for the following reasons. First, experimental data are readily available, as the engine had been studied extensively by Kushida et al.<sup>31</sup>. The second reason is the flowfield through the nozzle is completely laminar resulting in a very thick boundary layer. The previous study<sup>31</sup> was done using the classical inviscid-boundary layer approach. The present study, using the VISPER code, should be able to address the adequacy of the latter approach.

This engine is a small station keeper engine using decomposed hydrazine as propellant. Hence, all of the PNS calculations were performed using 3 species,  $NH_3$ ,  $N_2$ , and  $H_2$ , and frozen chemistry. The chamber operating conditions were as described in Reference 31, and are repeated here as Table 3. Six chamber pressures ranging from 25 psi to 132 psi were considered. Performance predictions, in terms of the thrust coefficient, were obtained for all six cases. However, the flowfield results are only discussed for the two extreme cases, namely the  $P_c = 25$  psi, and  $P_c = 132$  psi. For the first case, with  $P_c = 25$ , Figures 5 and 6 show the pressure and Mach number contour line. The thickness of the boundary layer, especially the sonic line, ( $M=1$ ) can be seen from Figure 6. Both Figures 5 and 6 show very clearly a compression wave coming from the attachment point in the nozzle contour and reflecting off the centerline. The magnitude of the compression wave can be seen from Figure 7, which shows that the pressure along the centerline increased significantly. It is interesting to note that this nozzle was designed as a boundary layer compensated Rao nozzle. The fact that a shock wave still exists in the nozzle indicates that this classical design method may not be applicable to flow situations having such a thick boundary layer. Figures 8 and 9 show the pressure and Mach number contours for the  $P_c = 132$  case. The boundary layer is still very thick, although not as thick as for the  $P_c = 25$  case.

For the performance prediction, the thrust coefficient,  $C_F$ , defined as total thrust divided by the product of the chamber pressure and the throat area, were obtained from the 6 cases using the PNS code and then compared to the results of Kushida<sup>31</sup> et al. In Reference 31, the experimental data were compared against the theoretical prediction of the JANNAF methodology using TDK/BLM<sup>29</sup>. In Figure 10 the results of Kushida are compared against the present theoretical performance predictions. It can be seen in Figure 10 that the TDK/BLM results compare surprisingly well with the experimental data, considering how thick the boundary layers are, especially in the low chamber pressure range. However, the PNS results are in better agreement with the data. Both codes, TDK/BLM and PNS, show excellent agreement at the highest chamber pressure, which is understandable given the thinner boundary layer.

Test Case 3: XLR-134 Nozzle

The Aerojet XLR-134 is a low thrust cryogenic engine being developed for the AFAL (Air Force Astronautic Laboratory). It is intended to provide low thrust propulsion for the delivery of large space structures to geosynchronous orbit<sup>32,33</sup>. The nozzle has an exit area ratio of 767. The injector uses a conventional coaxial element in which the gaseous fuel flows in an annulus around the liquid oxidizer. To minimize the amount of heat transfer from the engine to the vehicle, the entire nozzle is regenerative cooled. It should be noted that the laminar-turbulent transition based on  $Re_\theta = 360$  (Reynold's number based on the momentum thickness) reveals that for the given operating conditions, the flow stays laminar till about one inch before the throat. As yet, hot firing data are not available for this engine. Thus, strictly speaking, the XLR-134 is not a validation case. However, it is useful for exploring the limits of the boundary layer method.

The calculations for this engine were performed with six (6) species ( $H$ ,  $H_2$ ,  $H_2O$ ,  $O$ ,  $OH$ ,  $O_2$ ) and eight (8) reaction rates. Figure 11 compares the pressure along the wall calculated by the VISPER code, against the TDK/MABL code. In this nozzle the boundary layer thickness,  $(\delta_{995/r})_{exit}$  is about 0.2, which can be considered a fairly thick shear layer.

This thickness implies that the viscous effects can extend beyond that of classical boundary layer predictions. Furthermore, the standard methodology, i.e., boundary layer/inviscid flow interaction, can underpredict the specific impulse  $I_{sp}$  (= thrust/mass flow rate), because, in general, it neglects part of the viscous effects in the nozzle, (see Table 4). Figure 12 compares the wall shear between the two codes. The pressure and Mach number contours depicted in Figures 13 and 14 reveal that the shock originating from the attachment point propagates to the axis and then reflects.

## Richardson Extrapolation

Table 4 shows the run time and  $I_{sp}$  for the XLR-134 nozzle in the presence and absence of the Richardson extrapolation. The first half of the table is for the results with Richardson extrapolation. The minimum step size used is 0.0001. The second half shows the results obtained with constant step sizes. It can be seen from this table that introducing more grid lines in  $\eta$  direction increases the run time by a factor of 1.5, while it does not have major impact on the accuracy of the results. To obtain the same accuracy without this technique the required computation time is increased by a factor of 11.

The result for  $I_{sp}$  without Richardson extrapolation for  $\Delta\xi = 0.001$  underpredicts the performance by about 3%, which is not acceptable. However, it should be noted that due to the extremely high gradients in supersonic nozzle flows the required accuracy ( $< 1\%$ ) is difficult to attain. It has been shown that similar PNS Codes yield even worse predictions for  $I_{sp}$ <sup>10,34</sup>.

## CONCLUDING REMARKS

The Richardson Extrapolation technique has been successfully implemented for a PNS solver. Its advantages are shown both in the computer run time and accuracy. This application of Richardson Extrapolation can be extended to any other marching flow solver, such as time-dependent Navier-Stokes solver, the only restriction is the flow cannot have strong shock wave.

The VISPER code has shown to be a viable tool for studying supersonic nozzle flows, especially those with thick viscous layers. Excellent agreement with experimental data were obtained for supersonic combustion and nozzle flows. With respect to the interaction of core flow/boundary layer, the classical decoupled approach seems to be valid to nozzle flows with a Reynold's number (based on throat radius) about 10,000 (test case 2). However, the VISPER code provides a better alternative to the decoupled approach. Not only are the results more accurate, but the computer execution time is much less, especially if a second order correction is performed on the core flow/boundary layer calculations by adjusting the body by the displacement thickness.

## ACKNOWLEDGMENT

This work was supported by the Air Force Astronautics Laboratory (AFAL) under Contract No. F04611-86-C-0055. The authors wish to thank Mr. Jay Levine for carefully reviewing the manuscript and Dr. Phil Kessel and Mrs. Elizabeth Slimak for their support in this work.

## REFERENCES

1. Tannehill, J. C., Venkatapathy, E., and Rakich, J. V., "Numerical Solution of Supersonic Viscous Flow Over Blunt Delta Wings", AIAA Journal, Vol. 20, 1982, pp. 203-210.
2. Kaul, V. K., and Chaussee, D. S., "AFWAL Parabolized Navier-Stokes Code: 1983 AFWAL/NASA Merged Baseline Versions", US Air Force Wright Aeronautical Lab., AFWAL-TR-83-3118, 1983.
3. Ferri, A., "Review of Problems in Application of Supersonic Combustion", Journal of the Royal Aeronautical Society, Vol. 68, Sept. 1964, pp. 575-597.
4. Moretti, G., "Analysis of Two-Dimensional Problems of Supersonic Combustion Controlled by Mixing", AIAA Journal, Vol. 3, Feb. 1965, pp. 223-229.
5. Edelman, R., and Weilerstein, G., "A Solution of the Inviscid-Viscid Equations with Applications to Bounded and Unbounded Multicomponent Reacting Flows", AIAA Paper 69-83, Jan. 1969.
6. Ferri, A., "Mixing Controlled Supersonic Combustion", Annual Review of Fluid Mechanics, Vol. 5, Annual Reviews Inc., Palo Alto, CA, 1973, pp. 301-338.
7. Buggeln, R. C., McDonald, H., and Levy, R., "Development of a Three-Dimensional Supersonic Inlet Flow Analysis", NASA Contractor Report 3218, Jan. 1980.
8. Chitsomborn, T., Kumax, A., and Tirvari, S. N., "Numerical Study of Finite-Rate Supersonic Combustion Using Parabolized Equations", AIAA Paper No. 87-0088, Jan. 1987.
9. Sinha, N., and Dash, S. M., "Parabolized Navier-Stokes Analysis of Ducted Turbulent Mixing Problems with Finite-Rate Chemistry", AIAA Paper No. 86-0004, Jan. 1986.
10. Kehtarnavaz, H., Coats, D. E., and Kronzon, Y., "Thick Boundary Layer Assessment for Nozzle Flow", AIAA Paper No. 88-3160, July 1988.
11. Briley, W. R., and McDonald, M., "Solution to the Multi-Dimensional Compressible Navier-Stokes Equations by a Generalized Implicit Method", Journal of Computational Physics, Vol. 24, August 1977, pp. 372-397.

- 12 Beam, R., and Warming, R. F., "An Implicit Factored Scheme for the Compressible Navier-Stokes Equations", AIAA Journal, Vol. 16, April 1978, pp. 393-402.
- 13 Vigneron, Y. C., Rakich, J. V., and Tannehill, J. C., "Calculation of Supersonic Viscous Flow Over Delta Wings with Sharp Subsonic Leading Edges", AIAA Paper 78-1137, Seattle, WA, 1978.
- 14 Vigneron, Y. C., Rakich, J. V., and Tannehill, J. C., "Calculation of Supersonic Viscous Flow Over Delta Wings with Sharp Subsonic Leading Edges", NASA TM-78500, 1978.
- 15 Thomas, P. D., and Lombard, C. K., "The Geometric Conservation Law - A Link Between Finite Difference and Finite-Volume Methods of Flow Computation on Moving Grids", AIAA Paper 78-1208, 1978.
- 16 Cebeci, T., "Calculation of Compressible Turbulent Boundary Layers with Heat and Mass Transfer", AIAA J., Vol. 9, No. 6, June 1971, pp. 1091-1097.
- 17 Cebeci, T., "Eddy-Viscosity Distribution in Thick Axisymmetric Turbulent Boundary Layers", J. of Fluid Engineering, Transactions of ASME, June 1973, pp. 319-326.
- 18 Jones, W. P., and Launder, B. E., "The Prediction of Laminarization with a Two-Equation Model of Turbulence", Int. J. Heat Mass Transfer, Vol. 15, 1972, pp. 301-314.
- 19 Jones, W. P., and Launder, B. E., "The Calculation of Low Reynolds Number Phenomena with a Two-Equation Model of Turbulence", Int. J. Heat Mass Transfer, Vol. 16, 1973, pp. 1119-1130.
- 20 Danberg, J. E., Van Gulick, P., and Kim J., "Turbulence Modeling for Steady Three-Dimensional Supersonic Flows", Army Ballistic Research Laboratory, Maryland, Contract Report BRL-CR-553.
- 21 Shirazi, S. A., and Truman, C. R., "Prediction of Turbulent Source Flow Between Corotating Disks with an Anisotropic Two-Equation Turbulence Model", ASME paper No. 87-GT-73, 1987, 8 pages.
- 22 Patankar, S. V., and Spalding, D. B., "Heat and Mass Transfer in Boundary Layers", Inter-text Books, London, 1970.
- 23 van Driest, E. R., "On Turbulent Flow Near a Wall", Journal of the Aeronautical Sciences, Vol. 23, 1956, p. 1007.
- 24 Arora, R., Kuo, K. K., and Razdan, M. K., "Turbulent Boundary Layer Flow Computations with Special Emphasis on the Near-Wall Region", AIAA paper No. 81-1001, also proceeding of the AIAA Computational Fluid Dynamics Conference, June 1981, pp. 295-305.
- 25 Arora, R., Kuo, K. K., and Razdan, M. K., "Near Wall Treatment for Turbulent Boundary Layer Computations", AIAA J. Vol. 20, No. 11, Nov. 1982, pp. 1481-1483.
- 26 Cebeci, T., and Chang, K. C., "Calculation of Incompressible Rough-Wall Boundary-Layer Flows", AIAA Journal, Vol. 16, No. 7, July 1978, pp. 730-735.
- 27 Dahlquist, G., and Bjorck, A., "Numerical Methods", Prentice Hall, NJ, 1974.
- 28 Thompson, J. F., Warri, Z. U. A., and V'ayne Mastine, C., "Numerical Grid Generation", North Holland, NY, 1985.
- 29 Kehtarnavaz, H., Coats, D. E., Nickerson, G. R., and Dang, A. L., "Two-Dimensional Kinetics (TDK) Nozzle Performance Computer Program-Thick Boundary Layer Version", Software and Engineering Associates, Inc., March 1987, prepared for the AFAL under Contract No. F04611-86-C-0055, Report No. AFAL-TR-87-031.
- 30 Burrows, M. C., and Kurlov, A. P., "Analytical and Experimental Study of Supersonic Combustion of Hydrogen in a Vitiated Airstream", NASA Lewis Research Center Report NO. N73-31828.
- 31 Kushida, R. O., Hermel, J., Apfel, S., and Zydowicz, M., "Performance of High Area Ratio Nozzles for a Small Rocket Thruster", AIAA paper No. 86-1573, 1986.
- 32 Nickerson, G. R., and Dang, L. D., "Two-Dimensional Kinetics Computer Program for Orbit Transfer Vehicles", 22nd JANNAF Combustion Meeting, Pasadena, CA, October 7-10, 1985.
- 33 Schneider, B. E., Michel, R. W., and Gibb, J. A., "Low Thrust Cryogenic Engine Technology", AIAA-87-1932, 23rd Joint Propulsion Conference, San Diego, CA, June 19 - July 2, 1987.
- 34 Kehtarnavaz, H., Coats, D. E., and Kronzon, Y., "Boundary Layer Study - Thick Boundary Layer Assessment", Final Report prepared for the Air Force Astronautic Laboratory by SEA, Inc., under Contract No. F04611-86-C-0055.

- 35 Dang, A., Kehtamavaz, H., and Coats, D., "Viscous Performance Code for Nozzle Flows with Finite Rate Chemistry", Final Report prepared for the Air Force Astronautics Laboratory by S.E.A., Inc., under Contract No. F04611-86-C-0055.
- 36 Keller, H. B., and Cebeci, T., "Accurate Numerical Methods For Boundary Layers Flows: Two-Dimensional Turbulent Flows", AIAA Journal, Vol. 10, 1972, pp. 1193-1199.
- 37 Blottner, F. G., "Variable Grid Scheme Applied To Turbulent Boundary Layers", Computer Methods in Applied Mechanics and Engineering, Vol 4, 1974, pp. 179-194.
- 38 Morrison, J. H. and Napilitano, M., "Efficient Solutions of Two-Dimensional Incompressible Steady Viscous Flows", Computers and Fluids, Vol 16, 1988, pp. 119-132.
- 39 Soliman, M.O. and Baker, A. J., "Accuracy and Convergence of a Finite Element Algorithm For Turbulent Boundary Layer Flow", Computer Methods in Applied Mechanics and Engineering, Vol. 28, 1981, pp. 81-102.
- 40 Hemker, P. W., "Defect Correction and Higher Order Schemes For The Multi-Grid Solution Of The Steady Euler Equations", N86-29172/1/XAB, Mathematisch Centrum, Amsterdam, Nov. 1985.
- 41 Lawrence, S. L., "Application Of An Upwind Algorithm To The Parabolized Navier-Stokes Equations", Ph.D. Thesis, Iowa State University, 1987.
- 42 Lawrence, S. L., Chaussee, D. S. and Tannehill, J. C., "Application Of An Upwind Algorithm To The Three-Dimensional Parabolized Navier-Stokes Equations", AIAA Paper 87-1112-CP, June, 1987.
- 43 Tannehill, J., Levalts, J., and Lawrence, S., "An Upwind Parabolized Navier-Stokes Code For The Real Gas Flows", AIAA Paper 88-0713, January, 1988.
- 44 Korte, J. J., and McRae, D. S., "Explicit Upwind Algorithm For The Parabolized Navier-Stokes Equations", AIAA Paper 88-0716, January, 1988.

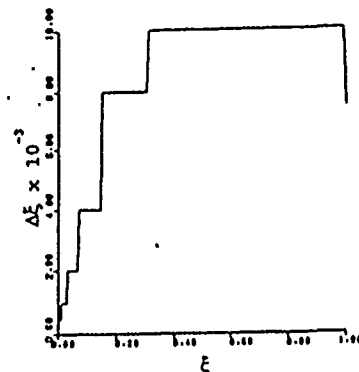


Figure 1. Step size variation as a function of  $\xi$

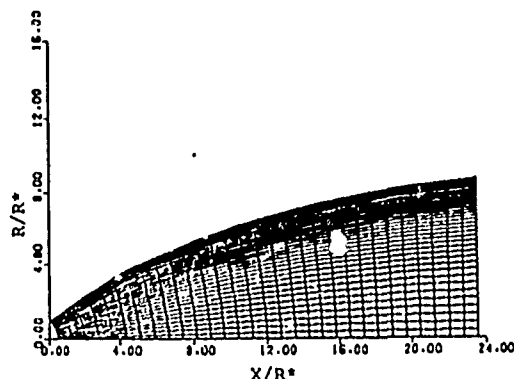


Figure 2. Sample grid used in this work

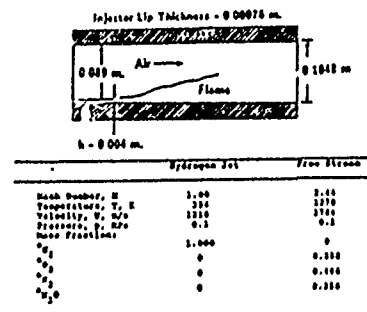


Figure 3. Schematic and parameters for the Burrows and Kurlov supersonic combustion

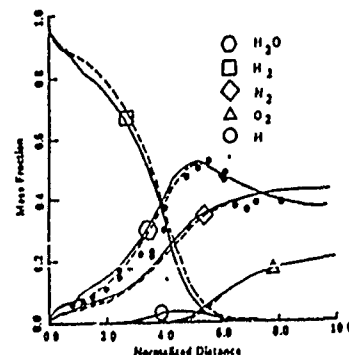


Figure 4. Burrows and Kurlov supersonic combustion test case. — mixing length model, ● experiment, Ref. 30



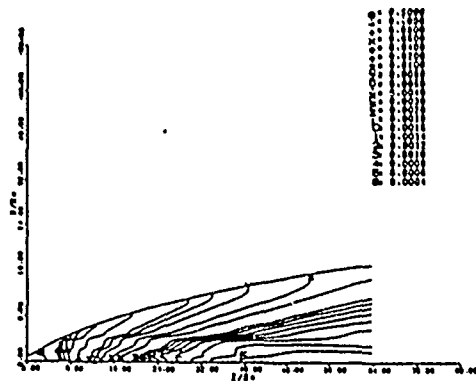


Figure 5. Pressure contours for SBS-1A engine for chamber pressure of 25 psi

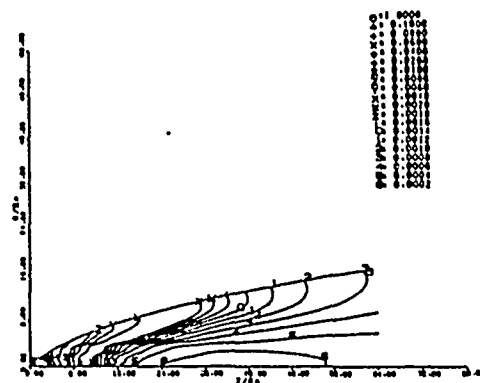


Figure 8. Pressure contours for SBS-1A engine for chamber pressure of 132 psi

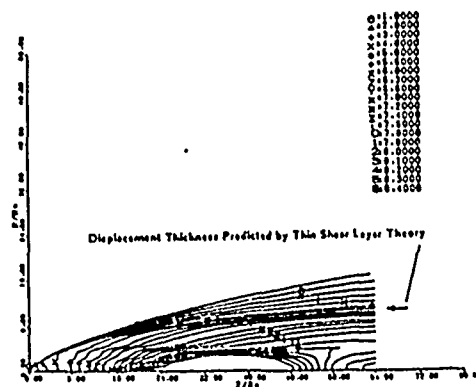


Figure 6. Mach number contours for SBS-1A engine for chamber pressure of 25 psi

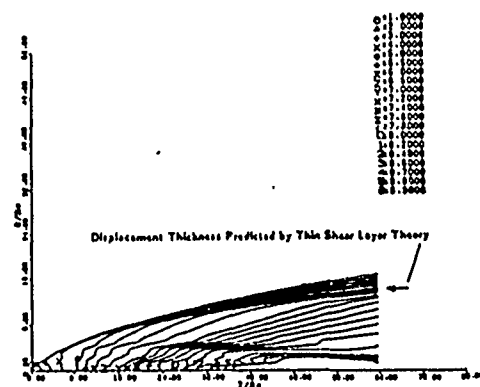


Figure 9. Mach number contours for SBS-1A engine for chamber pressure of 132 psi

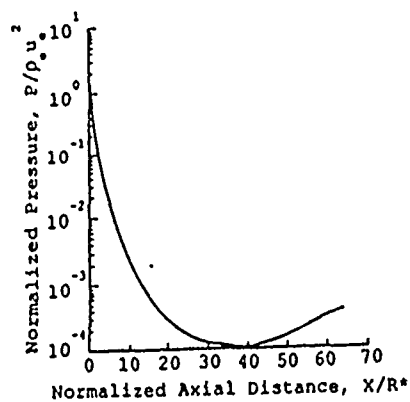


Figure 7. Pressure on the contour for the SBS-1A, P=25 psi

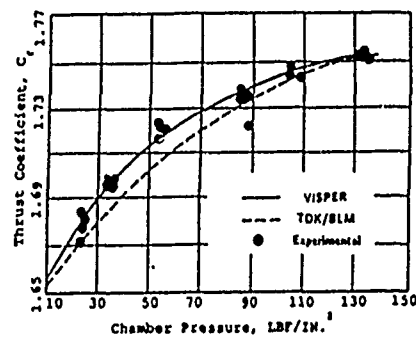


Figure 10. Comparison of thrust coefficient for experimental and predicted data

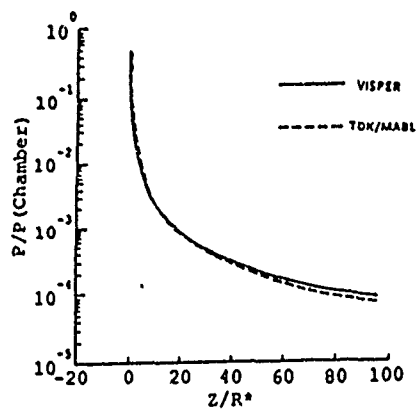


Figure 11. Comparison of pressure along the wall for XLR-134 engine

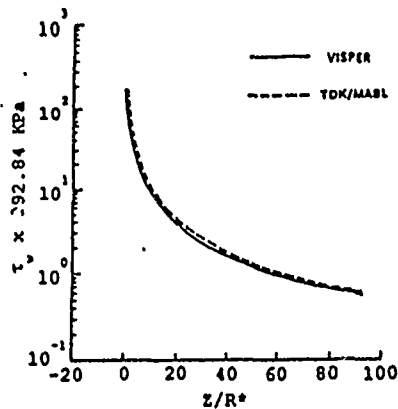


Figure 12. Comparison of the wall shear for the XLR-134 engine

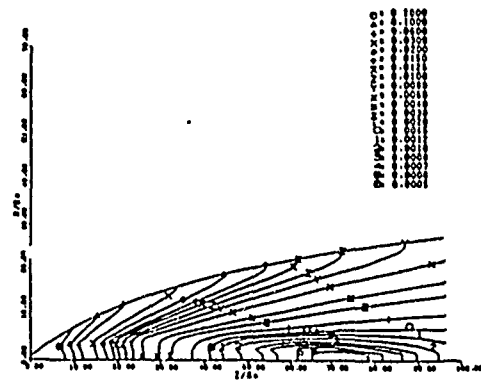


Figure 13. Pressure contours for XLR-134 engine as predicted by the VISPER code

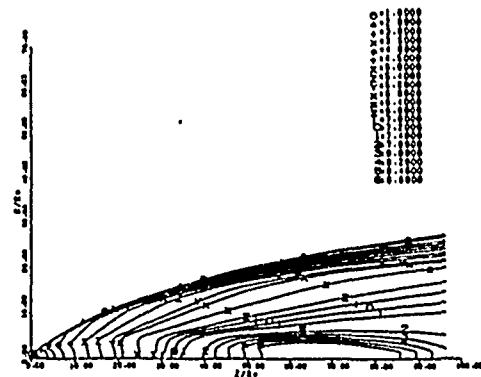


Figure 14. Mach number contours for XLR-134 engine as predicted by the VISPER code

Table 1: Specifications of the Engine

ENGINE	APPLICATION	PROPELLANT	THRUST (lb <sub>f</sub> )	CHAMBER PRESSURE (psia)	THROAT AREA, in <sup>2</sup> (inches)	EXIT AREA, in <sup>2</sup> (inches)	EXPANSION RATIO
SR-134 (Hughes Spacecraft Engine)	Spacecraft	H <sub>2</sub> /O <sub>2</sub>	245	100	.0033	2.00 x 10 <sup>5</sup>	300:1
XLR-134	OTV	LOX/GH <sub>2</sub>	311	310	.300	1.00 x 10 <sup>5</sup>	767:1

Table 2: Boundary Layer Thickness at the Exit Plane for the Missile Test Cases as Predicted by the Boundary Layer Approximation

Missile	Area Ratio	Transverse Radius at the Exit Plane, inches	Boundary Layer Thickness, inches	$\delta_{99.5}/r$
XLR-134	767:1	10.07	0.00	100
Hughes SR-134	300:1	1.01	0.01	200

Table J: Chamber Operating Conditions<sup>11</sup>

Propellant: decomposed hydrazine  
 Nozzle Throat Diameter: 0.185 in  
 Thermal expansion coefficient (L605):  $9.4 \text{ by } 10^{-4} \text{ in/in } ^\circ\text{F}$

Chamber Pressure	Supply Pressure	Char. Vel	Chamber Temp.	Mean Mol Wt.	Fraction Ammonia	Throat Wall Temp.	Throat Adj. Displacement	Throat Momentum	Throat Reynolds Number	Throat Reynolds Number	Throat Velocity	Mass Flow	
$P_c$ psia	$P_s$ psia	$C^*$ fps	$T_c$ °R	$W_m$	Dissoc. X	$T_{pw}$ °R	Throat Radius In R*	Thickness $\delta^*$ in.	Thickness $\delta$ in.	$Re_g$	$Re_g$	Coeff. $C_v$ $\frac{m}{lb_m/sec}$	
25	40	4125	1700	11.20	0.900	1665	.0935	.001030	3.557E-4	121.5	42.0	11029	.99566 .005215
35	60	4150	1745	11.36	0.870	1700	.0935	8.599E-4	3.142E-4	138.2	50.5	15027	.99567 .007284
54	100	4200	1830	11.67	0.810	1763	.0936	6.771E-4	2.729E-4	160.0	64.5	22118	.99566 .01117
86	185	4280	1965	12.22	0.719	1852	.0937	5.244E-4	2.426E-4	183.1	84.7	32716	.99567 .01755
106	250	4310	2030	12.50	0.668	1888	.0937	4.674E-4	2.293E-4	194.8	95.6	39052	.99567 .02152
132	350	4325	2070	12.69	0.645	1905	.0937	4.166E-4	2.112E-4	211.6	107.3	47592	.99568 .02672

## FRACTION DISSOCIATION:

$$N_2H_4 = (4/3)(1-X) NH_3 + \left[ (1+2X/3) N_2 + 2X H_2 \right]$$

Table K: The Effect of Richardson Extrapolation on the Performance and Computation Time for SLB 134 Nozzle

$\Delta f_{\text{mod}}$	With Richardson Extrapolation				Without Richardson Extrapolation			
	.01	.001	.0001	.00001	.01	.001	.0001	.00001
$q$	100	150	100	150	100	150	100	150
time, sec	400.0	740.0	2311.0	3176.7	1103.0	1671.0	5600.0	6513.0
$\frac{I_{sp}}{lb_m}$	450.03	450.03	450.03	450.03	449.30	449.12	450.72	450.00

$I_{sp}$  from the TME/PVAL to 457.45  $\frac{lb_f}{lb_m}$   
 Time refers to IBM 4/100 Computer

PNS SOLUTION OF NON-EQUILIBRIUM  
REACTING FLOW IN ROCKET NOZZLES

A. L. Dang\*, H. Kehtarnavaz\*\*, and D. E. Coats†  
Software and Engineering Associates, Inc.  
Carson City, Nevada

ABSTRACT

A Parabolized Navier-Stokes Code (PNS) which calculates the internal flow of turbulent and non-equilibrium reacting gases has been developed. A second order method with automatic step size control, based on the Beam-Warming scheme and Richardson extrapolation technique, is used to solve the flowfield equations. The results from this code are compared against the existing JANNAF performance prediction methodology calculations. The results indicate very good agreement and reveals the advantages of the Richardson extrapolation technique, both in terms of accuracy and computer execution time. Two turbulence models, mixing length and  $k - \epsilon$ , are used to resolve the wall shear layer.

INTRODUCTION

Parabolized Navier-Stokes (PNS) equations are a subset of the Navier-Stokes (NS) equations which are valid for supersonic flows<sup>1,2</sup>. The PNS equations neglect the streamwise diffusion term which, along with special treatment of the subsonic region of the boundary layer, removes the spatial ellipticity from the steady form of the equations and permits a solution using a streamwise marching computational technique. Although the PNS models were developed in the early 1960's, they were not widely used until the 1970's and 1980's.

As the interest in understanding of high speed flows and performance of propulsive nozzles increases, there is need for development of more precise computational techniques. It has been shown that the adequacy of the standard JANNAF methodology<sup>3</sup> is questionable for high expansion ratio nozzles. The current procedure consists of uncoupling the inviscid flow and viscous layer which loses validity when there is extensive interactions between the viscous layer and the core flow.

The PNS equations are integrated throughout the viscous and inviscid regions of the flow. This procedure eliminates the need to specify the edge conditions in matching boundary layer and inviscid solutions, i.e. the conventional inviscid-viscous interaction. Furthermore, the PNS equations are obtained by implicit methods. Notable algorithms of this type are those by Briley and McDonald<sup>4</sup> and Beam and Warming<sup>5</sup>.

GOVERNING EQUATIONS

For body fitted coordinates  $(\xi, \eta)$ , with  $\xi = \xi(x, r)$  and  $\eta = \eta(x, r)$ , the PNS equations for axisymmetric flow in conservation form are:

$$\frac{\partial}{\partial \xi} \left( r \frac{\xi E + \xi F}{J} \right) + \frac{\partial}{\partial \eta} \left( r \frac{\eta (E + E_v) + \eta (F + F_v)}{J} \right) + \frac{G}{J} = 0, \quad (1)$$

where

$$\begin{aligned} E &= (\rho u, \rho u^2 + p, \rho uv, \rho hu) \\ E_v &= (0, r_{xx}, r_{xr}, u_r + v_r + q_x) \\ F &= (\rho v, \rho uv, \rho v^2 + p, \rho hv) \\ F_v &= (0, r_{xr}, r_{rr}, u_r + v_r + q_r) \\ G &= (0, 0, -p, -ur - vr) \\ J &= \begin{vmatrix} \xi_x & \xi_r \\ \eta_x & \eta_r \end{vmatrix} \end{aligned} \quad \begin{aligned} r_{xx} &= -\mu \left( \frac{4}{3} \eta_x - \frac{2}{3} \eta_r \right) \\ r_{xr} &= -\mu \left( u_{\eta r} + v_{\eta x} \right) \\ r_{rr} &= -\mu \left( \frac{4}{3} \eta_r - \frac{2}{3} u_x \right) \\ q_x &= -\frac{\mu}{pr} h_{\eta x} \\ q_r &= -\frac{\mu}{pr} h_{\eta r} \end{aligned}$$

\* Senior Numerical Analyst  
\*\* Research Scientist  
† Vice President

Approved for public release; distribution is unlimited.

For planar flow, simply remove  $r$  and  $G$  from equation (1). In the above equations, the viscosity,  $\mu$ , represents the effective viscosity, i.e., for laminar flow,  $\mu$  is the laminar viscosity, while for turbulent flow,  $\mu$  is the sum of the laminar and turbulent viscosity. Similarly, for turbulent flow, the effective thermal conductivity is represented by

$$\frac{\mu}{pr} = \frac{\mu_L}{pr_L} + \frac{\mu_T}{pr_T}$$

The thermodynamic properties are related to the species mass fractions,  $c_i$ , as follows:

$$h = \sum_i c_i h_i(T) \quad cp = \sum_i c_i cp_i(T) \quad R_G = \sum_i c_i R_{Gi}(T)$$

The species continuity equations (unity Lewis number) for axisymmetric flow in transformed coordinates are:

$$\bar{u} \frac{\partial c_i}{\partial \xi} + \bar{v} \frac{\partial c_i}{\partial \eta} = \frac{\partial}{\partial \eta} \left( \frac{\mu}{pr} \frac{\partial c_i}{\partial \eta} \right) \eta_x \eta_x + \frac{\partial}{\partial \eta} \left( \frac{\mu}{pr} \frac{\partial c_i}{\partial \eta} \right) \eta_r \eta_r + \omega_i + \frac{1}{r} \frac{\mu}{pr} \frac{\partial c_i}{\partial \eta} \eta_r \quad (2)$$

For planar flow, simply remove the  $\frac{1}{r}$  term in equation (2). In equation (2),

$$\bar{u} = u \xi_x + v \xi_r \quad \bar{v} = u \eta_x + v \eta_r \quad \omega_i = \text{species production terms.}$$

The following normalization is implemented

$$\begin{aligned} x &= \xi/x^* & v &= \bar{v}/u_\infty & p &= \bar{p}/\rho_\infty u_\infty^2 \\ r &= \bar{r}/x^* & T &= \bar{T}/T_\infty & \mu &= \bar{\mu}/\rho_\infty u_\infty^2 \\ u &= \bar{u}/u_\infty & h &= \bar{h}/h_\infty & \omega_i &= \bar{\omega}_i \bar{r}^*/\rho_\infty u_\infty^2 \end{aligned}$$

and consequently equations (1) and (2) remain exactly the same.

#### FINITE DIFFERENCE EQUATIONS

The numerical scheme used for equation (1) is the Beam-Warming<sup>12</sup> method, while the scheme used for equation (2) is the implicit Euler. Treatment of departure solution is done using the Vigneron<sup>13,14</sup> technique. The flux vectors are linearized according to the Geometric Conservation Law<sup>15</sup>.

Thus, equation (1) is rewritten as:

$$\frac{\partial}{\partial \xi} (\hat{E}) + \frac{\partial}{\partial \xi} (\hat{P}) + \frac{\partial}{\partial \eta} (\hat{F}) + \hat{G} = 0 \quad (3)$$

$$\text{where } \hat{E} = r \frac{\xi_x E + \xi_r F}{j} - \hat{P} \quad \hat{P} = r(0, \xi_x(1-\omega)p, \xi_r(1-\omega)p, 0)$$

$$\hat{F} = r \frac{\eta_x(E+E_v) + \eta_r(F+F_v)}{j} \quad \hat{G} = \frac{G}{j}$$

In the Beam-Warming scheme, the flux vectors  $\hat{E}$ ,  $\hat{F}$ ,  $\hat{G}$  need to be linearized about the present station. Each of the flux vectors can be represented as of the sum of terms of the form  $fW$ , where  $f$  is a grid related quantity such as  $\xi_x r/J$ ,  $\eta_x r/J$  or  $1/J$ , and  $W$  is a flux vector, such as  $E$ ,  $F$ , or  $G$ . Denote by  $j$  the index for  $\eta$ , and  $i$  the index for  $\xi$ . Then,

$$\Delta(fW)_j = (fW)_j^{i+1} - (fW)_j^i = (\Delta f)_j^{i+1} W_j^i + f_j^{i+1} \Delta W_j^i \quad (4)$$

Using Taylor's expansion to first order:

$$\Delta W_j^i = W_j^{i+1} - W_j^i = \frac{\partial W}{\partial Q} \Delta Q_j + \frac{\partial W}{\partial Q_\eta} \Delta Q_{\eta,j} = \frac{\partial W}{\partial Q} \Delta Q_j + \frac{\partial W}{\partial Q_\eta} \frac{\partial}{\partial \eta} (\Delta Q)_j \quad (5)$$

where

$$Q = (\rho, u, v, h)$$

$$Q_\eta = \frac{\partial Q}{\partial \eta}$$

When linearization of the form (4) and (5) are applied to equation (3), a tridiagonal block structure results which can be solved efficiently for the increment,

$$\Delta Q_j = Q_j^{i+1} - Q_j^i.$$

Once a solution for the fluid dynamic equations (1) is obtained at the forward station, the species continuity equations can be solved at the same station, using the implicit Euler scheme.

#### BOUNDARY CONDITIONS

At the solid wall, the following boundary conditions are implemented:

$$u = 0 \quad v = 0 \quad \partial p / \partial n = 0, \quad (\partial h / \partial n = 0 \text{ or } T = T_w).$$

At the centerline, symmetric conditions are implemented:

$$\frac{\partial u}{\partial n} = 0 = \frac{\partial \rho}{\partial n} = \frac{\partial h}{\partial n}, \quad v = 0,$$

where  $n$  is the normal vector to the wall and/or axis.

#### TURBULENT MODELS

Mixing length<sup>16,17</sup> and  $k-\epsilon$  models<sup>18,19</sup> for the effective viscosity have been incorporated into the PNS code. An extensive discussion about the  $k-\epsilon$  model can be found in Ref. [20]. The method used to obtain the starting conditions for the  $k-\epsilon$  model were based on the philosophy that the starting solution must at least satisfy the approximate governing equations for  $k$  and  $\epsilon$ . To obtain profiles for  $k$  and  $\epsilon$  a local similarity solution of the mean-flow governing equations was obtained using the mixing length model at the starting marching step.

This solution included approximate profiles for the eddy viscosity and the Reynolds shear stresses. The initial profiles for  $k$  and  $\epsilon$  could then be evaluated.

Some uncertainty regarding the nature of turbulence flow when the local Reynolds number is low still exists. For example, the no-slip boundary condition for flow over a solid surface ensures that viscous effects will be dominant in the immediate vicinity of the surface, leading to low local Reynolds numbers. Jones & Launder<sup>19</sup> extended the  $k-\epsilon$  model to the wall region without using a near wall analysis. However, their model has not yet been thoroughly verified.

Patankar and Spalding<sup>22</sup> have applied the  $k-\epsilon$  model, incorporating a Cuyette flow analysis for the near wall region and using a modified van Driest formula<sup>23</sup>. Arora, et al.<sup>24,25</sup> have compared several sets of experimental data, including planar and axisymmetric, incompressible and compressible, laminar and turbulent, reacting and non-reacting and both subsonic and supersonic flows.<sup>26</sup> Their results indicate that the modified van Driest formula suggested by Cebeci and Chng<sup>26</sup> is suitable for a wide range of boundary layer flows. The same methodology has been used in this work.

## ARTIFICIAL DISSIPATION

In all the test cases presented in this paper, no artificial damping is used. Although the usual 4th order explicit and 2nd order implicit smoothing terms for PNS solvers have been included into the code, it has been found that activating either of them is detrimental to the accuracy of the code. For test case 2 for example, using just 10% of the recommended amount for the explicit smoothing causes the  $I_{sp}$  to rise by 1%, which is not acceptable. This fact is especially noteworthy since the 4th order smoothing term does not affect the formal accuracy of a lower order method.

## STEP CONTROL

An elaborate step control procedure has been developed for the PNS solver. This method is based on Richardson extrapolation technique<sup>33</sup> which has been used successfully in numerical solutions of ordinary differential equations and other numerical calculations. In order to make use of the Richardson extrapolation technique for the present application, the PNS is casted in a strictly marching procedure. At each marching step from  $\xi$  to  $\xi + \Delta\xi$ , the solutions at  $\xi + \Delta\xi$  are obtained two ways. The first way takes a step of size  $\Delta\xi$  from  $\xi$  to  $\xi + \Delta\xi$ . The second way takes 2 steps of size  $\Delta\xi/2$  from  $\xi$  to  $\xi + \Delta\xi/2$  and then to  $\xi + \Delta\xi$ . The results at  $\xi + \Delta\xi$  obtained with one step and 2 steps are then compared to determine the local error, which in turn decides on the next step size. The procedure works quite well for smooth flow situations, but requires more work for flow with a strong shock.

## GRID

A simple algebraic grid, based on transfinite interpolation<sup>34</sup>, is used in all the test cases presented in this paper. A sample grid, for the SSME, is shown in Figure 1.0.

## TRANSONIC SOLUTION

The initial start line for the PNS is obtained by taking the transonic analysis from the Two-Dimensional Kinetics Code (TDK)<sup>32</sup> and attaching a boundary layer next to the wall. This approach is justifiable in view of the very thin boundary layer at the throat. One other advantage in using a TDK based transonic solution is that a direct comparison with TDK/BLM (TDK/Boundary Layer Module) and/or TDK/HABL (TDK/Mass Addition Boundary Layer) codes can be made.

## RESULTS AND DISCUSSION

Four test cases were selected to verify the code. The test cases are:

1. Burrows & Kurlov<sup>27</sup> supersonic combustion to verify the combustion and mixing models in the code.
2. SBS-1A spacecraft engine.
3. XLR-134 engine.
4. SSME (Space Shuttle Main Engine).

The specifications of these three engines are given in Table 1.

### Test Case 1: Burrows & Kurlov Supersonic Combustion

This test case was employed to verify the validity of the turbulence models within the PNS code. Figure 1.1 is the schematic of the test case and Figure 1.2 compares the experimental data for the mass fraction of  $H_2O$  with what is predicted by the PNS code using mixing length and  $k-\epsilon$  turbulence models. From these results it can be concluded that both turbulent models yield fairly satisfactory results for supersonic combustion.

### Test Case 2: SBS-1A Spacecraft Engine

A Hughes Aircraft Corporation (HAC) small thruster, HE-54, was used to validate the theoretical performance prediction of the PNS code. This engine was selected for our study for the following reasons. First, experimental data are readily available, as the engine had been studied extensively by Kushida et al.<sup>31</sup>. The second reason is the flowfield through the nozzle is completely laminar from the throat on, resulting in a very thick boundary layer. The previous study<sup>31</sup> was done using the classical inviscid-boundary layer

approach. The present study, using the PNS code, should be able to address the adequacy of the latter approach.

This engine is a small station keeper engine using decomposed hydrazine as propellant. Hence, all of the PNS calculations are performed using 3 species,  $\text{NH}_3$ ,  $\text{N}_2$ , and  $\text{H}_2$ , and frozen chemistry. The chamber operating conditions are as described in Reference 31, and are repeated here as Table 2. Six chamber pressures ranging from 25 psi to 132 psi were considered. Performance predictions, in terms of the thrust coefficient, were obtained for all six cases. However, the flowfield results are only discussed for the two extreme cases, namely the  $P_c = 25$  psi, and  $P_c = 132$  psi. For the first case, with  $P_c = 25$ , Figures 2.1 and 2.2 show the pressure and Mach number contour line. The thickness of the boundary layer, especially the sonic line, ( $M=1$ ) can be seen from Figure 2.2. Both Figures 2.1 and 2.2 show very clearly a compression wave coming from the attachment point in the nozzle contour and reflecting off the centerline. The magnitude of the compression wave can be seen from Figure 2.3, which shows that the pressure along the centerline increased significantly. It is interesting to note that this nozzle was designed as a boundary layer compensated Rao nozzle, in fact by SEA, Inc. for Hughes Aircraft Corporation.

The fact that a shock wave is still in the nozzle shows that this classical design method may not be applicable to flow situations having such a thick boundary layer. Figures 2.4 and 2.5 show the pressure and Mach number contours for the  $P_c = 132$  case. The boundary layer is still very thick, although not as much as the  $P_c = 25$  case.

For the performance prediction, the thrust coefficient,  $C_F$ , defined as total thrust divided by the product of the chamber pressure and the throat area, are obtained from the 6 cases using the PNS code and then compared to the results of Kushida et al. In Reference 31, the experimental data were compared against the theoretical prediction of the JANNAF methodology using TDK/BLM<sup>32</sup>. In Figure 2.6 the results of Kushida are compared against the present theoretical performance predictions. It can be seen in Figure 2.6 that the TDK/BLM results compare surprisingly well with the experimental data, considering how thick the boundary layers are, especially in the low chamber pressure range. The PNS results, however, are in excellent agreement with the data. Both codes, TDK/BLM and PNS, show excellent agreement at the highest chamber pressure, which correlates well with the thinner boundary layer.

#### Test Case 3: XLR-134 Nozzle

The Aerojet XLR-134 is a low thrust cryogenic engine being developed for the AFAL (Air Force Astronautic Laboratory). It is intended to provide low thrust propulsion for the delivery of large space structures to geosynchronous orbit<sup>28,29</sup>. The chamber has an exit area ratio of 7.7. The injector uses a conventional coaxial element in which the gaseous fuel flows in an annulus around the liquid oxidizer. The injector faceplate is a thick copper section to provide adequate cooling and is integral with the injector body. One of the major considerations in nozzle design was to minimize the amount of heat transfer from the engine to the vehicle. For this reason, regenerative cooling to the exit of the nozzle was required. It should be noted that the laminar-turbulent transitions based on Re (Reynold's number based on the momentum thickness) reveals that for the given operating conditions, the flow stays laminar till about one inch before the throat. As yet, engine firing data is not available for this engine.

The calculations for this engine are performed with six (6) species ( $\text{H}$ ,  $\text{H}_2$ ,  $\text{H}_2\text{O}$ ,  $\text{O}$ ,  $\text{OH}$ ,  $\text{O}_2$ ) and eight (8) reaction rates. Figure 3.1 compares the pressure along the wall calculated by the PNS code, against the TDK/MABL code. It can be seen that PNS predicts about 0.126% more loss than the TDK/MABL code. In this nozzle the boundary layer thickness,  $(\delta_{995/r})_{\text{exit}}$ , is about 0.2, which can be considered a fairly thick shear layer.

Computer Code	$I_{sp}$ , lbf/lbm-sec
TDK/MABL	457.45
PNS	456.87

This thickness implies that the viscous effects can extend beyond that of classical boundary layer predictions. Furthermore, the standard methodology, i.e., boundary layer/inviscid flow interaction, can overpredict the specific impulse because, in general, they neglect part of the viscous effects in the nozzle. Figure 3.2 compares the wall shear between the two codes. The pressure and Mach number plots depicted in Figures 3.3 and 3.4 reveals that the shock originating from the attachment point develops to the axis and then reflects.



#### Test Case 4: Space Shuttle Main Engine (SSME)

The Space Shuttle Main Engine (SSME), which is a flight engine, utilizes a thrust chamber that is constructed in two sections: 1) a Main Combustion Chamber (MCC) assembly; and 2) an expansion nozzle assembly<sup>30,35</sup>. The nozzle assembly is bolted to the MCC at a nozzle attach flange. The expansion ratio at the attachment position is 5:1. The nozzle expansion assembly extends to an expansion ratio of 77.5:1.

The SSME uses a hydrogen expander cycle with oxygen preheating and a nozzle that is regeneratively cooled with hydrogen. Nozzle geometry and operating conditions for the SSME current design nozzle (109% power level) were obtained from NASA/MSFC.

The laminar-turbulent transition based on  $Re_\theta$  indicates that the flow in the chamber and nozzle is completely turbulent. The boundary layer is very thin in this nozzle,  $(W.995/r)^{exit} = 0.04$ , and the conventional inviscid-viscous interaction yields good results for the performance calculations. The PNS calculations for the SSME were done with six (6) species ( $H$ ,  $H_2$ ,  $H_2O$ ,  $O$ ,  $OH$ ,  $O_2$ ) and eight (8) reaction rates.

Figures 4.1 and 4.2 compare the pressure and total wall shear along the nozzle wall between the TDK/MABL and PNS. From Figure 4.2 it can be seen that PNS predicts more loss (higher shear at the wall).

Computer Code	$I_{sp}$ lbf/lbm.sec.
TDK/MABL	455.96
PNS	451.03

The difference in  $I_{sp}$ 's is due to the fact that the chemistry in this engine is in equilibrium<sup>36</sup> and the resulting equations become stiff. The present version of the PNS code does not properly account for this effect. The code will be modified to handle these severe conditions. Figures 4.3 and 4.4 show the calculated pressure and Mach Number contours. The compression wave originating from the attachment point can be clearly seen.

#### CONCLUDING REMARKS

The results obtained in this paper, although still preliminary, are very encouraging. The PNS code has shown to be a viable tool for performance prediction over a wide range of conditions for a variety of rocket engines. The results are especially good for flows with thick boundary layers. Some problems still remain to be investigated and resolved. For example, the 1% underprediction of the SSME, and for nozzles with strong shocks. For the latter, an upwind scheme may be required.

#### ACKNOWLEDGMENT

This work was supported by the Air Force Astronautics Laboratory (AFAL) under Contract No. F04611-86-C-0055. The authors wish to thank Dr. Phil Kessel, Mrs. Elizabeth Slimak, and Mr. Jay Levine of the AFAL.

#### REFERENCES

- 1 Tannehill, J. C., Venkatapathy, E., and Rakich, J. V., "Numerical Solution of Supersonic Viscous Flow Over Blunt Delta Wings," AIAA Journal, Vol. 20, 1982, pp. 203-210.
- 2 Kaul, V. K., and Chaussee, D. S., "AFWAL Parabolized Navier-Stokes Code: 1983 AFWAL/NASA Merged Baseline Versions," US Air Force Wright Aeronautical Lab., AFWAL-TR-83-3118, 1983.
- 3 Ferri, A., "Review of Problems in Application of Supersonic Combustion," Journal of the Royal Aeronautical Society, Vol. 68, Sept. 1964, pp. 575-597.
- 4 Moretti, G. "Analysis of Two-Dimensional Problems of Supersonic Combustion Controlled by Mixing," AIAA Journal, Vol. 3, Feb. 1965, pp. 223-229.
- 5 Edelman, R., and Weilerstein, G., "A Solution of the Inviscid-Viscid Equations with Applications to Bounded and Unbounded Multicomponent Reacting Flows," AIAA Paper 69-83, Jan. 1969.
- 6 Ferri, A., "Mixing Controlled Supersonic Combustion," Annual Review of Fluid Mechanics, Vol. 5, Annual Reviews Inc., Palo Alto, CA, 1973, pp. 301-338.

- 7 Buggeln, R. C., McDonald, H., and Livy, R., "Development of a Three-Dimensional Supersonic Inlet Flow Analysis," NASA Contractor Report 3218, Jan. 1980.
- 8 Chitsomborn, T., Kumax, A., and Tirvari, S. N., "Numeric Study of Finite-Rate Supersonic Combustion Using Parabolized Equations," AIAA Paper No. 87-0088, Jan. 1987.
- 9 Sinha, N., and Dash, S. M., "Parabolized Navier-Stokes Analysis of Ducted Turbulent Mixing Problems with Finite-Rate Chemistry," AIAA Paper No. 86-0004, Jan. 1987.
- 10 Kehtarnavaz, H., Coats, D. E., and Kronzon, Y., "Thick Boundary Layer Assessment for Nozzle Flow," AIAA Paper No. 88-3160.
- 11 Briley, W. R., and McDonald, H., "Solution to the Multi-Dimensional Compressible Navier-Stokes Equations by a Generalized Implicit Method," Journal of Computational Physics, Vol. 24, August 1977, pp. 372-397.
- 12 Bena, R., and Warming, R. F., "An Implicit Factored Scheme for the Compressible Navier-Stokes Equations," AIAA Journal, Vol. 16, April 1978, pp. 393-402.
- 13 Vigneron, Y. C., Rakich, J. V., and Tannehill, J. C., "Calculation of Supersonic Viscous Flow Over Delta Wings with Sharp Subsonic Leading Edges, AIAA Paper 78-1137, Seattle, WA, 1978.
- 14 Vigneron, Y. C., Rakich, J. V., and Tannehill, J. C., "Calculation of Supersonic Viscous Flow Over Delta Wings with Sharp Subsonic Leading Edges, NASA TM-78500, 1978.
- 15 Thomas, P. D., and Lombard, C. K., "The Geometric Conservation Law - A Link Between Finite Difference and Finite-Volume Methods of Flow Computation on Moving Grids," AIAA Paper 78-1208, 1978.
- 16 Cebeci, T., "Calculation of Compressible Turbulent Boundary Layers with Heat and Mass Transfer", AIAA J., Vol. 9, No. 6, pp. 1091-1097, June 1971.
- 17 Cebeci, T., "Eddy-Viscosity Distribution in Thick Axisymmetric Turbulent Boundary Layers", J. of Fluid Engineering, Transactions of ASME, pp. 319-326, June 1973.
- 18 Jones, W. P., and Launder, B. E., "The Prediction of Laminarization with a Two-Equation Model of Turbulence", Int. J. Heat Mass Transfer, Vol. 15, pp. 301-314, 1972.
- 19 Jones, W. P., and Launder, B. E., "The Calculation of Low Reynolds Number Phenomena with a Two-Equation Model of Turbulence" Int. J. Heat Mass Transfer, Vol. 16, p. 1119-1130, 1973.
- 20 Dinnborg, J. E., Van Gulick, P., and Kim J., Turbulence Modeling for Steady Three-Dimensional Supersonic Flows, Army Ballistic Research Laboratory, Maryland, Contract Report BRL-CR-553.
- 21 Shirazi, S. A., and Truman, C. R., "Prediction of Turbulent Source Flow Between Corotating Disks with an Anisotropic Two-Equation Turbulence Model", ASME paper No. 87-GT-73, 8 pgs, 1987.
- 22 Patankar, S. V., and Spalding, D. B., Heat and Mass Transfer in Boundary Layers, Inter-Text Books, London, 1970.
- 23 van Driest, E. R., "On Turbulent Flow Near a Wall", Journal of the Aeronautical Sciences, Vol. 23, 1956, p. 1007.
- 24 Arora, R., Kuo, K. K., and Razdan, M. K., "Turbulent Boundary Layer Flow Computations with Special Emphasis on the Near-Wall Region", AIAA paper No. 81-1001, also proceeding of the AIAA Computational Fluid Dynamics Conference, June 1981, pp. 295-305.
- 25 Arora, R., Kuo, K. K., and Razdan, M. K., "Near Wall Treatment for Turbulent Boundary Layer Computations", AIAA J. Vol. 20, No. 11, pp. 1481-1483, Nov. 1982.
- 26 Cebeci, T., and Chang, K. C., "Calculation of Incompressible Rough-Wall Boundary-Layer Flows", AIAA Journal, Vol. 16, No. 7, July 1978, pp. 730-735.
- 27 Burrows, M. C., and Kurlov, A. P., "Analytical and Experimental Study of Supersonic Combustion of Hydrogen in a Vitiated Airstream", NASA Lewis Research Center Report NO. N73-31828.

- 28 Nickerson, G. R., and Dang, L. D., "Two-Dimensional Kinetics Computer Program for Orbit Transfer Vehicles", 22nd JANNAF Combustion Meeting, Pasadena, CA, October 7-10, 1985.
- 29 Schneider, B. E., Michel, R. W., and Gibb, J. A., "Low Thrust Cryogenic Engine Technology", AIAA-87-1932, 23rd Joint Propulsion Conference, San Diego, CA, June 19 - July 2, 1987.
- 30 Prezekwas, A. J., and Gross, K., "SSME Thrust Chamber Modeling with Navier-Stokes Equations", AIAA paper No. 86-1517, 1986.
- 31 Kushida, R. O., Hermel, J., Apfel, S., and Zydwicz, M., "Performance of High Area Ratio Nozzles for a Small Rocket Thruster", AIAA paper No. 86-1573, 1986.
- 32 Kehtarnavaz, H., Coats, D. E., Nickerson, G. R., and Dang, A. L., "Two-Dimensional Kinetics (TDK) Nozzle Performance Computer Program-Thick Boundary Layer Version", Software and Engineering Associates, Inc., March 1987, prepared for the AFAL under Contract No. F04611-86-C-0055, Report No. AFAL-TR-87-031.
- 33 Dahlquist, G., and Bjorck, A., Numerical Methods, Prentice Hall, NJ, 1974.
- 34 Thompson, J. F., Warri, Z. U. A., and Wayne Mastine, C., Numerical Grid Generation, North Holland, NY, 1985.
- 35 Nickerson, G. R., and Dang, A. L., "Performance Predictions for an SSME Configuration with an Enlarged Throat," Report prepared for MSFC, SEA, Inc. Contract No. NAS8-35931, November, 1985.
- 36 Dang, A. L., Kehtarnavaz, H., and Nickerson, G. R., "Solution of the Boundary Layer Equations with Non-Equilibrium Reacting Chemistry in Rocket Nozzles," SEA, Inc. presented at 25th JANNAF Combustion Meeting, Huntsville, AL, October, 1988.

Table 1: Specifications of the Engines

ENGINE	APPLICATION	PROPELLANT	THRUST (lb <sub>f</sub> )	CHAMBER PRESSURE (psia)	THROAT RADIUS, R* (inches)	REYNOLD'S NUMBER Re <sub>R*</sub>	EXPANSION RATIO
SBS-1A (Hughes Spacecraft Engine)	Spacecraft	N <sub>2</sub> H <sub>4</sub>	5.45	106	.0925	3.90 x 10 <sup>4</sup>	300:1
XLR-134	OTV	LOX/CH <sub>2</sub>	511	510	.396	1.80 x 10 <sup>5</sup>	761:1
SSME (Space Shuttle Main Engine)	SSTO	LOX/CH <sub>2</sub>	463,000	3285	5.1527	1.18 x 10 <sup>7</sup>	77.5:1

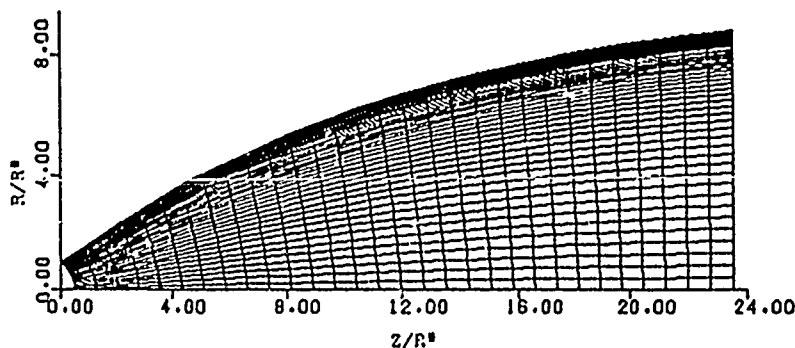


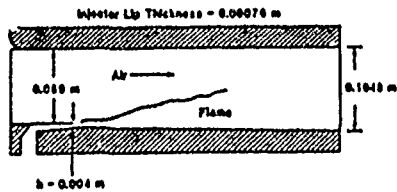
Figure 1.0. Physical Grids.

Table 2. Chamber Operating Conditions<sup>31</sup>

Propellant: decomposed hydrazine  
 Nozzle throat diameter: 0.185 in.  
 Thermal expansion coefficient (L605):  $9.4 \text{ by } 10^{-6} \text{ in./in. } ^\circ\text{F}$

Chamber Pressure $P_c$ psia	Supply Pressure $P_s$ psia	Char. Velocity $C^*$ fps	Chamber Temp. $T_c$ °R	Mean Mol. Wt. $M$	Fraction Ammonia Dissoc. $X$	Throat Wall Temp. $T_w$ °R	Throat Radius in. $A^*$	Throat Displacement Thickness $\delta^*$ in.	Throat Momentum Thickness $\theta$ in.	Throat Reynolds Number $Re_{A^*}$	Throat Velocity Coeff. $C_v$	Mass flow $\dot{m}$ lbm/sec		
25	40	4125	1700	11.20	0.900	1665	.0935	.001030	3.557E-4	121.5	42.0	11029	.99568	.005215
35	60	4150	1745	11.36	0.870	1700	.0935	8.599E-4	3.142E-4	138.2	50.5	15027	.99567	.007284
54	100	4200	1830	11.67	0.810	1743	.0936	6.771E-4	2.729E-4	160.0	64.8	22118	.99566	.01117
86	185	4.80	1965	12.22	0.719	1852	.0937	5.244E-4	2.426E-4	183.1	84.7	32716	.99567	.01755
106	250	4310	2030	12.50	0.668	1888	.0937	4.674E-4	2.293E-4	194.8	95.6	39032	.99567	.02152
132	350	4325	2070	12.69	0.645	1905	.0937	4.166E-4	2.112E-4	211.6	107.3	47592	.99568	.02672

FRACTION DISSOCIATION:



	Hydrogen Jet	Free Stream
Mach Number, M	1.00	3.44
Temperature, T, K	254	1270
Velocity, u, m/s	1216	1744
Pressure, p, MPa	0.1	0.1
Mass Fractions:		
$\text{H}_2$	1.000	0
$\text{N}_2$	0	0.258
$\text{O}_2$	0	0.486
$\text{H}_2\text{O}$	0	0.256

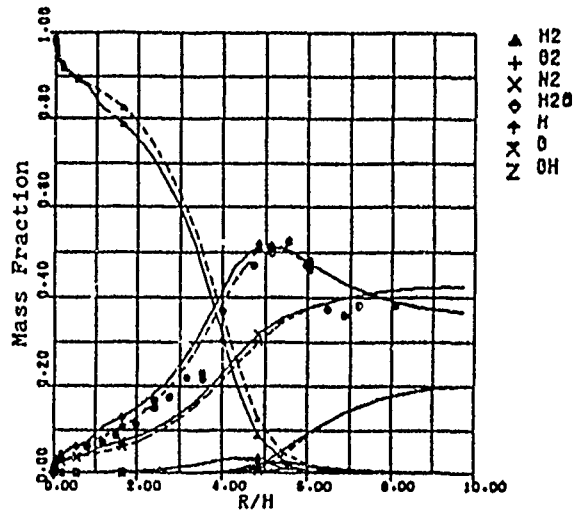


Figure 1.1. Combustion Validation Test Case Parameters.

Figure 1.2. Burrows & Kurlov Supersonic Combustion Test Case.

— k-c  
 --- mixing length model  
 • experiment, Ref. (27)

$\phi = 0.0002$   
 $\phi = 0.0004$   
 $\phi = 0.0006$   
 $\phi = 0.0008$   
 $\phi = 0.0010$   
 $\phi = 0.0012$   
 $\phi = 0.0014$   
 $\phi = 0.0016$   
 $\phi = 0.0018$   
 $\phi = 0.0020$   
 $\phi = 0.0022$   
 $\phi = 0.0024$   
 $\phi = 0.0026$   
 $\phi = 0.0028$   
 $\phi = 0.0030$   
 $\phi = 0.0032$   
 $\phi = 0.0034$   
 $\phi = 0.0036$   
 $\phi = 0.0038$   
 $\phi = 0.0040$   
 $\phi = 0.0042$   
 $\phi = 0.0044$   
 $\phi = 0.0046$   
 $\phi = 0.0048$   
 $\phi = 0.0050$   
 $\phi = 0.0052$   
 $\phi = 0.0054$   
 $\phi = 0.0056$   
 $\phi = 0.0058$   
 $\phi = 0.0060$   
 $\phi = 0.0062$   
 $\phi = 0.0064$   
 $\phi = 0.0066$   
 $\phi = 0.0068$   
 $\phi = 0.0070$   
 $\phi = 0.0072$   
 $\phi = 0.0074$   
 $\phi = 0.0076$   
 $\phi = 0.0078$   
 $\phi = 0.0080$   
 $\phi = 0.0082$   
 $\phi = 0.0084$   
 $\phi = 0.0086$   
 $\phi = 0.0088$   
 $\phi = 0.0090$   
 $\phi = 0.0092$   
 $\phi = 0.0094$   
 $\phi = 0.0096$   
 $\phi = 0.0098$   
 $\phi = 0.0100$   
 $\phi = 0.0102$   
 $\phi = 0.0104$   
 $\phi = 0.0106$   
 $\phi = 0.0108$   
 $\phi = 0.0110$   
 $\phi = 0.0112$   
 $\phi = 0.0114$   
 $\phi = 0.0116$   
 $\phi = 0.0118$   
 $\phi = 0.0120$   
 $\phi = 0.0122$   
 $\phi = 0.0124$   
 $\phi = 0.0126$   
 $\phi = 0.0128$   
 $\phi = 0.0130$   
 $\phi = 0.0132$   
 $\phi = 0.0134$   
 $\phi = 0.0136$   
 $\phi = 0.0138$   
 $\phi = 0.0140$   
 $\phi = 0.0142$   
 $\phi = 0.0144$   
 $\phi = 0.0146$   
 $\phi = 0.0148$   
 $\phi = 0.0150$   
 $\phi = 0.0152$   
 $\phi = 0.0154$   
 $\phi = 0.0156$   
 $\phi = 0.0158$   
 $\phi = 0.0160$   
 $\phi = 0.0162$   
 $\phi = 0.0164$   
 $\phi = 0.0166$   
 $\phi = 0.0168$   
 $\phi = 0.0170$   
 $\phi = 0.0172$   
 $\phi = 0.0174$   
 $\phi = 0.0176$   
 $\phi = 0.0178$   
 $\phi = 0.0180$   
 $\phi = 0.0182$   
 $\phi = 0.0184$   
 $\phi = 0.0186$   
 $\phi = 0.0188$   
 $\phi = 0.0190$   
 $\phi = 0.0192$   
 $\phi = 0.0194$   
 $\phi = 0.0196$   
 $\phi = 0.0198$   
 $\phi = 0.0200$   
 $\phi = 0.0202$   
 $\phi = 0.0204$   
 $\phi = 0.0206$   
 $\phi = 0.0208$   
 $\phi = 0.0210$   
 $\phi = 0.0212$   
 $\phi = 0.0214$   
 $\phi = 0.0216$   
 $\phi = 0.0218$   
 $\phi = 0.0220$   
 $\phi = 0.0222$   
 $\phi = 0.0224$   
 $\phi = 0.0226$   
 $\phi = 0.0228$   
 $\phi = 0.0230$   
 $\phi = 0.0232$   
 $\phi = 0.0234$   
 $\phi = 0.0236$   
 $\phi = 0.0238$   
 $\phi = 0.0240$   
 $\phi = 0.0242$   
 $\phi = 0.0244$   
 $\phi = 0.0246$   
 $\phi = 0.0248$   
 $\phi = 0.0250$   
 $\phi = 0.0252$   
 $\phi = 0.0254$   
 $\phi = 0.0256$   
 $\phi = 0.0258$   
 $\phi = 0.0260$   
 $\phi = 0.0262$   
 $\phi = 0.0264$   
 $\phi = 0.0266$   
 $\phi = 0.0268$   
 $\phi = 0.0270$   
 $\phi = 0.0272$   
 $\phi = 0.0274$   
 $\phi = 0.0276$   
 $\phi = 0.0278$   
 $\phi = 0.0280$   
 $\phi = 0.0282$   
 $\phi = 0.0284$   
 $\phi = 0.0286$   
 $\phi = 0.0288$   
 $\phi = 0.0290$   
 $\phi = 0.0292$   
 $\phi = 0.0294$   
 $\phi = 0.0296$   
 $\phi = 0.0298$   
 $\phi = 0.0300$   
 $\phi = 0.0302$   
 $\phi = 0.0304$   
 $\phi = 0.0306$   
 $\phi = 0.0308$   
 $\phi = 0.0310$   
 $\phi = 0.0312$   
 $\phi = 0.0314$   
 $\phi = 0.0316$   
 $\phi = 0.0318$   
 $\phi = 0.0320$   
 $\phi = 0.0322$   
 $\phi = 0.0324$   
 $\phi = 0.0326$   
 $\phi = 0.0328$   
 $\phi = 0.0330$   
 $\phi = 0.0332$   
 $\phi = 0.0334$   
 $\phi = 0.0336$   
 $\phi = 0.0338$   
 $\phi = 0.0340$   
 $\phi = 0.0342$   
 $\phi = 0.0344$   
 $\phi = 0.0346$   
 $\phi = 0.0348$   
 $\phi = 0.0350$   
 $\phi = 0.0352$   
 $\phi = 0.0354$   
 $\phi = 0.0356$   
 $\phi = 0.0358$   
 $\phi = 0.0360$   
 $\phi = 0.0362$   
 $\phi = 0.0364$   
 $\phi = 0.0366$   
 $\phi = 0.0368$   
 $\phi = 0.0370$   
 $\phi = 0.0372$   
 $\phi = 0.0374$   
 $\phi = 0.0376$   
 $\phi = 0.0378$   
 $\phi = 0.0380$   
 $\phi = 0.0382$   
 $\phi = 0.0384$   
 $\phi = 0.0386$   
 $\phi = 0.0388$   
 $\phi = 0.0390$   
 $\phi = 0.0392$   
 $\phi = 0.0394$   
 $\phi = 0.0396$   
 $\phi = 0.0398$   
 $\phi = 0.0400$   
 $\phi = 0.0402$   
 $\phi = 0.0404$   
 $\phi = 0.0406$   
 $\phi = 0.0408$   
 $\phi = 0.0410$   
 $\phi = 0.0412$   
 $\phi = 0.0414$   
 $\phi = 0.0416$   
 $\phi = 0.0418$   
 $\phi = 0.0420$   
 $\phi = 0.0422$   
 $\phi = 0.0424$   
 $\phi = 0.0426$   
 $\phi = 0.0428$   
 $\phi = 0.0430$   
 $\phi = 0.0432$   
 $\phi = 0.0434$   
 $\phi = 0.0436$   
 $\phi = 0.0438$   
 $\phi = 0.0440$   
 $\phi = 0.0442$   
 $\phi = 0.0444$   
 $\phi = 0.0446$   
 $\phi = 0.0448$   
 $\phi = 0.0450$   
 $\phi = 0.0452$   
 $\phi = 0.0454$   
 $\phi = 0.0456$   
 $\phi = 0.0458$   
 $\phi = 0.0460$   
 $\phi = 0.0462$   
 $\phi = 0.0464$   
 $\phi = 0.0466$   
 $\phi = 0.0468$   
 $\phi = 0.0470$   
 $\phi = 0.0472$   
 $\phi = 0.0474$   
 $\phi = 0.0476$   
 $\phi = 0.0478$   
 $\phi = 0.0480$   
 $\phi = 0.0482$   
 $\phi = 0.0484$   
 $\phi = 0.0486$   
 $\phi = 0.0488$   
 $\phi = 0.0490$   
 $\phi = 0.0492$   
 $\phi = 0.0494$   
 $\phi = 0.0496$   
 $\phi = 0.0498$   
 $\phi = 0.0500$   
 $\phi = 0.0502$   
 $\phi = 0.0504$   
 $\phi = 0.0506$   
 $\phi = 0.0508$   
 $\phi = 0.0510$   
 $\phi = 0.0512$   
 $\phi = 0.0514$   
 $\phi = 0.0516$   
 $\phi = 0.0518$   
 $\phi = 0.0520$   
 $\phi = 0.0522$   
 $\phi = 0.0524$   
 $\phi = 0.0526$   
 $\phi = 0.0528$   
 $\phi = 0.0530$   
 $\phi = 0.0532$   
 $\phi = 0.0534$   
 $\phi = 0.0536$   
 $\phi = 0.0538$   
 $\phi = 0.0540$   
 $\phi = 0.0542$   
 $\phi = 0.0544$   
 $\phi = 0.0546$   
 $\phi = 0.0548$   
 $\phi = 0.0550$   
 $\phi = 0.0552$   
 $\phi = 0.0554$   
 $\phi = 0.0556$   
 $\phi = 0.0558$   
 $\phi = 0.0560$   
 $\phi = 0.0562$   
 $\phi = 0.0564$   
 $\phi = 0.0566$   
 $\phi = 0.0568$   
 $\phi = 0.0570$   
 $\phi = 0.0572$   
 $\phi = 0.0574$   
 $\phi = 0.0576$   
 $\phi = 0.0578$   
 $\phi = 0.0580$   
 $\phi = 0.0582$   
 $\phi = 0.0584$   
 $\phi = 0.0586$   
 $\phi = 0.0588$   
 $\phi = 0.0590$   
 $\phi = 0.0592$   
 $\phi = 0.0594$   
 $\phi = 0.0596$   
 $\phi = 0.0598$   
 $\phi = 0.0600$   
 $\phi = 0.0602$   
 $\phi = 0.0604$   
 $\phi = 0.0606$   
 $\phi = 0.0608$   
 $\phi = 0.0610$   
 $\phi = 0.0612$   
 $\phi = 0.0614$   
 $\phi = 0.0616$   
 $\phi = 0.0618$   
 $\phi = 0.0620$   
 $\phi = 0.0622$   
 $\phi = 0.0624$   
 $\phi = 0.0626$   
 $\phi = 0.0628$   
 $\phi = 0.0630$   
 $\phi = 0.0632$   
 $\phi = 0.0634$   
 $\phi = 0.0636$   
 $\phi = 0.0638$   
 $\phi = 0.0640$   
 $\phi = 0.0642$   
 $\phi = 0.0644$   
 $\phi = 0.0646$   
 $\phi = 0.0648$   
 $\phi = 0.0650$   
 $\phi = 0.0652$   
 $\phi = 0.0654$   
 $\phi = 0.0656$   
 $\phi = 0.0658$   
 $\phi = 0.0660$   
 $\phi = 0.0662$   
 $\phi = 0.0664$   
 $\phi = 0.0666$   
 $\phi = 0.0668$   
 $\phi = 0.0670$   
 $\phi = 0.0672$   
 $\phi = 0.0674$   
 $\phi = 0.0676$   
 $\phi = 0.0678$   
 $\phi = 0.0680$   
 $\phi = 0.0682$   
 $\phi = 0.0684$   
 $\phi = 0.0686$   
 $\phi = 0.0688$   
 $\phi = 0.0690$   
 $\phi = 0.0692$   
 $\phi = 0.0694$   
 $\phi = 0.0696$   
 $\phi = 0.0698$   
 $\phi = 0.0700$   
 $\phi = 0.0702$   
 $\phi = 0.0704$   
 $\phi = 0.0706$   
 $\phi = 0.0708$   
 $\phi = 0.0710$   
 $\phi = 0.0712$   
 $\phi = 0.0714$   
 $\phi = 0.0716$   
 $\phi = 0.0718$   
 $\phi = 0.0720$   
 $\phi = 0.0722$   
 $\phi = 0.0724$   
 $\phi = 0.0726$   
 $\phi = 0.0728$   
 $\phi = 0.0730$   
 $\phi = 0.0732$   
 $\phi = 0.0734$   
 $\phi = 0.0736$   
 $\phi = 0.0738$   
 $\phi = 0.0740$   
 $\phi = 0.0742$   
 $\phi = 0.0744$   
 $\phi = 0.0746$   
 $\phi = 0.0748$   
 $\phi = 0.0750$   
 $\phi = 0.0752$   
 $\phi = 0.0754$   
 $\phi = 0.0756$   
 $\phi = 0.0758$   
 $\phi = 0.0760$   
 $\phi = 0.0762$   
 $\phi = 0.0764$   
 $\phi = 0.0766$   
 $\phi = 0.0768$   
 $\phi = 0.0770$   
 $\phi = 0.0772$   
 $\phi = 0.0774$   
 $\phi = 0.0776$   
 $\phi = 0.0778$   
 $\phi = 0.0780$   
 $\phi = 0.0782$   
 $\phi = 0.0784$   
 $\phi = 0.0786$   
 $\phi = 0.0788$   
 $\phi = 0.0790$   
 $\phi = 0.0792$   
 $\phi = 0.0794$   
 $\phi = 0.0796$   
 $\phi = 0.0798$   
 $\phi = 0.0800$   
 $\phi = 0.0802$   
 $\phi = 0.0804$   
 $\phi = 0.0806$   
 $\phi = 0.0808$   
 $\phi = 0.0810$   
 $\phi = 0.0812$   
 $\phi = 0.0814$   
 $\phi = 0.0816$   
 $\phi = 0.0818$   
 $\phi = 0.0820$   
 $\phi = 0.0822$   
 $\phi = 0.0824$   
 $\phi = 0.0826$   
 $\phi = 0.0828$   
 $\phi = 0.0830$   
 $\phi = 0.0832$   
 $\phi = 0.0834$   
 $\phi = 0.0836$   
 $\phi = 0.0838$   
 $\phi = 0.0840$   
 $\phi = 0.0842$   
 $\phi = 0.0844$   
 $\phi = 0.0846$   
 $\phi = 0.0848$   
 $\phi = 0.0850$   
 $\phi = 0.0852$   
 $\phi = 0.0854$   
 $\phi = 0.0856$   
 $\phi = 0.0858$   
 $\phi = 0.0860$   
 $\phi = 0.0862$   
 $\phi = 0.0864$   
 $\phi = 0.0866$   
 $\phi = 0.0868$   
 $\phi = 0.0870$   
 $\phi = 0.0872$   
 $\phi = 0.0874$   
 $\phi = 0.0876$   
 $\phi = 0.0878$   
 $\phi = 0.0880$   
 $\phi = 0.0882$   
 $\phi = 0.0884$   
 $\phi = 0.0886$   
 $\phi = 0.0888$   
 $\phi = 0.0890$   
 $\phi = 0.0892$   
 $\phi = 0.0894$   
 $\phi = 0.0896$   
 $\phi = 0.0898$   
 $\phi = 0.0900$   
 $\phi = 0.0902$   
 $\phi = 0.0904$   
 $\phi = 0.0906$   
 $\phi = 0.0908$   
 $\phi = 0.0910$   
 $\phi = 0.0912$   
 $\phi = 0.0914$   
 $\phi = 0.0916$   
 $\phi = 0.0918$   
 $\phi = 0.0920$   
 $\phi = 0.0922$   
 $\phi = 0.0924$   
 $\phi = 0.0926$   
 $\phi = 0.0928$   
 $\phi = 0.0930$   
 $\phi = 0.0932$   
 $\phi = 0.0934$   
 $\phi = 0.0936$   
 $\phi = 0.0938$   
 $\phi = 0.0940$   
 $\phi = 0.0942$   
 $\phi = 0.0944$   
 $\phi = 0.0946$   
 $\phi = 0.0948$   
 $\phi = 0.0950$   
 $\phi = 0.0952$   
 $\phi = 0.0954$   
 $\phi = 0.0956$   
 $\phi = 0.0958$   
 $\phi = 0.0960$   
 $\phi = 0.0962$   
 $\phi = 0.0964$   
 $\phi = 0.0966$   
 $\phi = 0.0968$   
 $\phi = 0.0970$   
 $\phi = 0.0972$   
 $\phi = 0.0974$   
 $\phi = 0.0976$   
 $\phi = 0.0978$   
 $\phi = 0.0980$   
 $\phi = 0.0982$   
 $\phi = 0.0984$   
 $\phi = 0.0986$   
 $\phi = 0.0988$   
 $\phi = 0.0990$   
 $\phi = 0.0992$   
 $\phi = 0.0994$   
 $\phi = 0.0996$   
 $\phi = 0.0998$   
 $\phi = 0.1000$

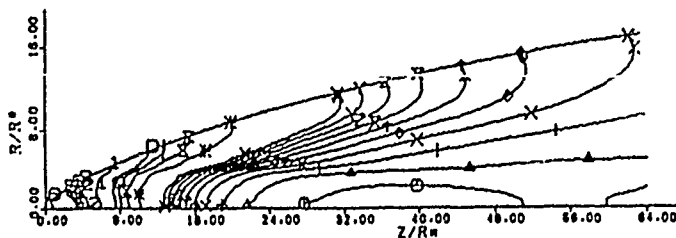


Figure 2.1. Pressure Contour for  $Po=25$  for the RAS-1A Spacecraft Engine.

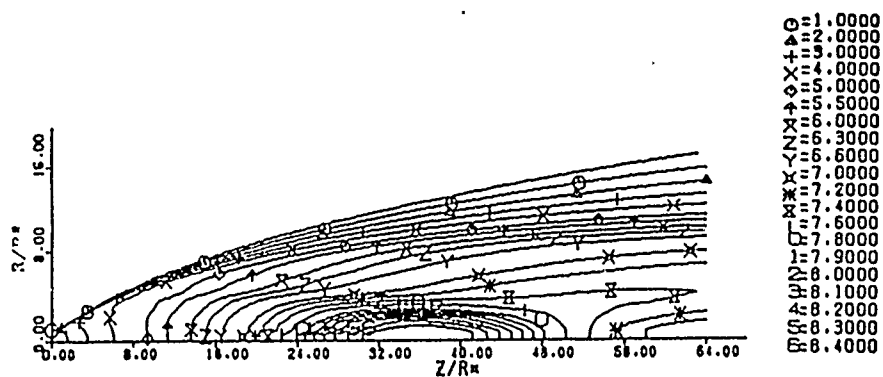


Figure 2.2. Mach Number Contour for  $P_c=25$  for the SRS-1A Spacecraft Engine.

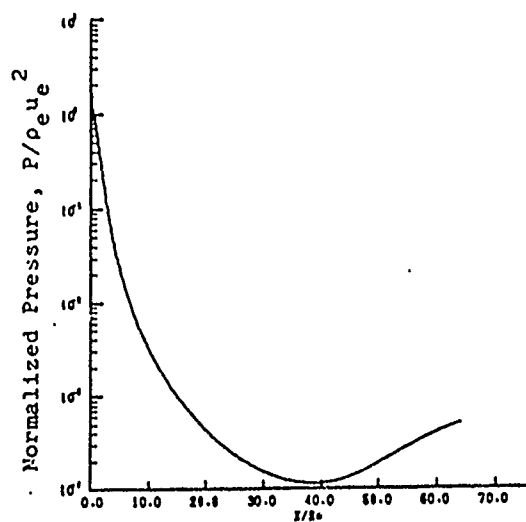


Figure 2.3. Pressure on Centerline  $P_c=25$  for the SRS-1A Spacecraft Engine.

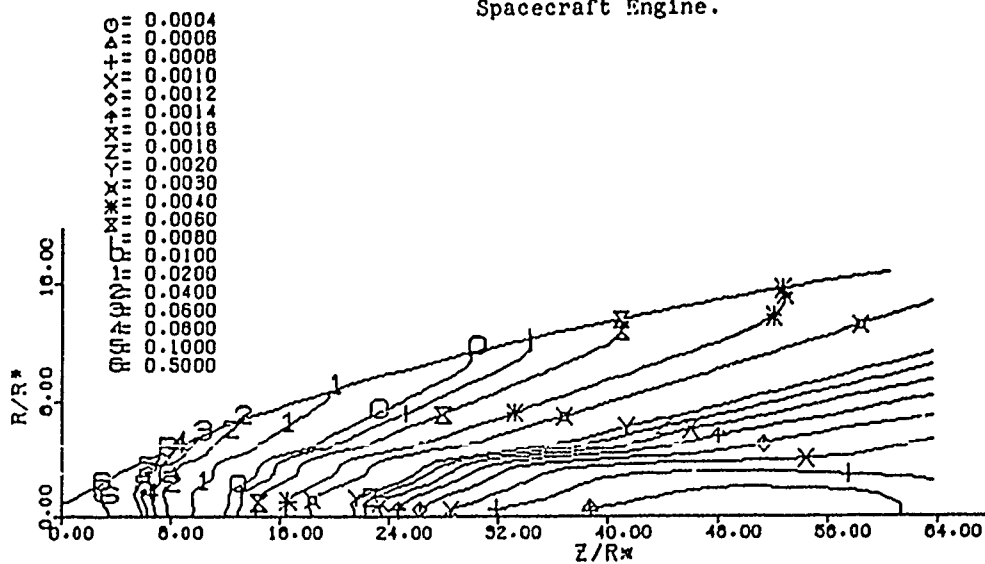


Figure 2.4. Pressure Contour for  $P_c=132$  for the SRS-1A Spacecraft Engine.

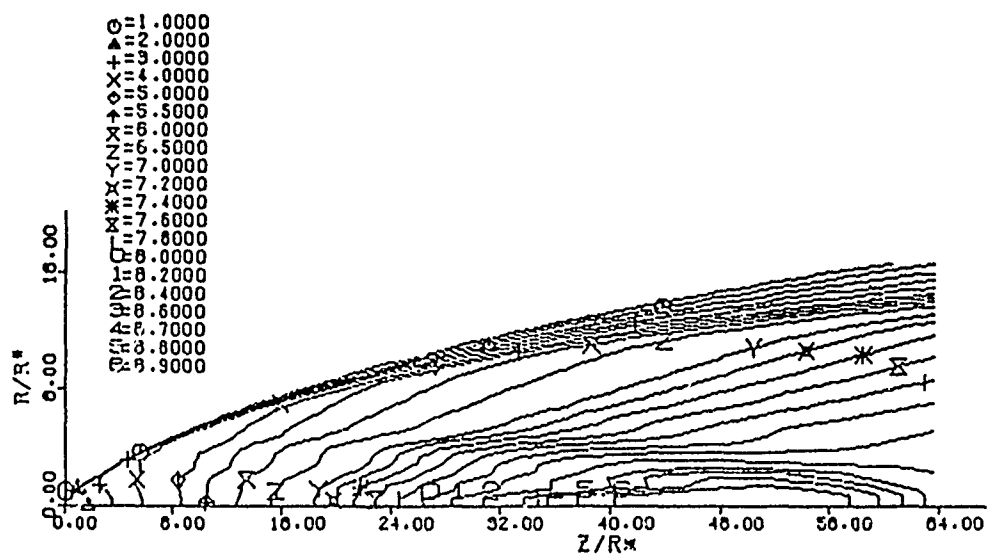


Figure 2.5. Mach Number Contour for  $P_c=132$  for the SBS-1A Spacecraft Engine.

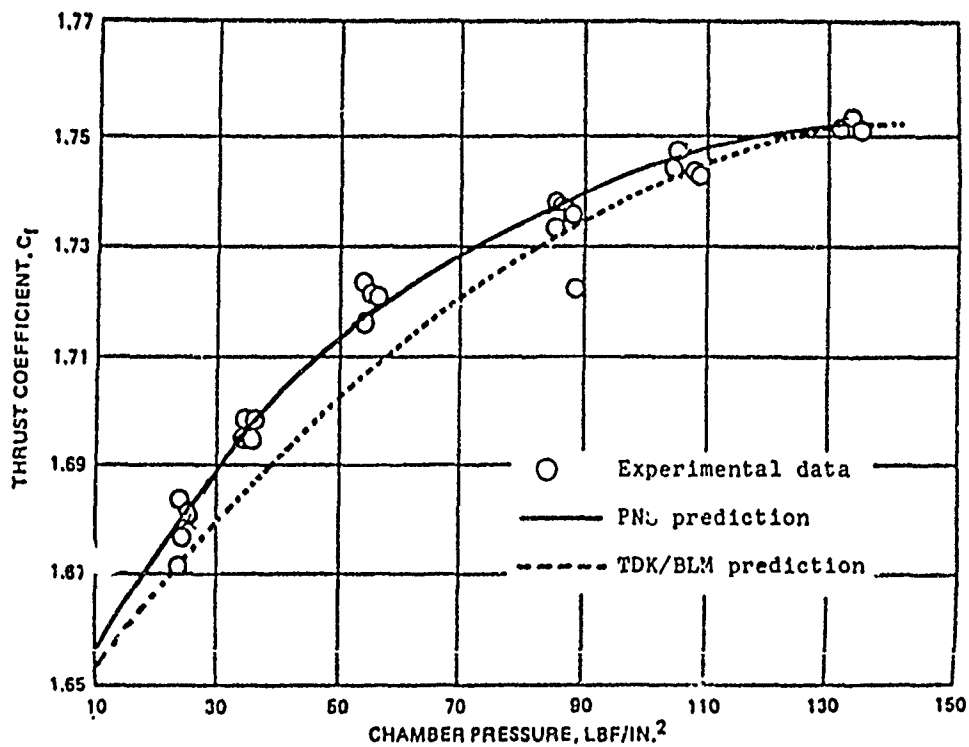


Figure 2.6. Comparison of Thrust Coefficient for Experimental and Predicted Data.

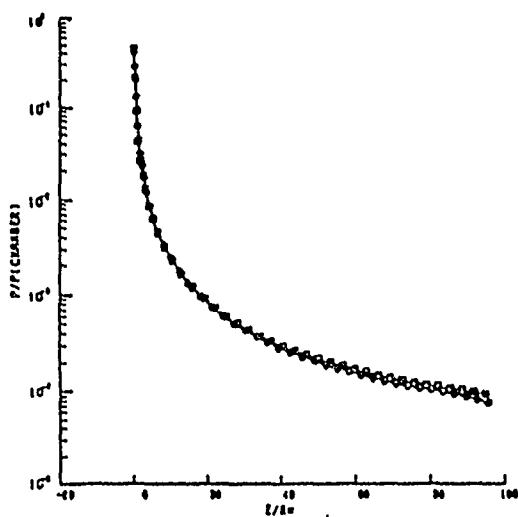


Figure 3.1. Pressure along the wall for turbulent flow with chemistry in XLR-134 nozzle.  
 o TDK/MABL  
 □ PNS

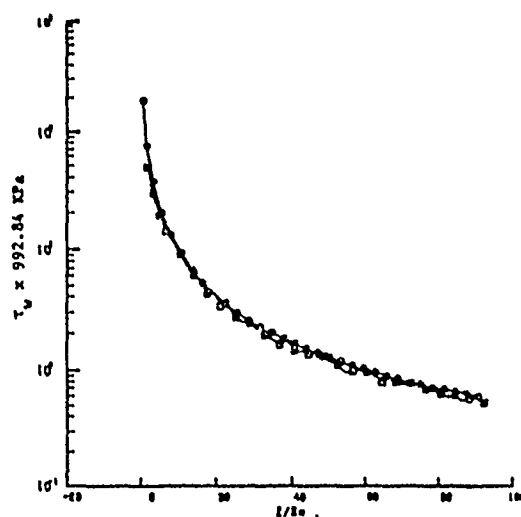


Figure 3.2. Shear stress along the wall for turbulent flow with chemistry in XLR-134 nozzle.  
 o TDK/MABL  
 □ PNS

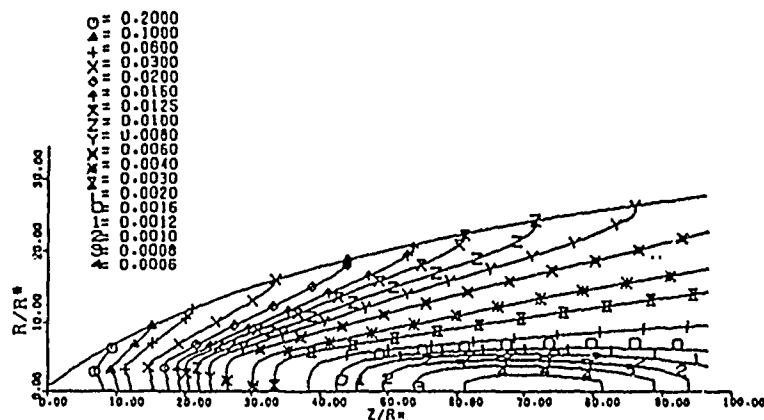


Figure 3.3. Pressure Contours for XLR-134 nozzle turbulent flow with chemistry.

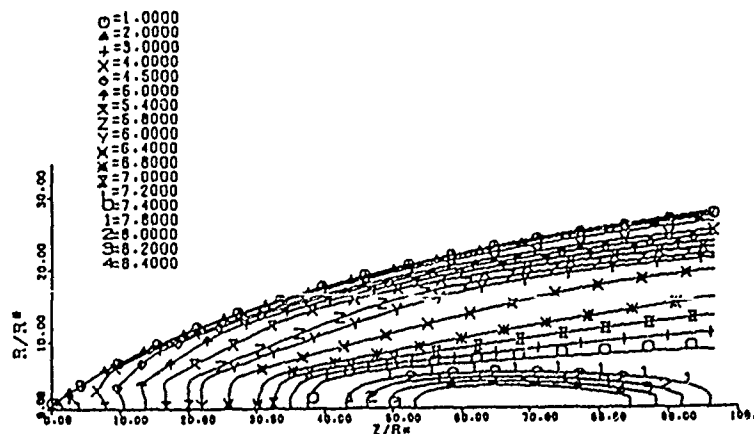


Figure 3.4. Mach Number Contours for XLR-134 nozzle turbulent flow with chemistry.

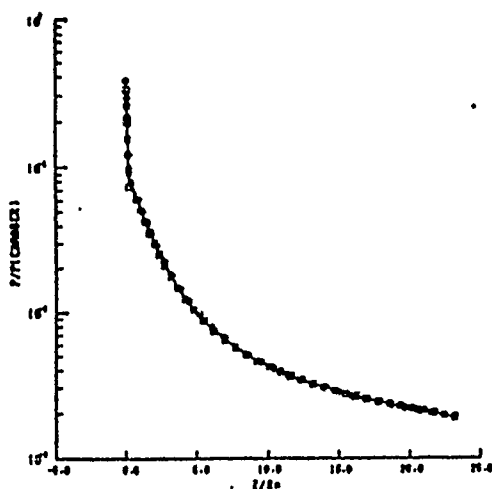


Figure 4.1. Pressure along the wall for turbulent flow with chemistry in SSME nozzle.  
 o TDK/MABL  
 □ PNS

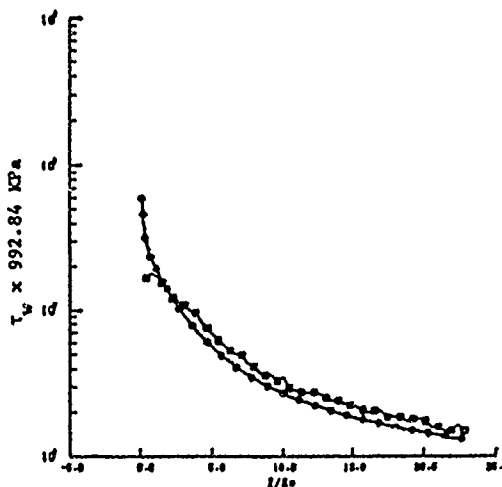


Figure 4.2. Shear stress along the wall for turbulent flow with chemistry in SSME nozzle.  
 o TDK/MABL  
 □ PNS

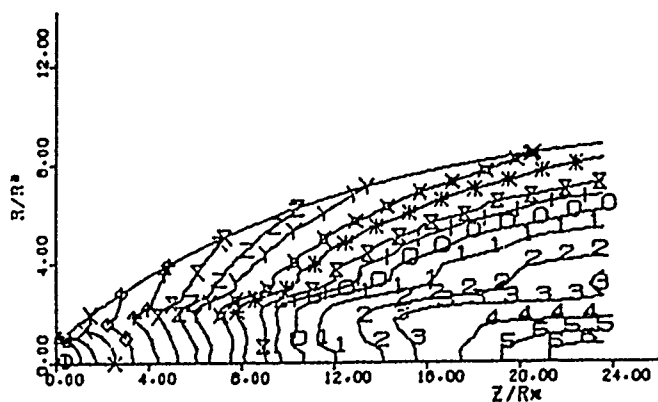


Figure 4.3. Pressure Contours for SSME nozzle turbulent flow with chemistry.

O=240.0000  
 Δ=100.0000  
 + =50.0000  
 x =20.0000  
 X =10.0000  
 ◆ =5.0000  
 † =3.0000  
 \* =2.0000  
 N =1.5000  
 Y =1.0000  
 x =0.8000  
 \* =0.6000  
 x =0.5000  
 † =0.4000  
 † =0.3000  
 † =0.2000  
 † =0.1500  
 † =0.1000  
 † =0.0700  
 † =0.0500

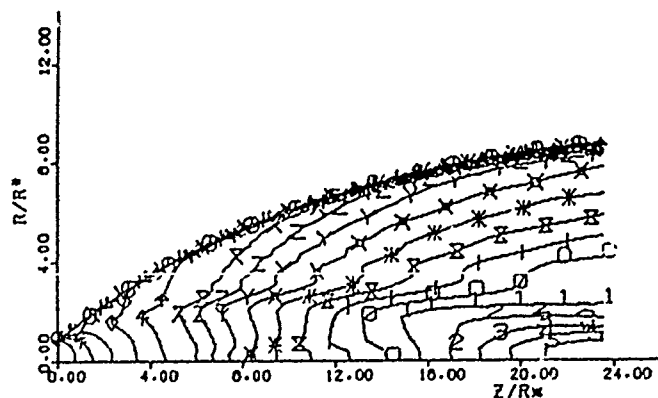


Figure 4.4. Mach Number Contours for SSME nozzle turbulent flow with chemistry.

O=1.0000  
 Δ=1.5000  
 + =2.0000  
 x =2.5000  
 X =3.0000  
 ◆ =3.4000  
 † =3.8000  
 \* =4.0000  
 N =4.2000  
 Y =4.4000  
 x =4.6000  
 \* =4.8000  
 † =5.0000  
 † =5.2000  
 † =5.4000  
 † =5.6000  
 † =5.8000  
 † =6.0000  
 † =6.2000  
 † =6.4000